博士論文

Synthesis of Zinc-Containing Zeolites with a Focus on Mixing Methods of Raw Materials

（原料混合手法に着目した亜鉛含有ゼオライトの合成）

Natsume Koike

（小池 夏萌）

Department of Chemical System Engineering,
The University of Tokyo
February 16th, 2018

A Dissertation Submitted in Partial Fulfillment of the
Requirements for the Degree of Doctor of Philosophy

Dissertation Committee;

Tatsuya OKUBO, Ph. D. (Supervisor)
Professor, Department of Chemical System Engineering
Dean, School of Engineering
The University of Tokyo

Masaru OGURA, Ph. D.
Professor, Department of Chemical System Engineering
The University of Tokyo

Ryuji KIKUCHI, Ph. D.
Associate Professor, Department of Chemical System Engineering
The University of Tokyo

Masashi OKUBO, Ph. D.
Associate Professor, Department of Chemical System Engineering
The University of Tokyo

Toru Wakihara, Ph. D.
Associate Professor, Department of Chemical System Engineering
The University of Tokyo

Kazuya YAMAGUCHI, Ph. D.
Professor, Department of Applied Chemistry
The University of Tokyo

Shigeo MARUYAMA, Ph. D.
Professor, Department of Mechanical Engineering
The University of Tokyo

Table of Contents

Chapter 1. General Introduction

1.1 Porous Materials

Porous materials, solid materials containing pores or voids in their interiors, have been playing important roles in both scientific and technological fields because of their specific interaction with guest atoms, ions and molecules.[1] They have been used as, for example, catalysts, ion-exchangers and adsorbents. Development of new classes of porous materials or finding new functionalities of them have been opening doors for many new applications. The sizes, shapes and volumes of the pores, and atoms and molecules that construct them directly affect their functions.

The pores within porous materials are classified by the pore sizes, as micropores (with pore sizes below 2 nm), mesopores (with pore sizes in the range from 2 nm to 50 nm) and macropores (with pore sizes above 50 nm), according to the International Union of Pure and Applied Chemistry (IUPAC) definition.[2] Controlled pore structure, uniformity of pore sizes, volumes and shapes of the pore interior are crucial for their properties. To achieve the desirable porous structures, various methods have been developed. The micropore structures are formed, for example, through hydrothermal treatment and controlled assembly of molecular building blocks.[3,4,5] The ordered mesoporous structures have been achieved mainly by using soft templates such as block copolymer micelles[6,7,8,9] or hard templates such as polystyrene beads and inorganic nanoparticles.[10,11,12] Mesoporous structures have also been prepared by controlled assembly of uniform colloidal particles.[13,14] Macroporous materials have been formed *via* processes, for example, partial sintering, hard templating and technique including bubble formation.[15] Secondary macro- and / or mesoporosity are often introduced to microporous structure to form hierarchal structure for overcoming problems such as restricted molecular diffusion and mass transportation in micropores.[16,17]

Porous materials are also categorized by the types of the material which creates the walls of the pores. Various porous materials composed of inorganic, organic and inorganic-organic hybrid materials have been reported. Zeolites are major inorganic microporous materials and will be deeply described in section 1.2. Other examples of microporous inorganic materials include various phosphates, such as those of zinc, beryllium, gallium, indium, and tin with the same topology as zeolite or newly found topology with the contents.[18] Among various inorganic mesoporous materials, such as metal (*e.g.* platinum,[19,20] zinc,[21] nickel and cobalt[22]) and metal oxide (*e.g.* niobia and titania[23]) mesoporous materials, mesoporous silicas are of particular importance because of their precisely controllable morphology, high stability and easily modified surface properties.[24] They were firstly reported in the early 1990s by Kuroda group and researchers in Mobil Company, indevidualy.[25,26] The most common mesoporous silica include MCM-41, MCM-48 and SBA-15, which have different pore sizes (2 to 10 nm) and structural characteristics (2D hexagonal and 3D cubic).[27] The periodic mesoporous materials are new generation of ordered porous materials with open pores greater than 2 nm, and have achieved remarkable drug/gene delivery systems, biosensors and bio-imaging applications.[24] They have also been utilized as efficient supports for active metals such as platinum.[28]

Carbonaceous adsorbents are common organic based porous materials which can be obtained economically using low-cost materials such as coal and agricultural solid wastes.[29] Activated carbons have been prepared *via* well-established activation method which produce high surface area and have been used as efficient adsorbents.[30,29] Ordered mesoporous carbons with defined pore structures have also been extensively studied due to their superior sorption and separation characteristics.[31] Porous crystalline covalent organic frameworks (COFs), which are other type of carbon-based microporous materials, are defined as crystalline microporous organic structures which building blocks constructed solely from light elements (H, B, C, N, and O) are linked by covalent bonds.[32] They are constructed by assembling reversible co-condensation reactions of the building blocks.[33] They have shown remarkable activities in, such as, catalysis[32] and gas storage[34] due to their designable structures and properties, easy processing and low density.

The inorganic-organic hybrid materials have recently been intensively studied because of their properties combining advantages of both inorganics (*e.g.* thermal and mechanical stability) and organics (*e.g.* flexibility and easily tunable functionality). Organosilicas are one major group of hybrid materials which usually made from $R'Si(OR)_3$ or $(RO)_3Si–R'–Si(OR)_3$ monomers or various oligosiloxanes.[35] Organosilicas with micropores can be formed as random silica network (aerogel and xerogel[36,37]) and more importantly, as ordered silicate structure. To form the latter ordered structure, bottom-up approach to build up small unit, such as, double four membered ring[38,39,40] and double three membered ring[41] has been successful. Organosilicas with periodic mesopores are formed mainly by three ways; grafting, which modifies mesoporous silicas by $R'_xSi(OR)_{4-x}$ type organosilans,[42] co-condensation, which uses both $Si(OR)_4$ type alkoxysilane and $R'Si(OR)_3$ type organosilans in the condensation process,[43,44] and the method using bridged organosilans $(RO)_3Si–R'–Si(OR)_3$.[45,46,47,48,49] Metal-Organic frameworks (MOFs) are another major hybrid porous materials with crystalline structures, which are formed by metal cations or clusters connected with organic linkers by coordinating bonds.[50] Their desirable and tunable structures and contents of the walls have enabled various new application such as adsorption and separation materials,[51] sensors, catalysts[52] and so on.

1.2 Zeolites

Zeolites are crystalline microporous inorganic materials constructed from tetrahedrally coordinated $TO_{4/2}$ primary units (where T is a tetrahedral atom such as Si, Al, Zn, and so on).[1] The first observation of zeolite was reported in 1756 by Swedish mineralogist. It named from Greek words “zeo” (to boil) and “lithos” (stone) because it behaved as if boiling in blowpipe flame.[53] Zeolites have been indispensable for several industries as adsorbents, ion-exchangers, and catalysts due to their unique crystalline structures, high (hydro)thermal stability, and several properties arising from their anionic frameworks. A zeolite is defined as an aluminosilicate, and molecular sieves with framework T atoms other than silicon and aluminum are not zeolites in strict speaking.[53] However, it has been widely accepted to call the latter materials also as zeolites, therefore in this dissertation the term ’zeolite’ is used also for various metallosilicates. 234 types of zeolite topologies have been identified, which can be recognized by three-letter framework type codes defined by the Structure Commission of the International Zeolite Association (IZA-SC).[54] The type codes with asterisks (*) and hyphens (-) mean that the topology contains polymorphs and interruptions, respectively.

In this chapter, the largest two classes of the zeolites; aluminosilicates and aluminophosphates, will be mainly described.

Since the first report of synthetic zeolites in 1862,[53] various synthetic version of natural zeolites and synthetic zeolites with no natural analogues, which was first accomplished in 1948,[55] have been synthesized artificially. In the early period, zeolite synthesis was attempted by mimicking geologic conditions with high temperatures (> 200 ^{o}C) and pressures (> 100 bar).[53] Then, in the late 1940s, synthesis of aluminum-rich LTA and FAU zeolites at around 100 ^{o}C and autogenous pressure was achieved using alkali cation and aluminosilicate gels.[56] Those findings enabled the large scale synthesis of zeolites in early 1950s.[53] The use of organic cation (*e.g.* tetramethylammonium for LTA zeolite synthesis[57]) fascinated synthesis of zeolite, especially those with high Si/Al ratio. Synthesis of aluminophosphate was reported in 1982, using acidic or mildly basic conditions and no alkali-metal ions.[58]

The mechanisms of zeolite synthesis are very complex due to the complicated reactions and heterogeneous system. Ostwald's law states that the phase formed first is replaced by a thermodynamically more stable phase until the most stable phase is formed. Zeolites are thermodynamically metastable phases, therefore, formation of zeolites cannot be explained only by the thermodynamics, and kinetics must be considered. Even if a structure is thermodynamically unfavorable, it can be obtained in a condition where the energy barrier for the more thermodynamically stable phase is high enough. It has been reported that careful control of the kinetic factors enables formation of desired zeolite in a certain condition. For example, careful investigation of very early stages of zeolite synthesis in colloidal system enabled synthesis of ultra-small EMT zeolite from template-free colloidal precursors at 30 ºC.[59,60] Multiple stages of zeolite phase transformation have also been reported in aluminosilicate gels and phase changes involving LTA, FAU, GIS, ANA, SOD and CAL depending on synthesis temperature and time was identified.[61] The sequence of stages progressed from low to high density structures (increasing thermodynamic stability), in accordance to the Ostwald's rule.[61]

Two major mechanisms of the zeolite formation have been proposed; the solution-mediated transport mechanism and the solid-phase transformation mechanism.[53] The former involves diffusion of silicate and aluminate species from the liquid phase to the nucleation site (*e.g.* synthesis of MOR zeolite from clear solution[62]). The latter case suggests that the solid hydrogel reorganizes to form zeolite structure (*e.g.* synthesis of FER and MFI zeolite from non-aqueous mixture[63]). It is quite difficult to distinguish the mechanisms except for the extreme cases, and it differs depending on the types of raw materials or other reaction conditions.[64]

In either cases, the zeolite crystallization has been described in the mechanistic pathways, including induction period, nucleation, and crystal growth.[3] Induction period is the time between the starting time of the reaction and the time crystalline product is firstly observed (usually by X-ray diffraction analysis). This period can be divided into three subunits: relaxation time, which is required for the system to establish distribution of silicate and aluminate species by mixing the chemicals and rising reaction

temperature, the time for the formation of a stable nucleus, and the time for the nucleus to grow to a detectable size.[3] In the relaxation time, the non-equilibrium 'primary amorphous phase' is considered to be converted to 'quasi-steady-state phase' or 'secondary amorphous phase', and regarded as very crucial period to determine the activation energy for crystallization process and obtained zeolite.[3,65] In the nucleation period, progressive ordering of the secondary amorphous phase is proceeded by breaking and connecting the T-O-T bonds by hydroxyl ion and related condensation reaction.[3,66] A crucial role in the ordering process is also played by the cations in the synthesis mixtures (*vide infra*). The nucleation step is considered to require high activation energies.[67,68] Finally, in the period of crystal growth, the nuclei increase in size *via* repeated cation mediated addition of silicate units. The activation energy of the crystal growth is considered to be lower than that in the nucleation period.[69]

As mentioned above, cations are not only the source to provide hydroxyl ions for fascinating the reactions, but play a crucial role in the zeolite synthesis as structure-directing agents. Structure-directing effect by the hydrated alkali-metal cations is proposed to involve the ordering of water around the cations with subsequent displacement by silicate and aluminate species to form regions of micro organization, which leads nucleation centers.[53] It was proposed that cation-water complexes stabilize small aluminosilicate anions that are responsible for forming zeolite structures through electrostatic and steric factors.[53,3] Use of cations other than alkali-metal cations has also been studied. For example, alkaline-earth-metal cations Ca^{2+}, Sr^{2+}, and Ba^{2+} produced synthetic counterparts of natural zeolites like harmotone (PHI), however, the relatively low solubilities of these ions (*e.g.* Ca^{2+}) in aqueous media limits the available composition ranges.[53] The scheme of cation-mediated assembly is depicted in Figure 1-1.[3]

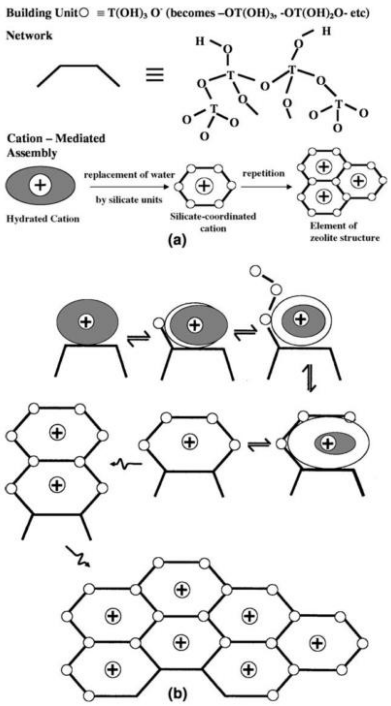

Figure 1-1 The basic mechanism for the cation-mediated assembly of ordered regions: (a) nomenclature and symbolism; (b) details of in-situ construction process by addition of solution units to a surface site.[3]

In addition to the use of inorganic cations, use of various organic structure-directing agents (OSDAs) have greatly broaden the structure and composition of available zeolites.[4,57,70] By the use of OSDAs, high-silica zeolites[71,72] and zeolites with extra-large pores (greater than 12-membered ring)[73,74,75] have been successfully obtained. The structure-directing mechanisms of OSDAs were investigated in the synthesis of pure-silica zeolites and a hydrophobic hydration model have been proposed (Burkett-Davis model, Figure 1-2[76]). In the model, a key step of structure-direction is explained as the replacement of water molecules in the hydration sphere of tetrapropylammonium (TPA) cation by silicate species through favorable overlap of hydration sphere around TPA and hydration domains of silicate to form inorganic-organic composite species.[77] The release of water molecules from the ordered hydrophobic hydration spheres into the bulk and subsequent favorable van der Waals interacts between the TPA and hydrophobic silica provide the entropic and enthalpic driving forces for the composite formation.[76,78,79]

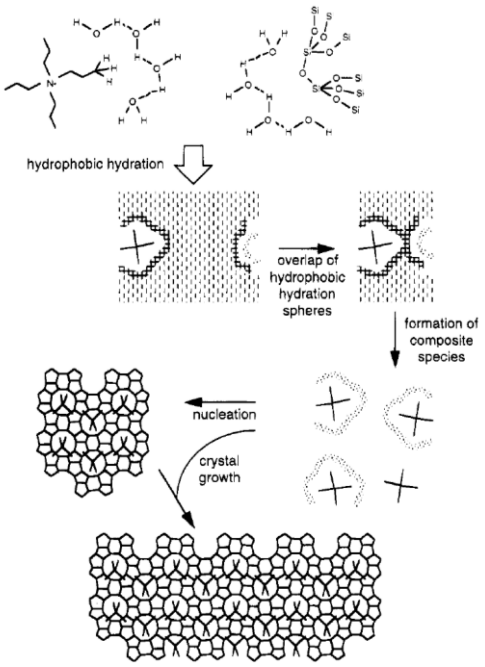

Figure 1-2 Proposed mechanism of structure direction in the TPA-mediated synthesis of pure-silica MFI zeolite (silicalite-1).[76]

Pure silica zeolites which are composed of only SiO_2 do not contain framework charge because silicon is tetravalent. On the other hand, introduction of other elements such as aluminum to zeolite frameworks forms negatively charged oxide frameworks (one negative charge is generated per framework A1(III) atom) that require extra-framework cations. Typical cations in natural zeolites are alkali metals, *e.g.* Na^+, K^+, and alkaline earth metals, *e.g.* Ca^{2+}, Ba^{2+}, and synthetic zeolites contain both inorganic and organic cations, *e.g.* quaternary ammonium ions. Those cations in zeolites can be exchanged by other cations. Therefore, zeolites are used for separation and purification applications (*e.g.* builders in detergent for removal of Ca^{2+} and Mg^{2+},[80] absorbents for capture and storage of radioactive ions[81]). The ion-exchanged metals can act as active sites in various catalytic applications, for example, zeolites exchanged with Cu^{2+} and Fe^{2+} are used as automobile catalysts to remove NO_x.[82,83] Ion-exchange with ammonium ions and subsequent heating to decompose NH_4^+ to NH_3 and H^+ introduce Brønsted acid sites to zeolites. Ultra-stable zeolite Y with those Brønsted acid sites have widely been used in fluid catalytic cracking of heavy petroleum distillates.[84,85]

1.3 Zeolites with Various Heteroatoms

Zeolites with partial substitution of various heteroatoms other than aluminum in their frameworks have been intensively investigated due to their special properties such as new active sites that can catalyze various reactions, depending on the type and environment of the heteroatoms.[86,87]

The properties of metal-substituted zeolites strongly depend on the type of heteroatom, zeolite framework and the synthesis conditions of zeolites. In this section, examples of metallosilicate zeolites and their properties, and several ingenious schemes in synthetic methods to incorporate the metal species to the zeolitic framework is described.

One of the important aspects is that introduction of isolated heteroatoms such as Sn, Ti, and Hf in zeolite frameworks generates isolated Lewis acid sites in zeolites. Shape-selectivity and support-induced stabilization of transition states or intermediates due to the zeolite pores comparable to those of reactant molecules greatly improve the catalytic activities.[88,89,90] Higher acid site stability with lower tendency of thermal sintering into bulk oxides compared to the metal sites on amorphous silicas is also a great advantage.[91] Especially, they have shown remarkable activity in water because of the hydrophobicity of the zeolite can prevent competitive adsorption of water on acid sites.[92,93] The Brønsted acidity of zeolites is also significantly affected by the type and environment of incorporated metals. For example, difference in properties of proton between MFI zeolites with incorporated Al(III), Ga(III) and B(III), respectively has been reported by using ^{1}H MAS NMR.[94]

Crystallization of zeolites under near neutral conditions using fluoride ions (F^-) as mineralizing agents opened the door for the introduction of metal species that are poorly soluble in basic media, such as Ti.[95] Titaniumsilicalite-1 (TS-1) with MFI topology is one of the most prominent Ti containing zeolites which has been utilized as an oxidation catalyst in various chemical processes such as phenol hydroxylation or propylene epoxidation using H_2O_2.[96,97] To increase the Ti content, it has been reported

that harmonizing hydrolysis rates of titanium alkoxide and silicate species with nucleation and crystal growth rates of zeolite is of great importance.[98] Addition of $(NH_4)_2CO_3$ to the synthesis mixture decreased the pH and reduced the crystallization rate, therefore Ti incorporation rate and crystallization rate became comparable, and the Si/Ti ratio was decreased from 58 to 34 without formation of extra-framework Ti species.[98] Titanosilicate zeolites with large pores, such as *BEA and Y zeolites, were firstly achieved by post-synthetic treatment using $TiCl_4$, however, the oxidation activities of those zeolites were poor probably because Ti atoms were not properly incorporated in the frameworks.[97] Titanoaluminosilicate[99,100] and titanosilicate[101] *BEA zeolites were then synthesized in OH^- media based on seeding procedures. They showed high activities in selective oxidation of large molecules with H_2O_2.[100,101] It should be noted that titanosilicate *BEA zeolites prepared in OH^- media had a large number of internal silanol groups since the charge of organic structure directing agent (OSDA), TEA^+, was balanced by SiO^- groups, which yield Si–OH after elimination of TEA^+.[101] Defect free Ti-*BEA can be prepared in F^- media since TEA^+ would be neutralized by F^-.[102,103]

Zeolites with Sn in their frameworks have also been intensively studied because of the good redox and Lewis acid properties. The Sn containing zeolite was first attempted to be synthesized as MFI structure with Si/Sn ratios between 33 and 133.[87,104] Sn was effectively incorporated only when the Si/Sn ratio is higher than 40, otherwise extraframework hexacoordinated species were formed. It was reported that order upon which the silica and Sn sources and the structure-directing agent were added in the synthesis gel strongly affected the crystallinity, particle size and Sn environment (Figure 1-3).[87,105] Large particles with poor crystallinity together with a considerable amount of SnO_2 were formed when $SnCl_4$ was added at last. It was likely because silicon polymerization was advanced when the Sn source was introduced and therefore Sn cannot be fully incorporated into the silicate structure.[87,105]

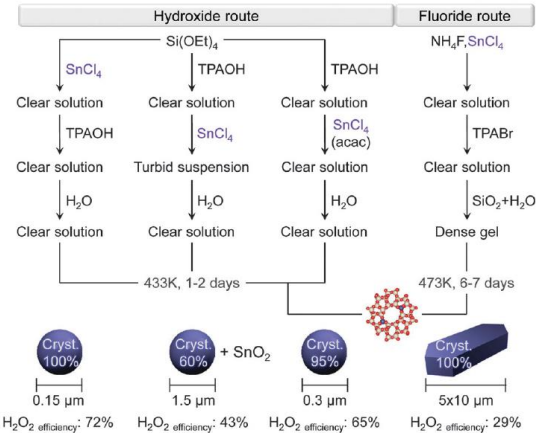

Figure 1-3 Procedures for the preparation of Sn-MFI zeolites and their impact on the morphology, Sn speciation and catalytic activity.[87]

Synthesis of Sn-*BEA was achieved by using dealuminated *BEA seed crystal in OH-media,[106] following the success of pure silica *BEA synthesis by seeding method.[107] It was assumed that *BEA could not nucleate in the absence of trivalent cations such as Al^{3+} or B^{3+}.[108] Sn-*BEA with improved crystallinity was prepared by fluoride mediated procedure with seed crystals and long crystallization time.[90] Increase in the Sn content (0, 1 and 1.8 wt%) led an increase in the crystallization time (4, 7 and 60 days, respectively), and changes in crystal morphology to plates with higher Sn concentrations in the outer shells.[109]

Top-down approaches have also been conducted to introduce various metals in the zeolite frameworks. In the method, a metallosilicate zeolite was treated to generate vacancies in the framework, and insertion of desired metal species is conducted (Figure 1-4(a)). Both gas-phase, such as $TiCl_4$, $AlCl_3$, $GaCl_3$ vapor,[110] and liquid-phase, such as Sn(II) acetate solution,[111] treatments have been successfully applied. Desilication based leaching rather than dealumination has also been found to be a promising method to introduce metals in a one-pot manner (Figure 1-4(b)).[112]

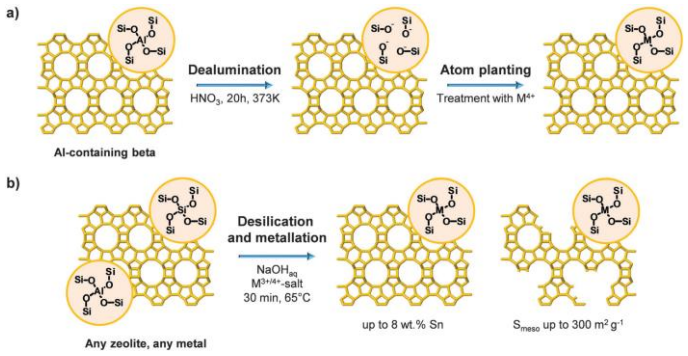

Figure 1-4 (a) Two-step and (b) one-step post-synthetic approaches for the preparation of metal-containing zeolites.[87]

It has been reported that the coordination states of the metal sites in zeolites significantly affect their catalytic activity. For example, isomorphously substituted Sn site connected to four silicon atom (so called closed site) and partially hydrolyzed Sn site (so called open site) in Sn containing zeolites have reported to show different activity (Figure 1-5). It has been reported that the partially hydrolyzed Sn site is more active in catalysis due to the enhanced Lewis acidic property (*e.g.* Sn-MFI for isomerisation of glyoxal and dihydroxyacetone to glycolic and lactic acid[113,112]).[88]

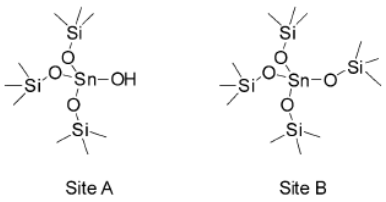

Figure 1-5 Isomorphously substituted (site A) and partially hydrolyzed (site B) tin sites.[88]

As was also mentioned above, the substitution by metal species in zeolite framework have been achieved by selecting appropriate precursors and reaction conditions. In the following sentences, various methods established to broaden available composition of zeolite frameworks (*i.e.* type and amount of incorporated metals) are further described.

Addition of agents to stabilize and mobilize the metal ions in the solution *via*

complexation is effective to prevent hydrolysis of metallic ion species before their incorporation into zeolite crystals.[114] Acetylacetone and oxalic acid was investigated as chelating agents for the preparation of Fe, Co, and Mn containing zeolites.[115,116] Citric acid was also used to form complex with Zn^{2+} species in the synthesis of MOR to prevent formation of oxides or hydroxides of zinc.[117]

Methods to prepare composite of silicon and other metal species prior to hydrothermal treatment have also provided a successful route to various metal-containing zeolites. For example, through acidic hydrolysis and condensation of silica precursors and alkali earth metal (Ae) salt, composite with desirable Si–O–Ae–O–Si linkage was formed.[118] The lower reaction rate allowed more opportunities for isolation and dispersion of metal ions and prompted the bond formation between metal ions and silanol groups.[118] By using the precursor, a direct hydrothermal synthesis of MFI zeolite with Mg, Ca, Sr and Ba was achieved (Figure 1-6).[118] Mechanochemical treatment has also been reported to be an effective method to prepare mixed silica and metal oxides by mechanical forces for the synthesis of metal-containing zeolites. For synthesis of Ti-MFI and Ti-*BEA zeolites, TiO_2 and fumed silica were treated by a planetary ball mill to obtain a composite material of Ti, Si, and O, which was subsequently used in hydrothermal treatment.[119,120] Mn containing MFI zeolite was also prepared by the same strategy.[121]

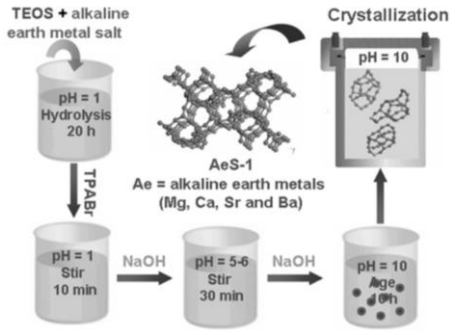

Figure 1-6 Schematic diagram of the synthesis procedure for alkaline-earth metal framework-substituted MFI zeolites.[118]

1.3.1 Zeolites with Zinc

Zinc is a common metal as Lewis acid site both in homogeneous[122,123] and heterogeneous catalysts.[124] Unlike the other first row transition metals (*e.g.*, Mn^{2+}, Fe^{2+}, Co^{2+}, Ni^{2+} and Cu^{2+}), the zinc ion (Zn^{2+}) has a filled *d* orbital (*d10*) and does not catalyze redox reactions but functions as a Lewis acid to accept a pair of electrons.[125] Because of the lack of redox activity, Zn can be considered as a suitable metal for reactions that require a redox-stable site to function as a Lewis acid site, such as proteolysis and the hydration of carbon dioxide.[126] Zn coordination observed most often is a slightly distorted tetrahedral (*e.g.* zinc metalloenzymes), and five-coordinated distorted trigonal bipyramidal geometry.[125] Bulk ZnO has been shown to activate hydrogen, hydocarbons, and olefins through a heterolytic cleavage.[127] The active site has been proposed to be a defect site.[128] By dehydration of two adjacent Zn−OH groups in the defect sites at elevated temperature to evolve H_2O, Zn−O−Zn site was formed, and hydrogen was thought to dissociate on the low coordinate Zn ions, forming Zn−H and a Zn−OH sites.[128] Amorphous silica materials with isolated Zn sites have been reported to be efficient catalysts for alkane dehydration.[124] The dehydrated Zn sites datively coordinate an oxygen of a neighboring silanol.[129]

In the case of zeolite-base catalysts, Zn^{2+} exchanged aluminosilicate zeolites have been used as catalysts for, for example, alkane activation under non-oxidative conditions *via* heterolytic dissociation of the C-H bonds over $Zn^{\delta+}$-$O^{\delta-}$ [130,131] and hydroamination reactions.[132] Those Zn^{2+} cations located in the ion-exchange sites of zeolites have been demonstrated to have very strong interactions with Lewis basic molecules such as acetonitrile and pyridine, with characteristic desorption temperatures higher than those observed in other Lewis acidic zeolites containing Ti, Zr, or Sn.[91,133] For those Zn^{2+} exchanged aluminosilicate zeolites, the Lewis acidic Zn sites are formed together with Brønsted acidic sites generated by unchanged Al sites in the zeolite frameworks, thereby providing bifunctional features suitable for several reactions such as conversion of light alkanes to aromatics.[131,134] Although the bifunctional property is desirable for some reactions, the presence of residual Brønsted acidity sometimes causes undesired side reactions and catalyst deactivation.

Therefore, zincosilicate zeolites with zinc in their frameworks is recently attracting increasing attention because of the strong Lewis acidity with the absence of Brønsted acidity. Based on FT-IR analysis using deuterated acetonitrile as a probe molecule, existence of different zinc sites is suggested (Figure 1-7).[91] CIT-6, a zincosilicate *BEA zeolite, showed high adsorption energies of Lewis basic molecules, and enable reactions previously not possible with Sn-, Ti- and Zr-zeolites, such as Diels–Alder cycloaddition–dehydration reactions of ethylene and dimethyl ester of furan-2,5-dicarboxilic acid to produce dimethyl terephthalate. (Figure 1-8).[91] From computational studies, it was suggested that the Zn incorporation into the zeolite framework is likely not through covalent bonding to framework oxygen atoms but rather through ionic bonding.[135]

Figure 1-7 Proposed framework Zn site structures in zincosilicates. M^+ is a monovalent cation, such as alkali or alkyl ammonium.[91]

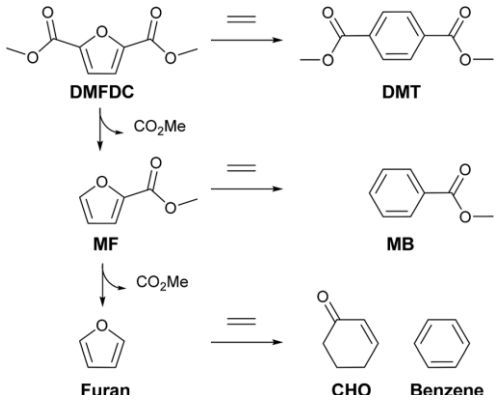

Figure 1-8 Full Diels–Alder cycloaddition–dehydration reaction diagram for dimethyl ester of furan-2,5-dicarboxilic acid as a substrate.[91]

Zincosilicate zeolites have also been focused on because of their features to promote three membered ring (3MR) formation. It have been reported that zeolite

structures built up from small rings, such as 3MR and 4MR, are expected to exhibit low framework density, which will address diffusion limitations in micropore channels.[136] VPI-7 (structure code: VSV) is a first synthetic zincosilicate zeolite with 3MR prepared in the presence of sodium and TEABr (not incorporated into the product) by hydrothermal treatment at 200 ºC for 12 days.[137] VPI-8 (VET) is a high-silica zincosilicate zeolite with unique 12MR pore system with novel 'pinwheel' building unit synthesized by using pore-filling TEA^+ cation and lithium.[138,139,140] VPI-9 (VNI) is prepared in the presence of Rb and composed of two types of layers joined *via* isolated tetrahedra.[141] The Zn atoms in the framework of VNI are all associated with 3MR.[141] Use of Cs gave a zincosilicate analog of analcime (ANA).[142] RUB-17 (RSN) was prepared by using both Na^+ and K^+, and the topology was revealed to have a projection in common with VSV topology with 3MR, 8MR and 9MR.[143] There are no pure-silica or aluminosilicate analogs for the high-zinc-content zincosilicates, VPI-7, VPI-9, VPI-10, and RUB-17. In the high-zinc series of zincosilicate zeolites, the type of inorganic cation is crucial to determine the phases. Zincosilicate analogue of sodalite zeolite (SOD) was prepared using TMA^+ and Na^+ (both as β-cage occupancies with the $(TMA^+ + Na^+)/2Zn$ ratio of almost 1) with Si/Zn = 6–7.[144]

CIT-6 is a zincosilicate analog of zeolite beta, which was first synthesized in 1999 from clear hydrogels containing Li, Zn and tetraethylammonium hydroxide (TEAOH).[145,146]. With longer synthesis time, VPI-8 is nucleated on the surface of CIT-6 crystals, which disappear finally.[147] It has been demonstrated that CIT-6 can be transformed to a pure silicate and subsequently be modified to an aluminosilicate through the insertion of aluminum into locations formerly occupied by zinc.[145]

The crystallization process of zincosilicate zeolites, especially the process of 3MR formation, and position of zinc in the zeolite topology have been investigated. Beryllo- and zincosilicates have reported to form topologies that contain 3MR. 3MRs have small T-O-T angles (130º) that are relatively unstable in pure-silicate or aluminosilicate frameworks.[144] Aluminosilicate zeolite with 3MR is reported to be only ZSM-18, synthesized using a very specific organic template.[148] Some zincosilicate zeolites contain the unit named *lov* (spiro-5) composed of two 3MR rings sharing one

vertex (Figure 1-9 left). The spiro-5 unit has been found in beryllosilicate lovdarite (LOV), with beryllium both in the center and the vertices,[149] and zincosilicate VPI-7 with zinc located at the vertices.[150] zincosilicate RUB-17 also contains spiro-5 unit, but the position of zinc is not known (Figure 1-9).[149] It have been revealed that the 3MR was formed during the induction period prior to other larger units in the crystallization of some zincosilicates such as RUB-17[149] and VPI-7.[151] It was assumed that 3MR formation during the induction period is the key step for the nucleation process of the 3MR containing-zincosilicate zeolites by some methods such as Raman spectroscopies.[149,151] Raman spectroscopies have been useful tool to determine the ring distribution in the product, although it is not always possible because the characteristics of isolated rings are lost when the clusters are embedded in a three-dimensional continuous oxide framework.[142]

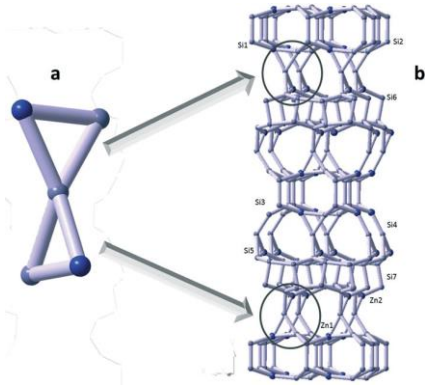

Figure 1-9 Close view of the lov (spiro-5) building unit (a) in the RSN framework (b) [149]

In contrast to the substitution by tetravalent metals (such as Sn(IV) and Ti(IV) shown in the previous section), which do not generate framework charge, substitution by trivalent (such as Al(III)) or divalent (such as Zn(II)) metals to zeolite frameworks forms negatively charged oxide frameworks that require extra-framework cations. The ion-exchange property due to the charged framework is one of the most important properties of zeolites, especially for separation and purification applications.[80,81] In addition, the ion-exchanged metals are effective active sites in various catalytic applications.[82,83] Ion-exchange with ammonium ions and subsequent heating to decompose NH_4^+ to NH_3 and H^+ introduce Brønsted acid sites to zeolites.[84,85] Those

extra framework cations have important roll to modify the properties of zeolites and find new applications. While one negative charge is generated per framework trivalent metal, two negative charges are generated per divalent metals incorporated in the framework in four coordination. Since zinc is a divalent ion, isomorphous substitution of Si(IV) by Zn(II) can generate two negative charges per framework zinc.[152] The two charges per the atom enable divalent cation exchange in 1 by 1 ratio leaving no unpaired charge centers like aluminosilicate zeolites (Figure 1-10).[152] Therefore, zincosilicate zeolites have been considered as an efficient platform for stabilization of extra-framework divalent cations (at ion-exchange sites). Divalent cation-exchanged zeolites such as Cu(II)- and Fe(II)-exchanged zeolites have been found to be promising catalysts for several important reactions, for example, selective catalytic reduction of nitrogen oxides[153] and methane conversion.[154] Also, unexchanged zinc sites are shown to exhibit significantly reduced acidity relative to the aluminum sites.[155] The absence of strong Brønsted acidity provides advantages to reduce side reactions and catalyst deactivation.[152] Catalytic activity of Ni^{2+} exchanged zincosilicate *BEA zeolite (CIT-6) was demonstrated in propylene oligomerization, and it showed higher selectivity into C_{3n} products compared to aluminosilicate *BEA zeolites likely because the reduced Brønsted acidity.[152] CIT-6 with Pt species introduced by ion-exchange method showed high activity in propane degydrogenation.[156] The high negative charge density of zincosilicate VPI-9 also lead high ionic conductivity arising from the charge-balancing cations.[157]

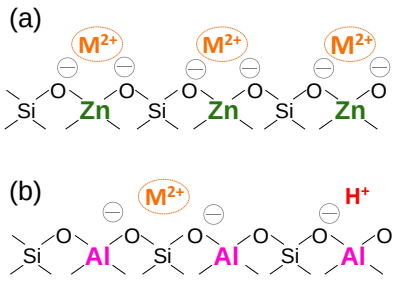

Figure 1-10 Schematic image of ion-exchange sites in (a) zincosilicate and (b) aluminosilicate zeolites.

The attempts to prepare efficient zeolites for divalent ion-exchange have been also conducted by focusing on paired Al sites in aluminosilicate zeolites. The paired Al sites are defined as local Al–O–(Si–O)$_n$–Al sequences (n = 1 or 2) which is close enough to accommodate a divalent cation.[158] The fraction of Al in Al–O–Si–O–Al sequences are generally reported to be low (*e.g.* less than 5% in ZSM-5[159]), therefore, most of Al pairs are considered to be represented by Al–O–(Si–O)$_2$–Al sequences.[158] The ratio of Al in pairs have been hard to calculate by direct experimental method. For example, ^{29}Si MAS NMR can only distinguish Al–O–Si–O–Al sequence. Recently, however, a method to estimate the fractions of Al pairs by using ion-exchanged Co^{2+} ions as probes for the Al pairs have been developed.[158,160] The concentration of Co^{2+} at the individual cationic sites reflects the spatial distribution of Al pairs.[158] By using the method, several synthetic methods have been shown to be effective to increase the ratio of paired Al sites.[161] For example, MFI zeolites prepared with $Al(OH)_3$ or metallic Al were shown to contain higher fractions of paired Al (more than 50%) than that prepared using $AlCl_3$, $Al(NO_3)_3$, Al_2O_3, Al-tri-sec-butoxide (7−33%).[162] On the other hand, ZSM-5 prepared by using different Si sources (tetraethoxyorthosilicate, fumed silica, colloidal silica, sodium silicate) contained similar paired Al fractions.[163] Increase in the amount of Na^+ in the synthetic gel resulted in lower paired Al fractions.[162,164] The presence of anions of decreasing polarization ability (OH^- > Cl^- = PO_4^{3-} > NO) leading to a lower positive charge on the N atom, results in a decreased population of Al pairs.[162] In the synthesis of CHA zeolites, it was reported that the fraction of Al in pairs can be increased by using equimolar amount of Na^+ together with *N*,*N*,*N*-trimethyl-1-adamantylammonium cation ($TMAda^+$). However, the paired Al densities cannot be increased more than that in random Al distribution at most (*e.g.* fraction of Al in pairs is reported to be ca. 17% for CHA with Si/Al = 15).[165]

Taken together, fractions of paired Al can be increased by carefully tuning the synthetic conditions, however, existence of isolated Al cannot be avoided in the synthesis of aluminosilicate zeolites even in the zeolites with high Al contents. Presence of isolated Al is suitable for stabilization of oxo-species of divalent cations, which are sometimes undesired. In addition, isolated Al sites can remain as Brønsted acid sites when counterbalanced by protons and hence cause side reactions and catalyst

deactivation. Therefore, the innate absence of Brønsted acidity and high ion-exchange ability for multivalent cations make zincosilicate zeolites preferable candidates for certain applications compared to existing aluminosilicate zeolites.

The zinc site four coordinated by framework lattice oxygen, so-called "closed" sites, create two negative charges, which is suitable for stabilization of bare divalent metal cations (Figure 1-7). On the other hand, Zn sites which is coordinated with a OH group atoms in the zeolite framework, so called "open" sites, are monocation ion-exchangeable sites and have been considered as active Lewis acid sites.[91] To target the ion-exchange of divalent metals, zincosilicate zeolites rich in the closed zinc sites are preferable because of the two negative charge enable the divalent cation exchange in one by one ratio. On the other hand, for the use as Lewis acid catalysts, zincosilicate zeolites with more open sites would be desirable because of the stronger Lewis acidity[91] and better accessibility to the sites by the reactant molecules. Therefore, the desirable zinc environment differs depending on the targeted use.

As described above, the zinc in zeolite framework can be considered as ion-exchange site or Lewis acid site. On the other hand, the Zn^{2+} cations, which are stabilized as extra framework cations at ion-exchanged site, have also been considered as strong Lewis acid catalysts for, for example, alkane activation under non-oxidative conditions *via* heterolytic dissociation of the C-H bonds over $Zn^{\delta+}$-$O^{\delta-}$ [130,131] and hydroamination reactions.[132] [91,133] In the case of those Zn^{2+} exchanged aluminosilicate zeolites, the Lewis acidic Zn sites are formed together with Brønsted acidic sites generated by unchanged Al sites in the zeolite framework, thereby providing bifunctional features suitable for several reactions such as conversion of light alkanes to aromatics.[131,134] Although the bifunctional property is desirable for some reactions, the presence of residual Brønsted acidity sometimes causes undesired side reactions and catalyst deactivation. Therefore, zincosilicate zeolites with zinc in their frameworks is desirable for certain application which requires strong Lewis acidity in the absence of Brønsted acidity.

1.4 Scope and Overview of This Dissertation

As described above, zinc-containing zeolites possess several unique features that cannot be found in other zeolites, such as, characteristic Lewis acidity and outstanding ion-exchange ability, which make the zinc-containing zeolites promising alternatives in various applications especially catalysis. However, introduction of zinc atoms to zeolite frameworks is difficult due to the different reactivity of zinc species compared to silicon and aluminum, resulting in formation of zinc oxide or hydroxide species out of zeolite frameworks. The longer Zn–O bond length (ca. 2 Å), compared with Si–O (ca. 1.6 Å) also makes the synthesis of zinc-containing zeolites difficult because significant distortion of the frameworks would inhibit the crystallization. These obstacles inhibit broadening available zeolite topologies and content of zinc-containing zeolites, therefore, in spite of the promising characteristics, there have been reported only about 10 framework types of zincosilicate zeolites among 232 zeolite framework types.

The objective of this dissertation is to develop synthesis methods for zinc-containing zeolites in various conditions with a focus on mixing method of raw materials. Figure 1-11 shows the structure of this doctoral dissertation. This dissertation describes the important factors to accomplish zinc introduction to zeolite frameworks in various conditions and aims to broaden available zeolite topologies and content of zinc-containing zeolites. In Chapter 1, a general background of porous materials, especially zeolites, is described. Then, researches about various metal containing zeolites and zinc-containing zeolites are briefly summarized. In Chapter 2, co-precipitation method is demonstrated to be an alternative method to prepare zinco(alumino)silicate gels with highly dispersed zinc species in silicate structures. The homogeneous gel was used for the synthesis of zinc-containing MOR zeolites with the expectation that zinc species already in the silicate structure can react with silicate easily to form zincosilicate zeolite framework. The successful zinc introduction to MOR framework without using any organic substances revealed the importance to prepare the homogeneous gel before hydrothermal treatment. Importance of aluminum species in the synthesis was also suggested. In Chapter 3, applicable scope of the zinc-containing zeolite synthesis using the co-precipitated gels was aimed to be broaden based on

‘composite-building unit (CBU)’ hypothesis, which has been developed as a strategy to achieve OSDA-free synthesis of aluminosilicate zeolites. Based on the hypothesis, *BEA and MFI zeolites which have same CBU as MOR zeolites were selected as target zeolites. By addition of the seed crystals of *BEA and MFI zeolites, synthesis of zinc-containing *BEA and MFI zeolites were achieved in a same manner as the synthesis of MOR zeolites, suggesting the applicability of CBU hypothesis to the synthesis of zinc-containing zeolites. Chapter 4 demonstrated a co-precipitation method conducted in the presence of organic structure-directing agent (OSDA). By the method, zincosilicate gels containing Tetraethylammonium cation (TEA^+) were prepared and used for the synthesis of *BEA zeolites, which have been synthesized by using TEA^+ as an OSDA. Successful introduction of high amount of zinc to zincosilicate *BEA zeolites compared to previous reports suggested that the OSDA containing co-precipitated gels had suitable features for synthesis of zincosilicate zeolites. Chapter 5 presents method to increase homogeneity of zinc and silicate species with a particular focus on mixing method of raw materials in liquid phase. By using the homogeneous mixture, new zincosilicate zeolites with CHA topology were successfully synthesized. The general conclusions of this dissertation and future perspectives for the research are described in Chapter 6.

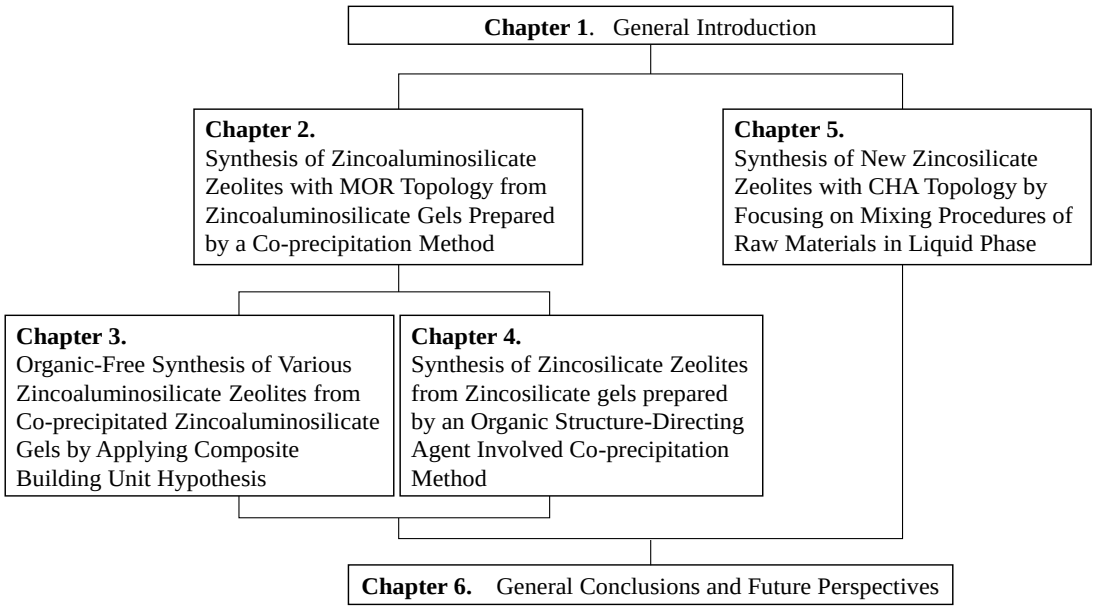

Figure 1-11 Structure of this dissertation

Chapter 2. Synthesis of Zincoaluminosilicate Zeolites with MOR Topology from Zincoaluminosilicate Gels Prepared by a Co-precipitation Method

2.1 Introduction

As described in the previous chapter, zeolites with Zn in the frameworks, zincosilicate zeolites, have recently attracted increasing attention for especially catalytic applications due to their ion-exchange capabilities and Lewis acidity.[91,152] However, there have been several obstacles that prevent zincosilicate zeolites from being used in practical applications. First, incorporation of Zn into zeolite frameworks is difficult due to the longer Zn–O bond length (*ca*. 2 Å), compared with Si–O (*ca*. 1.6 Å). To overcome this problem, Al is incorporated, together with Zn, into the zeolite frameworks, yielding zincoaluminosilicate zeolites.[166] For example, AEI, CHA, and GME zincosilicate zeolites are hardly synthesized but they have been successfully achieved recently as zincoaluminosilicates.[166] In addition, the framework Al can improve (hydro)thermal stability and the obtained zincoaluminosilicate zeolites are described to be more applicable under harsher conditions than zincosilicate counterparts.[166]

The second obstacle is a use of organic structure-directing agents (OSDAs) in synthesis of many zincosilicate zeolites. Among reported zincosilicate zeolites, only VPI-7,[137] VPI-9,[141] and RUB-17,[149] are synthesized without using OSDAs. All of them are present only as zincosilicates *(i.e.,* no pure silica or aluminosilicate analogs) with high contents of Zn. The structures of these 3 zeolites are composed of three-ring (3MR), which is considered to be stabilized by framework Zn.[151] For other zincosilicate zeolites without 3MR, on the other hand, OSDAs are required, for example, *BEA,[145] MFI,[167] MOR,[117] SOD,[144] and VET.[139] The cost of OSDAs is often responsible for most of the total costs of raw materials and thus can inhibit commercialization of zeolites.[168] In addition, calcination is required to remove OSDAs occluded in the pores/cavities of the as-synthesized zeolites, which can hinder the structure integrity of zeolites and the

local environments of Zn. In the absence of OSDAs, another advantage is that zeolites with higher substituting contents of Zn can be obtained because the charge density of alkali metal cations is higher than that of OSDAs, resulting in higher-charged zeolites. In the case of aluminosilicate zeolites, our group has established an OSDA-free synthesis method with the assistance of seed crystals for synthesis of many industrially important aluminosilicate zeolites, including *BEA,[169170] MEL,[169] MTW,[171] and MWW.[172] However, the only successful example for seed-assisted, OSDA-free synthesis of zincosilicate zeolite is VET.[173] It still remains a significant challenge to broaden the types of zinc-containing zeolites that can be synthesized without using any OSDAs.

Similar to other metal-substituted zeolites (*e.g.*, Ti-, Zr-, and Sn-zeolites), another obstacle in synthesis of Zn-zeolites is the precipitation of zinc oxides or hydroxides during hydrothermal treatment. A complex agent is sometimes needed for stabilization of Zn species under alkali conditions of zeolite synthesis and subsequently for successful incorporation of Zn into the zeolite frameworks.[117] The addition of such a complex agent makes zeolite synthesis more complicated and again increases total manufacturing costs of zeolites. Therefore, it is desired to develop a facile synthesis method for zinc-substituted zeolites that can avoid the formation of oxide/hydroxide by-products without using additional organic compounds.

To solve the abovementioned problems, homogeneous zincoaluminosilicate gels, in which both Zn and Al atoms are substituted in silicate matrix, were used as starting materials for synthesis of zincoaluminosilicate zeolites without using any organics. The homogeneous zincoaluminosilicate gels are prepared by co-precipitation of basic silicate solution and acidic solution containing dissolved Zn and Al species.

2.2 Experimental Section

2.2.1 Materials

The following chemicals were used as received for synthesis of zeolites: sodium silicate solution (JIS No.3, Fuji Kagaku CORP), aluminum sulfate solution (Taimei Chemicals

Co., Ltd.), zinc sulfate (Wako Pure Chemical Industries, Ltd.), sodium hydroxide solution (Wako Pure Chemical Industries, Ltd.), sulfuric acid solution (Wako Pure Chemical Industries, Ltd.), fumed silica (Cab-O-Sil M-5, Cabot Co.), sodium aluminate (Wako Pure Chemical Industries, Ltd.), and zinc acetate (Wako Pure Chemical Industries, Ltd.).

2.2.2 Preparation of Zincoaluminosilicate Gels

The zincoaluminosilicate gels were prepared by mixing sodium silicate solution (8.25 wt% SiO_2) and acidic solution of aluminum sulfate and zinc sulfate using peristaltic pumps (Figure 2-1). The mixing and the precipitation were performed in a vessel with an overflow tube under neutral pH at 40 °C. The desired amounts of aluminum sulfate and zinc sulfate used for preparation of gels were calculated with Zn/(Zn+Al) molar ratios of 0.1, 0.2, 0.4, 0.6, 0.8, and 1, while keeping Si/(Zn+Al) at 8.0. The feed ratio of the sodium silicate solution and the sulfate solution was kept at 4:1 (by volume). The averaged residence time of the gel slurry (= vessel volume/total feed rate) was kept at around 15 min, so that the vessel volume and both of the feed rates were optimized. For example, in the typical procedure, 1000 cm^3 of sodium silicate solution and 250 cm^3 sulfate solution was prepared and mixed at the feeding rate of 20 cm^3/min and 5 cm^3/min, respectively. The neutralized suspension containing the zincoaluminosilicate gel was collected and recovered by a centrifugal separator. The gel was thoroughly washed with deionized water. The water content in the gel was measured from a weight loss after calcination at 600 °C for 4 h.

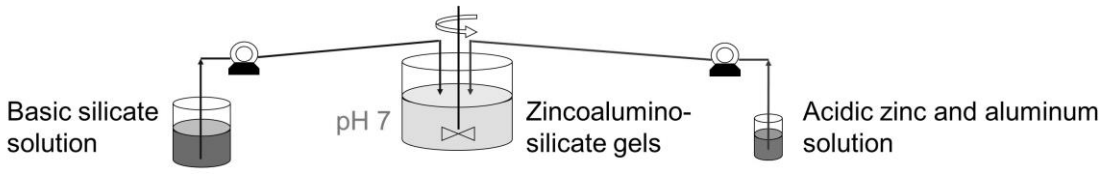

Figure 2-1 Schematic image of the co-precipitation to obtain zincoaluminosilicate gels

2.2.3 Synthesis of MOR Zeolites from Zincoaluminosilicate Gels

Zincoaluminosilicate MOR zeolites were synthesized using the co-precipitated gels. First, seed crystals of MOR zeolite (Tosoh, HSZ-640NAA, Si/Al = 9.0) were dispersed in sodium hydroxide aqueous solution. Then, the zincoaluminosilicate gel was added and mixed vigorously. The chemical compositions of the reaction mixtures (without seed crystals) were 1.84 Na_2O: 0.5(1-*x*) Al_2O_3: *x* ZnO: 8.0 SiO_2: 120 H_2O, where *x* was varied as 0.1, 0.2, 0.4, 0.6, 0.8, and 1. The weight of seed crystals was fixed at 10 wt% (on a basis of SiO_2). The hydrothermal synthesis was carried out in a 60-mL autoclave at 150 °C for 20–96 h under a static condition. After completion, the solid product was recovered by filtration and washed with deionized water until the filtrate reached pH 7–8. The product was dried at 80 °C overnight before subsequent characterizations. A product without Zn was also prepared using aluminosilicate gel in a same manner (*i.e.*, *x* = 0).

For comparison, synthesis of MOR zeolites using conventional sources of Si, Al, and Zn, namely, fumed silica, sodium aluminate, and zinc acetate, respectively, was also carried out. Typically, sodium aluminate and zinc acetate were dissolved in sodium hydroxide aqueous solution. Then, seed MOR crystals were dispersed in the resulting solution. Finally, fumed silica was added and the mixture was stirred vigorously. The resulting homogeneous mixture was transferred to an autoclave and hydrothermal synthesis was conducted similarly as described above.

2.2.4 Characterization

Powder X-ray diffraction (XRD) analysis was conducted to determine the crystal structure of the products using a diffractometer (Rigaku Ultima IV) operated with Cu Kα monochromatized radiation at 40 kV and 40 mA. Elemental analysis of the products was performed by inductively coupled plasma-atomic emission spectrometry (ICP-AES, Thermo iCAP 6300) after dissolving the products in hydrofluoric acid or potassium hydroxide solutions. To observe crystal size and morphology, field-emission scanning electron microscopy (FE-SEM) images were obtained from JFM-7500FA (JEOL) at an accelerating voltage of 15 kV. Nitrogen adsorption–desorption measurements were performed on Quantachrome Autosorb-iQ2-MP at liquid nitrogen temperature. Prior to

the measurements, the samples were degassed at 350 °C for 6 h under vacuum. Diffuse reflectance (DR) UV–vis spectra in the range over 190 nm were recorded on a JASCO V-670 spectrometer in the 190−800 nm wavelength range using barium sulfate as a reference. To obtain UV–vis spectra below 190 nm, a Shimadzu SolidSpec-3700DUV spectrometer was used. FT-IR spectra using pyridine and acetonitrile-d_3 (CD_3CN) as probe molecules were corrected using a JASCO FT-IR 6100 spectrometer equipped with a mercury cadmium telluride (MCT) detector. Spectra in a range of 4000–700 cm^{-1} were acquired with a resolution of 4 cm^{-1}. For the FT-IR measurements, the as-synthesized samples were ion-exchanged with ammonium nitrate to form NH_4-type MOR zeolites. The samples (15–18 mg) were pressed at around 30 MPa for 5 min to form self-standing pellets with diameter of 2 cm. The pellets were placed in a vacuum cell. While evacuating, the samples were heated to 500 ^oC at a heating rate of 10 ^oC/min and held at this temperature for 1 h. Then, the samples were cooled to 80 ^oC and probe molecules, pyridine (Wako Pure Chemical Industries, Ltd.) or CD_3CN (Sigma-Aldrich Co. LLC, 99.8% D atoms) were dosed to the samples until the spectra became unchanged. After collecting the first spectra, the cell was evacuated at 80 ^oC and FT-IR spectra were recorded after 1 h. Then, the cell was heated to 150 ^oC and subsequently to 250 ^oC under vacuum. After holding at each targeted temperature for 1 h (pyridine) or 30 min (CD_3CN), the cell was cooled to 80 ^oC and FT-IR spectra were then recorded. The resulting spectra were subtracted with the spectra obtained at 80 ^oC but without dosing probe molecules. Solid-state magic-angle-spinning (MAS) nuclear magnetic resonance (NMR) experiments were conducted on a JNM-ECA 500 (JEOL). ^{27}Al MAS NMR spectra were recorded at 130.3 MHz with a pulse length ($\pi/2$) of 3.2 μs, a recycle delay of 5 s, and a spinning frequency of 14 kHz. ^{29}Si MAS NMR spectra were recorded at 99.3 MHz with a pulse length ($\pi/2$) of 5.0 μs, a recycle delay of 60 s, and a spinning frequency of 10 kHz. Raman spectroscopy was employed to characterize the ring statistics for the elucidation of the crystallization process. Raman spectra were obtained using a Raman spectrometer (JASCO Corp., NRS-1000) equipped with green laser (532 nm). Raman spectra were recorded over the range 300 and 800 cm^{-1}, and integrated for 30 s at least twice.

2.2.5 Ion-exchange experiments

To characterize local environments of Zn in the obtained zeolites, ion-exchange experiments with Ni(II) was performed. 0.01 M of nickel nitrate aqueous solution was prepared from nickel(II) nitrate hexahydrate (Wako Pure Chemical Industries, Ltd.). pH of the solution was adjusted to 6.0–6.5 by adding a few drops of ammonia aqueous solution (3 wt%). The solid samples (0.3 g) were dispersed in the nickel nitrate solution (100 mL) and then stirred at 500 rpm and room temperature. After stirring for 2 days, the samples were separated from the solution by centrifugation and re-dispersed in 100 mL of fresh nickel nitrate solution. The ion-exchange procedure was repeated for 3 times. Finally, the ion-exchanged products were thoroughly washed with deionized water and dried at 80 °C. The content of Ni was determined by ICP-AES (Thermo iCAP 6300).

For the further investigation of the ion-exchange properties of the obtained MOR zeolites, ion-exchange isotherms describing mono-divalent ion-exchange of Na^+ type MOR with Ni^{2+} was conducted. The isotherms were constructed at 29 ^oC in a bath shaker (AsOne MyBL-100L) using exchange solutions with total concentration of 0.1 mol equiv./L (1 mol equiv. is equals to 1 mol of unit positive charge of cations). The ion-exchange period was determined by the long-time exchange experiments up to 5 days to confirm that the system reached the exchange equilibrium. In every experiment, the isotherm points were obtained by contacting 0.05 g of zeolites with 50 mL solutions. After the equilibration, the zeolites were separated by centrifugation or filtration from the exchange solutions. The separated zeolite samples were washed by deionized water. The chemical compositions of zeolites and ion-exchange solutions were determined by ICP-AES (Thermo iCAP 6300).

2.2.6 Catalytic reactions

The catalytic performances of obtained MOR zeolites in propylene oligomerzation reactions were tested after the ion exchange with Ni^{2+}, in a tubular fixed-bed reactor (quartz, inner diameter of 0.3 cm) at atmospheric pressure. For the measurements, 0.1 g of Ni exchanged aluminosilicate MOR (Zn0 MOR) and zincoaluminosilicate MOR with Zn/(Zn+Al) ratio of 0.4 (Zn0.4 MOR) samples were

introduced to the reactor. Before the activity testing, the catalysts were pretreated in nitrogen flow at 400 ^{o}C for 2 h. After the pretreatment, the temperature was fixed to 200 ^{o}C. Then, a mixture of propylene (0.25 sccm) and nitrogen (1.0 sccm) was supplied to the qualtz tubular reactor. Products were detected by on-line gas chromatography (Shimadzu, GC2014) with a thermal conductivity detector (TCD). The propylene conversion, carbon balance, and product selectivity were calculated as described below, where n_i stands for moles of species *i*.

Conversion of propylene (X_{pro});

$$X_{pro} = \left(\frac{n_{i,total} - n_{propylene}}{n_{i,total}} \right) \times 100\%$$

Carbon balance (CB)

$$CB = \left(\frac{\sum Carbon\,number \times n_i}{3 \times n_{propylene,inlet}} \right) \times 100\%$$

Selectivity to species *i* (S_i)

$$S_i = \left(\frac{n_i}{n_{i,total}} \right) \times 100\%$$

2.3 Results and Discussion

2.3.1 Characterization of Zincoaluminosilicate Gels

The chemical compositions of the co-precipitated zincoaluminosilicate gels are shown in Table 1. The ratios of Zn/(Zn+Al) of the gels were almost identical to the initial ratios of the solutions of zinc sulfate and aluminum sulfate used in the co-precipitation.

As is widely known, tetrahedral Al sites in the silicate frameworks generate one anionic charge per Al atom whereas tetrahedral Zn sites generate two negative charges per zinc atom which is accompanied by a charge-balancing cation in the silicate framework. Recently, however, it has also been reported that Zn in the silicate frameworks can possess a structure that creates only one charge per Zn.[91] As shown in Table 1, the ratios of Na/(Zn+Al) were nearly constant at 1.0–1.1, regardless of the zinc contents, suggesting that both Zn and Al created monocation ion-exchangeable sites (one negative charge per Zn/Al atom) in the zincoaluminosilicate gels. It can also imply that both Zn and Al are highly dispersed in the silicate structures.

To verify the stability of the zincoaluminosilicate gels and the dispersity of zinc

species, the obtained gels were calcined at 800 °C for 8 h in air. DR UV–vis spectra of the calcined gels in comparison to a calcined physical mixture of fumed silica and zinc acetate are shown in Figure 2-2. The physical mixture exhibited an absorption band assigned to ZnO, which is observed at around 360–380 nm due to the $O^{2-} \rightarrow Zn^{2+}$ ligand-to-metal charge transfer transition.[173] On the other hand, in the case of the zincosilicate (Zn/(Zn+Al) = 1.0) and zincoaluminosilicate (Zn/(Zn+Al) = 0.8) gels, the absorption band due to ZnO was not observed in spite of the high zinc content. This suggests that Zn in the gels was stable against the formation of ZnO, providing additional evidence of the high dispersity of Zn in the silicates. The dispersity and the stability against ZnO formation of Zn in the zinco(alumino)silicate gels are highly desirable for the synthesis of zeolites with Zn in the frameworks.

Table 1 Chemical Compositions of the co-precipitated zincoaluminosilicate gels

Initial Zn/(Zn+Al)	Compositions of co-precipitated gels[a]		
	Zn/(Zn+Al)	Si/(Zn+Al)	Na/(Zn+Al)
0	0.00	7.5± 0.01	1.1± 0.00
0.2	0.20 ± 0.005	7.4 ± 0.00	1.1 ± 0.01
0.4	0.39 ± 0.001	7.4 ± 0.01	1.1 ± 0.01
0.6	0.58 ± 0.002	7.3 ± 0.02	1.0 ± 0.01
0.8	0.78± 0.001	7.3 ± 0.01	n.d.[b]
1.0	1.0 ± 0.000	7.3 ± 0.02	n.d.[b]

[a]Determined by ICP-AES. [b]Not determined.

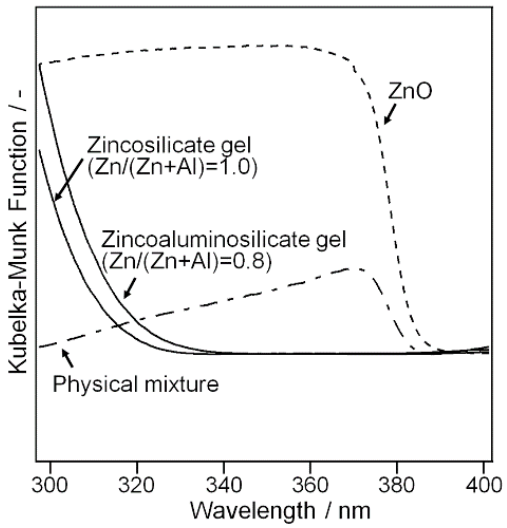

Figure 2-2 DR UV-Vis spectra of zincosilicate gel (Zn/(Zn+Al) = 1.0), zincoaluminosilicate gel (Zn/(Zn+Al) = 0.8), and physical mixture of zinc acetate and fumed silica after calcination at 800 °C for 8 h in air. A spectrum of ZnO is shown for comparison.

To verify the effects co-precipitation conditions toward the formed zincoaluminosilicate gels, feeding rate and temperature of the solutions were varied, respectively. Figure 2-3 shows DR UV-Vis spectra of zincoaluminosilicate gels with Zn/(Zn+Al) of 0.6 prepared at standard condition (40 ^{o}C), 0 ^{o}C and 80 ^{o}C, and physical mixture of zinc acetate and fumed silica after heat treatment at 800 °C for 8 h in air. As described above, the absorption band due to ZnO was not observed in the zincoaluminosilicate gel prepared by the standard condition, while the physical mixture exhibited an absorption band assigned to ZnO. When the co-precipitation was conducted at 0 ^{o}C in the ice bath, the absorption band assigned to ZnO was slightly increased (Figure 2-3(b)). It is likely because the reaction between Zn and Si species was suppressed in the decreased temperature and Zn-O-Zn bonds were formed, which makes the gel unstable against the formation of ZnO. When the temperature was increased to 80 ^{o}C, the clear absorption band due to ZnO was not observed (Figure 2-3(b)), however, an additional band at around 210 nm appeared (Figure 2-3(a)). The assignment of the additional peak is still not clear, but likely assigned to Zn-O-Zn dimers formed due to the enhanced polymerization in the high temperature.

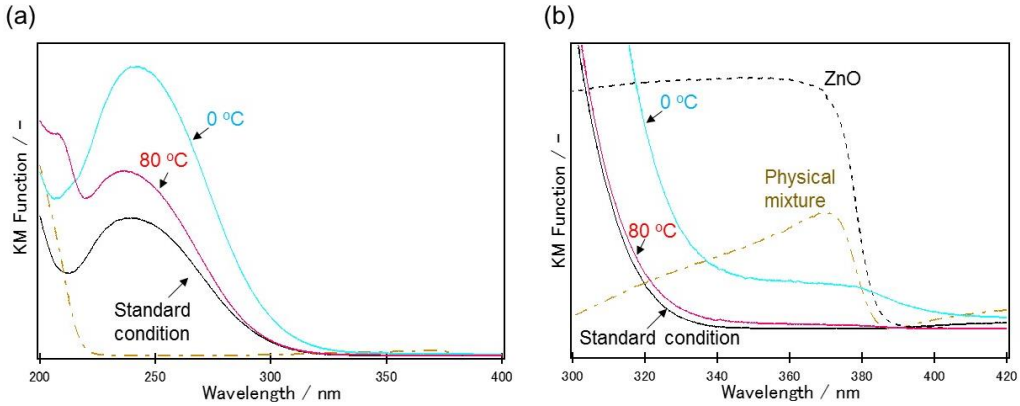

Figure 2-3 DR UV-Vis spectra in the range of (a) 200–400 nm and (b) 300–420 nm of zincoaluminosilicate gels (Zn/(Zn+Al) = 0.6) prepared at standard condition (40 °C), 0 °C and 80 °C, and physical mixture of zinc acetate and fumed silica after calcination at 800 °C for 8 h in air. A spectrum of ZnO is shown for comparison in (b).

In the standard condition, sodium silicate solution and solution of aluminum sulfate and zinc sulfate were mixed by using peristaltic pumps with the feeding rate of 20 mL/min and 5 mL/min, respectively. To see the effect of the mixing condition, the control experiments were conducted as follows; sodium silicate solution was added to the solution of aluminum sulfate and zinc sulfate by peristaltic pumps in the feeding rate of 5 mL/min (Si-5 mL) or 20 mL/min (Si-20 mL). In the other control experiments, the solution of aluminum sulfate and zinc sulfate was added to sodium silicate solution by peristaltic pumps in the feeding rate of 5 mL/min (Zn-5 mL) or 20 mL/min (Zn-20 mL) (Figure 2-4).

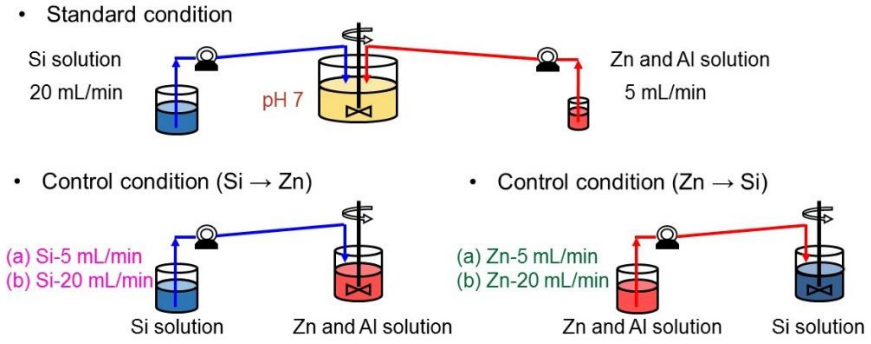

Figure 2-4 Schematic image of the standard condition and control conditions for the co-precipitation to obtain the zincoaluminosilicate gels.

Figure 2-5 shows DR UV-Vis spectra of zincoaluminosilicate gels with Zn/(Zn+Al) of 0.6 prepared at standard condition, control conditions (Si-5 mL, Si-20 mL, Zn-5 mL and Zn-20 mL), and physical mixture of zinc acetate and fumed silica after heat treatment at 800 °C for 8 h in air. In contrast to the zincoaluminosilicate gel prepared by standard condition which shows no absorption band due to ZnO, trace absorption band assigned to ZnO was observed (Figure 2-5 (b)). It is likely because when the one solution was added to the other solution, the formed gel is expected to have less homogeneity than the gels prepared by the standard solution. Formation of Zn-rich part may result in the ZnO formation after the heat treatment. The absorption band assigned to ZnO is more intense in the gels formed in the conditions of Si-5 mL and Zn-5 mL, compared to that formed in the conditions of Si-20 mL and Zn-20 mL. In the control experiments, when the feeding of solutions proceeded, gelation occurred in the middle of the experiments. With the feeding rate of 5 mL, larger amount of solutions were added after the gelation compared to the case with feeding rate of 20 mL. Therefore, the polymerization was expected to be advanced when the additional solution was introduced and Zn and Si species cannot be fully mixed to form the zincosilicate structure

From these results, the co-precipitation conditions are shown to have a considerable effect to realize high dispersity of Zn in the silicates.

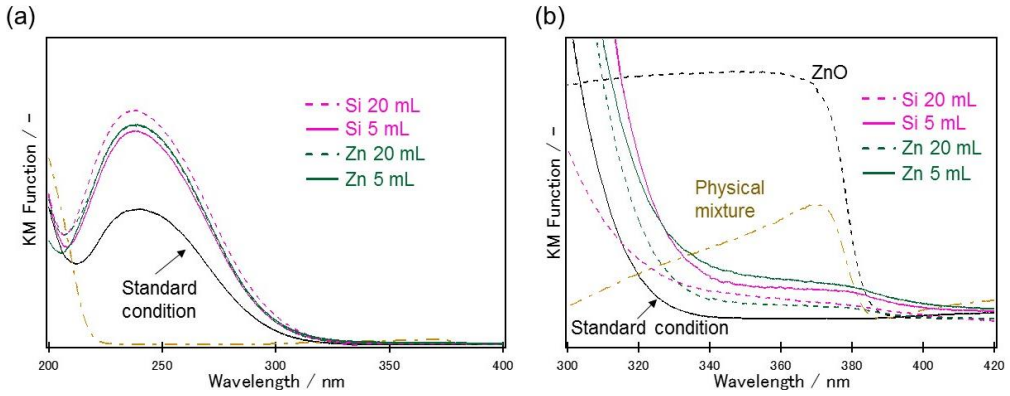

Figure 2-5 DR UV-Vis spectra in the range of (a) 200–400 nm and (b) 300–420 nm of zincoaluminosilicate gels (Zn/(Zn+Al) = 0.6) prepared at standard condition, Si 20 mL, Si 5 mL, Zn 20 mL and Zn 5 mL, and physical mixture of zinc acetate and fumed silica after calcination at 800 °C for 8 h in air. A spectrum of ZnO is shown for comparison in (b).

2.3.2 Synthesis of MOR Zeolites from the Zincoaluminosilicate Gels

Powder XRD patterns of the products obtained from the zincoaluminosilicate gels with different Zn/(Zn+Al) ratios after hydrothermal synthesis at 150 °C for 72 h are shown in Figure 2-6. In spite of the high contents of Zn, no peaks from impurities such as ZnO (2θ = 31.6, 34.2, and 36.1) were observed, indicating that the formation of Zn–O–Zn bonds and subsequent ZnO formation can be avoided under the present synthesis conditions. The absence of ZnO species was also supported by UV-vis spectroscopic measurements (*vide infra*). MOR zeolites were obtained when the gels with Zn/(Zn+Al) of 0, 0.1, 0.2, 0.4, and 0.6 were used. Hereafter, the MOR samples prepared using the gels with Zn/(Zn+Al) of *x* are denoted as Zn*x* MOR.

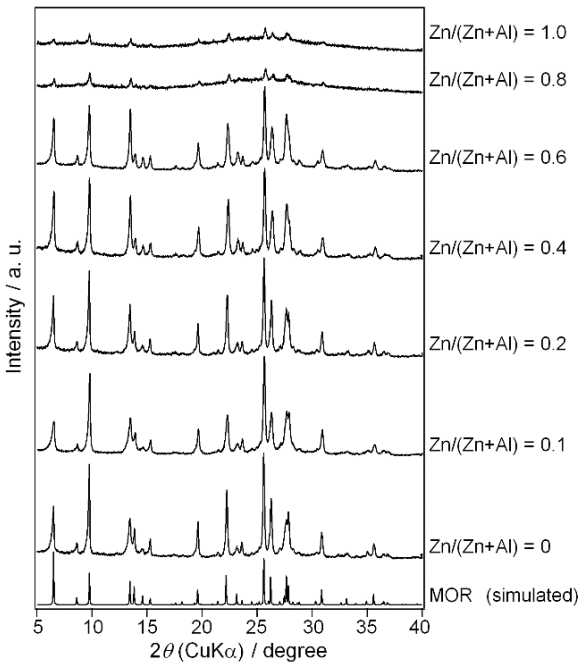

Figure 2-6 Powder XRD patterns of products synthesized from co-precipitated gels with Zn/(Zn+Al) of 0, 0.1, 0.2, 0.4, 0.6, 0.8, and 1.0 at 150 °C for 72 h. Peaks seen in products of Zn/(Zn+Al) = 0.8 and 1.0 are due to seed crystals.

Figure 2-7 shows powder XRD patterns of the products collected after hydrothermal treatment for different periods of time with the crystallization curves plotted in Figure 2-8. The crystallinity was calculated from the total areas of XRD peaks at around 19.7°, 22.4°, 25.8°, and 26.4°. It was clear that the synthesis time increased as

the Zn contents were increased. When the gels with Zn/(Zn+Al) of 0.8 and 1.0 were used, however, no any zeolite products were observed (See Figure 2-6). Note that XRD peaks seen in the products when Zn/(Zn+Al) was 0.8 and 1.0 are ascribed to the MOR seed crystals because the similar patterns were also observed in the samples before the hydrothermal treatment (see Figure 2-7). The necessity of Al is probably because the longer bond length of Zn–O (ca. 2 Å) compared with Si–O (1.58–1.64 Å) and Al–O (1.70–1.73 Å) can cause significant distortions of the zeolite framework and inhibit the formation of MOR zeolite. The presence of Al in the framework is thus considered to stabilize the framework, resulting in zincoaluminosilicate zeolites.

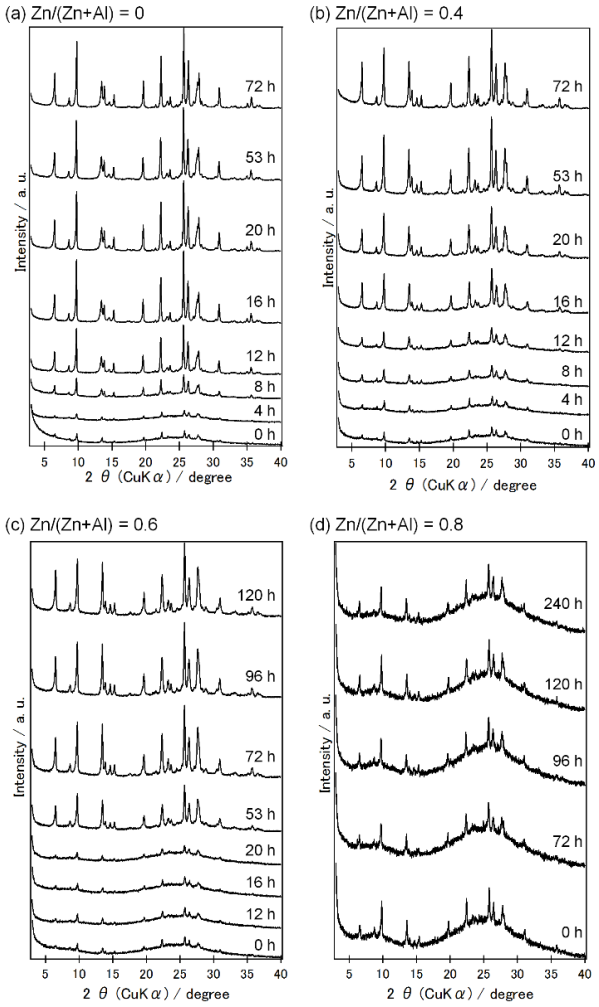

Figure 2-7 Powder XRD patterns of products synthesized for different periods of time from co-precipitated gels with Zn/(Zn+Al) of (a) 0, (b) 0.4, (c) 0.6, and (d) 0.8.

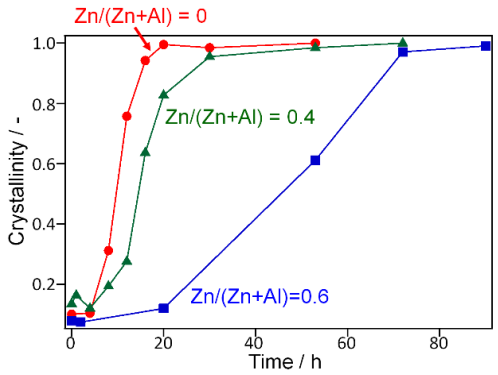

Figure 2-8 Crystallization curves of products synthesized from co-precipitated gels with Zn/(Zn+Al) of 0, 0.4, and 0.6. The crystallinity was calculated from the total areas of XRD peaks at around 19.7°, 22.4°, 25.8°, and 26.4°.

Raman spectra of the zincosilicate samples obtained after different time of hydrothermal treatment is shown in Figure 2-9. It has been reported that bands in the 200-600 cm^{-1} region are sensitive to the T-O-T bond angle and the size of the ring in the framework. Previous Raman investigations on zeolite have assigned bands at ca. 370-430 cm^{-1} to 5MR, ca. 470-530 cm^{-1} to 4MR, and 550-600 cm^{-1} to 3MR. When zincoaluminosilicate gels with Zn/(Zn+Al) of 0, 0.4 and 0.6 were used, intensity of bands attributed to 5MR and 4MR increases with crystallization of MOR zeolite progresses (Figure 2-9 (a)–(c)). On the other hand, when zincoaluminosilicate gels with Zn/(Zn+Al) = 0.8 were used, remarkable changes in the ring distribution was not observed (Figure 2-9 (d)). After 120 hours of hydrothermal treatment, a band close to 3MR region was observed. The 3MR formation is likely induced due to the high content of zinc.[151]

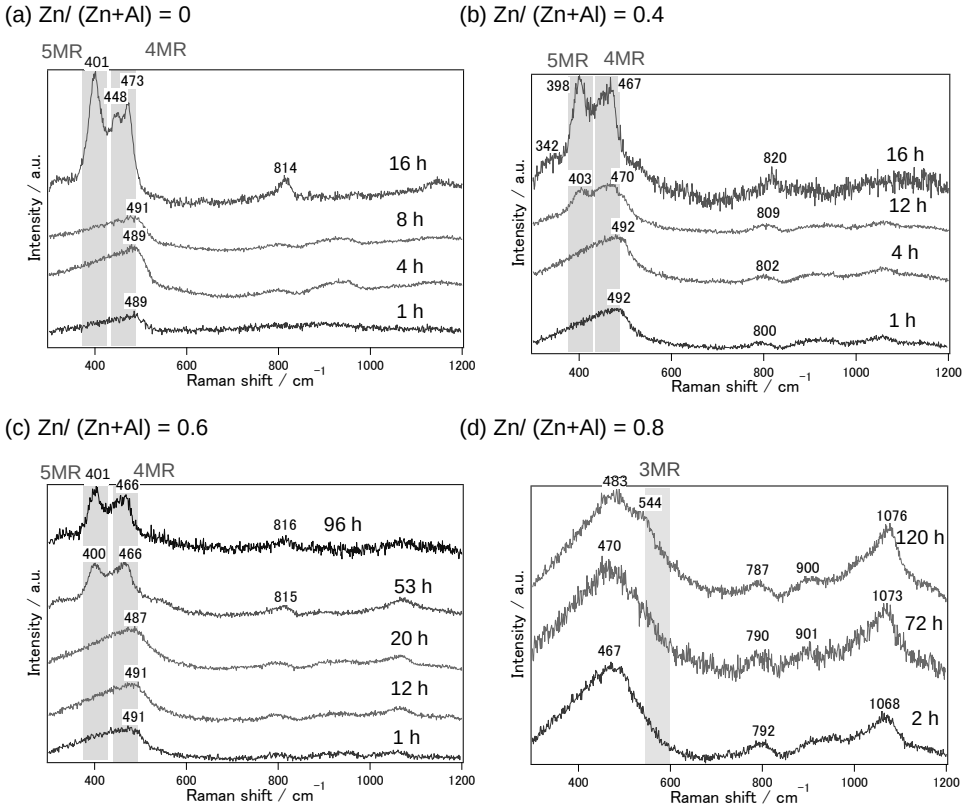

Figure 2-9 Raman spectra of the samples synthesized for different periods of time from co-precipitated gels with Zn/(Zn+Al) of (a) 0, (b) 0.4, (c) 0.6, and (d) 0.8.

Figure 2-10 shows powder XRD patterns of the products synthesized from co-precipitated gels with Zn/(Zn+Al) of 0.1 and 0.6 at 150 °C for varied time with and without MOR seed crystals. Obviously, the crystallization of zincoaluminosilicate MOR zeolites proceeded without using the seed crystals. However, when the XRD patterns of the products were compared with that obtained with seed crystals, the speed of crystallization was quite slow. By using the zincoaluminosilicate gel with Zn/(Zn+Al) of 0.1, crystallinity of MOR zeolite obtained after 19 days was lower than that obtained with seed crystals after 72 hours of hydrothermal treatment. The crystallization of MOR was almost completed after 28 days. On the other hand, with Zn/(Zn+Al) of 0.6, the crystallinity of MOR product was lower than that obtained with seed crystals after 72 hour of hydrothermal treatment even after 28 days. From these results, it

is suggested that nucleation of zincoaluminosilicate MOR zeolites from the zincoaluminosilicate is possible without seed, but the crystallization time is significantly increased. The increase in the crystallization time with the increase of the metal content have been reported for many metallosilicate zeolites.[109]

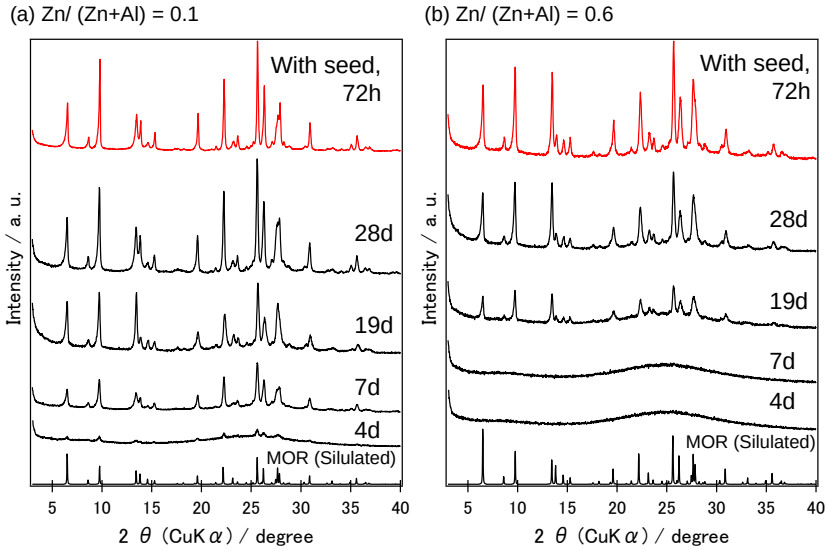

Figure 2-10 Powder XRD patterns of products synthesized from co-precipitated gels with Zn/(Zn+Al) of (a) 0.1 and (b) 0.6 at 150 °C for varied time with and without MOR seed crystals. The XRD pattern of the product without annotation was obtained without using seed crystals.

Chemical compositions of the MOR zeolites obtained with seed crystals analyzed by ICP-AES are summarized in Table 2. The molar Zn/(Zn+Al) ratios of the zeolite products were almost the same as those of the initial zincoaluminosilicate gels. It was also confirmed that the obtained MOR zeolites had high micropore volumes. For the Zn0.4 MOR and Zn0.6 MOR products, nitrogen uptakes were very small in their as-synthesized, Na-form (V_{micro} < 0.1 cm^3/g). However, the proton-forms of Zn0.4 MOR and Zn0.6 MOR showed reasonably high micropore volumes. The decreases in micropore volumes of the Na-form samples with increasing Zn contents are presumably because of the increasing contents of Na^+ cations that fill and/or block the zeolite cavities and the heavier weights of Zn compared to Al. Similar observation was also reported for Rb-MOR.[175]

Table 2 Chemical compositions, solid yields, and micropore volumes of the MOR products

Sample	Initial	Compositions of products[a]				Yield	V_{micro}
	Zn/(Zn+Al)	Zn/(Zn+Al)	Si/(Zn+Al)	Si/Zn	Si/Al	(%)	(cm^3/g)[b]
Zn0 MOR[c]	0	0.00	5.22± 0.002	∞	5.3± 0.01	71	0.15[d]
Zn0.1 MOR[c]	0.1	0.09 ± 0.004	5.32 ± 0.015	66.5 ± 3.15	5.8 ± 0.01	72	0.14[d]
Zn0.2 MOR[c]	0.2	0.19 ± 0.001	5.37 ± 0.018	28.8 ± 0.11	6.6 ± 0.02	69	0.14[d]
Zn0.4 MOR[c]	0.4	0.39 ± 0.002	5.93 ± 0.017	14.9 ± 0.11	9.9 ± 0.02	75	0.13[e]
Zn0.6 MOR[c]	0.6	0.58 ± 0.001	6.34 ± 0.004	10.9 ± 0.01	15.2 ± 0.04	79	0.12[e]
Zn0.4 MOR (control)[f]	0.4	0.055 ± 0.004	4.81± 0.007	88.3 ± 5.54	5.10± 0.016	51	n.d.[g]
Zn0.6 MOR (control)[f]	0.6	0.48 ± 0.018	6.08 ± 0.206	12.7 ± 0.19	11.7 ± 0.04	82	n.d.[g]

[a]Determined by ICP-AES. [b]Micropore volumes determined by a *t*-plot method. [c]Synthesized from the co-precipitated gels. [d]Calculated from as-synthesized, Na-form MOR products. [e]Calculated from H-form MOR products prepared by ion-exchange of as-synthesized products with ammonium nitrate aqueous solution and subsequent calcination. [f]Controlled samples synthesized using fumed silica, sodium aluminate, and zinc acetate. [g]Not determined.

For comparison, synthesis of MOR zeolites was conducted using conventional raw materials, that is, fumed silica, sodium aluminate, and zinc acetate, while keeping other conditions the same as in the cases of the zincoaluminosilicate gels described above. As shown in Figure 2-11, XRD patterns of the products obtained at Zn/(Zn+Al) = 0.4 and 0.6 indicate the formation of MOR zeolite. In the sample synthesized with Zn/(Zn+Al) of 0.4, however, the content of Zn was significantly lower than that of the reaction mixture (Zn0.4 MOR (control) in Table 2). At Zn/(Zn+Al) of 0.6, on the contrary, the product prepared using conventional raw materials possessed the Zn content (Zn0.6 MOR (control) in Table 2, Zn/(Zn+Al) = 0.48) slightly lower than that found in the product obtained from the zincoaluminosilicate gels (Zn/(Zn+Al) = 0.58) but the crystallinity of the Zn0.6 MOR (control) sample was lower than Zn0.6 MOR. In addition, the formation of ZnO in the Zn0.6 MOR (control) sample was confirmed by

UV-vis measurement but was not observed in the Zn0.6 MOR sample (Figure 2-12). This is probably because the high concentration of Zn species in the reaction mixture caused the ZnO formation. These results suggest that MOR zeolites with high contents of Zn incorporated in the zeolite framework cannot be obtained using conventional Si and Zn sources in the absence of organics, which is consistent with the previous report[117] that the formation of zincosilicate MOR zeolites is not favored in the absence of additional organics capable of forming the complex with Zn to decrease the concentration of "free" Zn species in the basic solution. It is also indicated that the zincoaluminosilicate gels prepared *via* co-precipitation are suitable precursors for the synthesis of MOR zeolites with framework Zn even without any organic compounds.

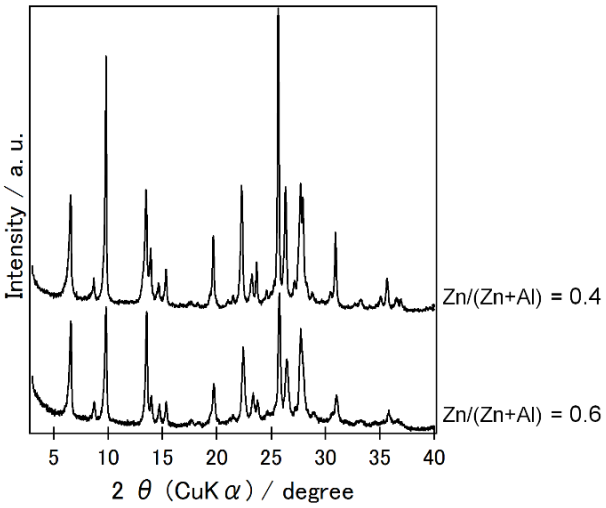

Figure 2-11 Powder XRD patterns of products synthesized using fumed silica, sodium aluminate, and zinc acetate at Zn/(Zn+Al) of 0.4 and 0.6.

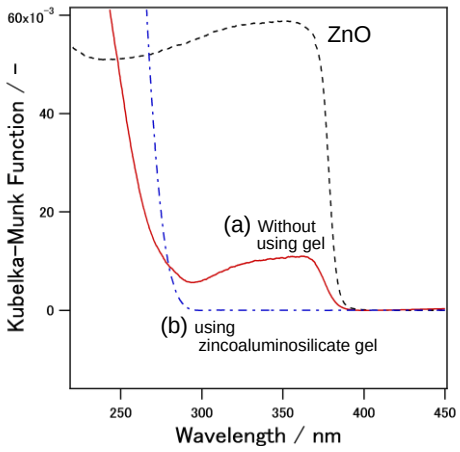

Figure 2-12 DR UV-vis spectra of products synthesized at Zn/(Zn+Al) of 0.6 using (a) conventional raw materials (fumed silica, sodium aluminate, and zinc acetate) and (b) co-precipitated zincoaluminosilicate gel.

FE-SEM images of the obtained MOR zeolites are shown in Figure 2-13. The MOR zeolite crystals were aggregates/intergrowths of primary nanosized crystals, which have needle-like morphology. The sizes of these needle-like primary nanosized crystals became smaller as the contents of Zn were increased (Figure 2-14). The secondary particles were with the diameters of 1–5 μm. With increasing the Zn contents, the secondary particles became more angular. Interestingly, the secondary particles of zeolites with Zn contained some macroporous cavities observed from the outside (the jar-like structure). The large hysteresis loops observed in the nitrogen adsorption–desorption isotherms of zincoaluminosilicate MOR zeolites (Figure 2-15) suggest that there existed macro- and/or mesopores inside the zeolite particles.[12]

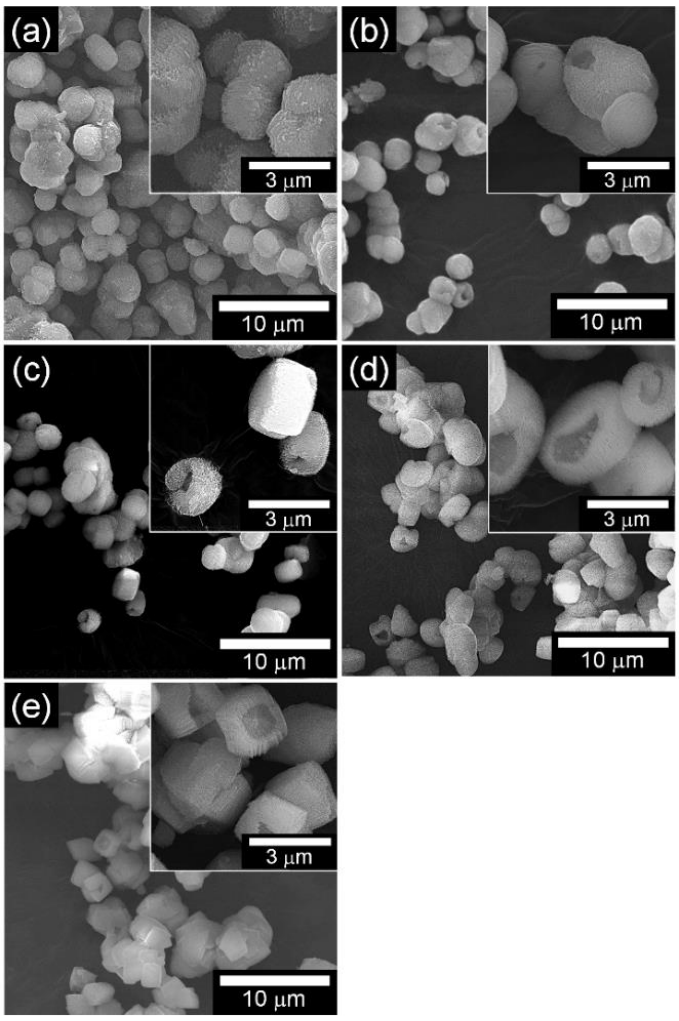

Figure 2-13 FE-SEM images of MOR zeolites prepared from co-precipitated gels with Zn/(Zn+Al) of (a) 0, (b) 0.1, (c) 0.2, (d) 0.4, and (e) 0.6.

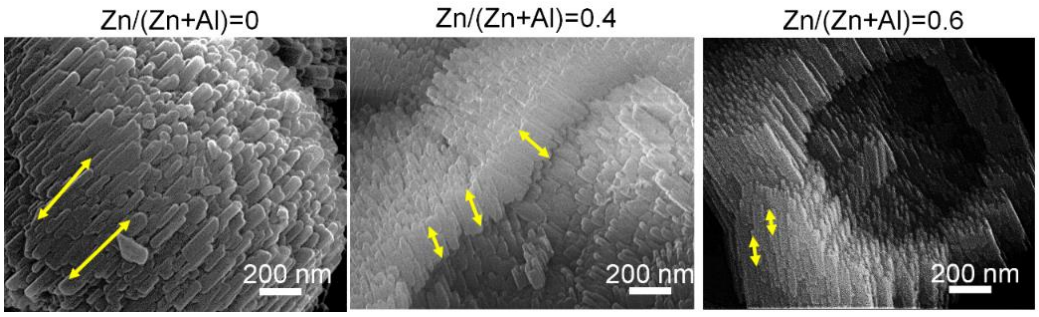

Figure 2-14 FE-SEM images of products synthesized from co-precipitated gels with Zn/(Zn+Al) of 0, 0.4, and 0.6.

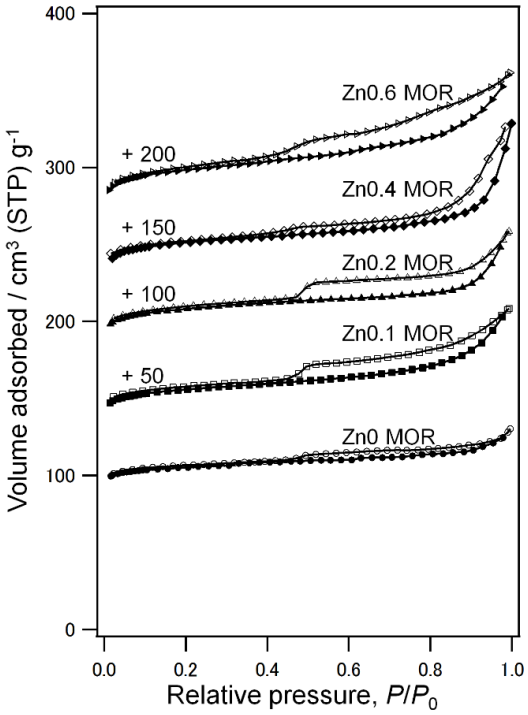

Figure 2-15 Nitrogen adsorption–desorption isotherms of Zn0 MOR, Zn0.1 MOR, Zn0.2 MOR, Zn0.4 MOR, and Zn0.6 MOR. The isotherms of Zn0.4 MOR and Zn0.6 MOR were obtained after ion-exchange with NH_4NO_3 and subsequent calcination.

To give some insights into the formation process, time course changes in the morphology of the products prepared from the zincoaluminosilicate gels with Zn/(Zn+Al) of 0.4 was observed. Time-evolved FE-SEM images of Zn0.4 MOR are shown in Figure 2-16, revealing that the zincoaluminosilicate gel had porous structures from the initial stage of the hydrothermal treatments, which may correspond to the macroporous cavities observed in the final Zn0.4 MOR product (Figure 2-13 (d)). By prolonging the treatment time, small primary crystals were observed with the retained macroporous jar-like structures, reflecting the relation between the macroporous cavities of the initial gel and the final zeolite product. This phenomenon may be considered as a type of pseudomorphic conversion of the amorphous zincoaluminosilicate gels into the crystalline zincoaluminosilicate zeolites without complete migration of the initial components into the solution phase. For the pseudomorphic conversion, slow hydrolysis (dissolution) of the initial gels and crystallization of zeolites are likely important because zeolites can be crystallized while retaining the initial morphology. In this case,

slower crystallization induced by Zn (Figure 2-8) is a key for the formation of MOR zeolites with the jar-like macroporous cavities.

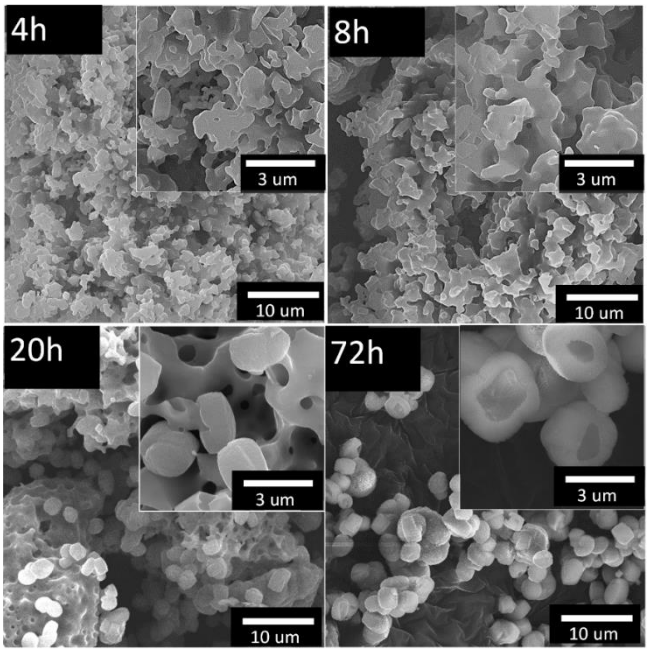

Figure 2-16 FE-SEM images of products synthesized from co-precipitated gels with Zn/(Zn+Al) of 0.4 at 150 °C for 4, 8, 20, and 72 h.

Solid-state ^{27}Al MAS NMR measurements were conducted to investigate the local environments of Al species in the zincoaluminosilicate gels and the obtained MOR zeolites. As shown in Figure 2-17, no octahedrally coordinated Al species, generally appearing at a chemical shift (δ) of ca. 0 ppm, were observed both in the zincoaluminosilicate gels and in the obtained MOR zeolites. In all samples, only one resonance at δ = 54.2–54.7 ppm, corresponding to tetrahedrally coordinated Al, was observed. This suggests that during the co-precipitation, all Al species reacted with silicates and were incorporated into the amorphous silicate structures in a four-coordination. One may further postulate that Zn species also reacted with silicates in the similar manner to Al species because both Zn and Al were dissolved and homogeneously mixed in the same acidic aqueous solution. ^{27}Al MAS NMR spectra of the MOR zeolites became sharper and slightly shifted from 54.2 ppm observed in the gels to 54.7 ppm, suggesting that the local environments of zincoaluminosilicate

became more ordered and the average Al–O–Si bond angles were almost unchanged during the formation of MOR zeolites.[176]

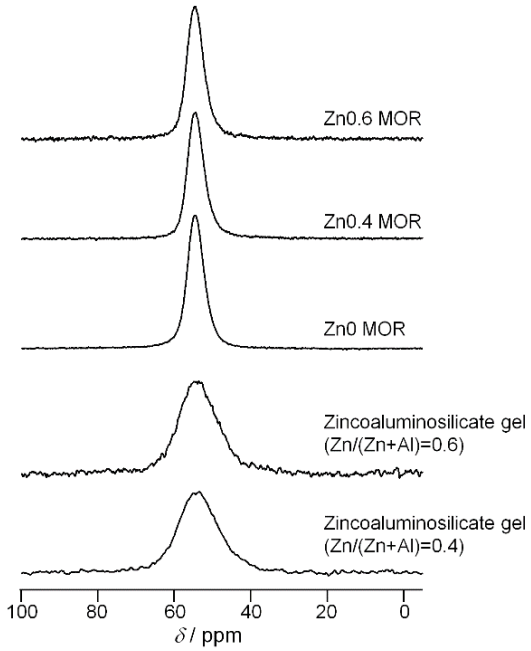

Figure 2-17 Solid-state ^{27}Al MAS NMR spectra of zincoaluminosilicate gels with Zn/(Zn+Al) of 0.4 and 0.6, and MOR zeolites obtained from gels with of Zn/(Zn+Al) of 0, 0.4, and 0.6 (i.e., Zn0 MOR, Zn0.4 MOR, and Zn0.6 MOR).

Figure 2-18 shows solid-state ^{29}Si MAS NMR spectra of Zn0 MOR, Zn0.4 MOR, and Zn0.6 MOR. The spectra were deconvoluted to three signals attributed to Q^4(0T) silicon species ($Si(OSi)_4$) at δ around −110 ppm, Q^4(1T) silicon species ($Si(OT)(OSi)_3$) at δ of ca. −105 ppm, and Q^4(2T) silicon species ($Si(OT)_2(OSi)_2$) at δ of ca. −98 ppm, where T stands for substituted Zn or Al atoms. It has been reported that chemical shift for silicon environments derived from adjacent Zn is larger than that derived from adjacent Al. Ranges of chemical shifts for Si(1Zn) and Si(2Zn) species in tectozincosilicates are reported to be from -85 ppm to -105 ppm and from -75 ppm to -85 ppm, respectively. However, in zincoaluminosilicate case, it has been difficult to distinguish Q^4(1Zn) and Q^4(1Al). Therefore, the peak shifts derived from substituted Zn and Al are calculated together here. The broader peak in low shift range is probably due to contribution from Zn species. Si/(Zn+Al) ratio was calculated for each samples from the peak areas of the

three peaks using following formula.

$$\left(\frac{\mathrm{Si}}{\mathrm{T}}\right)\mathrm{NMR} = \sum_{n=0}^{4} I_{\mathrm{Si}(n\mathrm{T})} \Big/ \sum_{n=0}^{4} \left(\frac{n}{4}\right) I_{\mathrm{Si}(n\mathrm{T})}$$

The Si/(Zn+Al) ratios calculated from the ^{29}Si MAS NMR spectra for Zn0 MOR, Zn0.4 MOR, and Zn0.6 MOR were 5.2, 5.7, and 5.5, respectively, which are close to the ratios obtained by ICP-AES analysis. The concurrence of the chemical compositions calculated from ^{29}Si MAS NMR and ICP-AES results suggests the successful incorporation of Zn and Al atoms into the zeolite frameworks. The zincoaluminosilicate MOR zeolites (*i.e.*, Zn0.4 MOR and Zn0.6 MOR) exhibited slightly smaller Si/(Zn+Al) ratios calculated from NMR spectra compared to those of ICP-AES results, likely indicating the presence of some silanol defects in the zeolites.

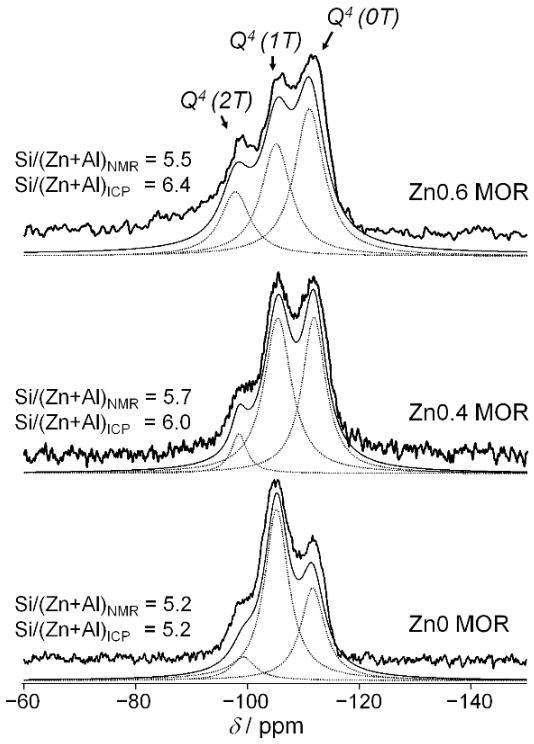

Figure 2-18 Solid-state ^{29}Si MAS NMR spectra and their peak deconvolution of MOR zeolites obtained from gels with of Zn/(Zn+Al) of 0, 0.4, and 0.6 (i.e., Zn0 MOR, Zn0.4 MOR, and Zn0.6 MOR).

2.3.3 Environments of Zn in the Zincoaluminosilicate MOR Zeolites

To analyze zinc coordination states in the obtained MOR zeolites, UV-vis spectra including a deep UV region were measured as depicted in Figure 2-19. For comparison, a Zn^{2+}-exchanged sample was also prepared by ion-exchange of the aluminosilicate MOR seed crystals with 1 M zinc nitrate aqueous solution. The spectra of Na- and H-type aluminosilicate MOR zeolites are also shown in Figure 2-19 (c) and Figure 2-19 (e), respectively. An absorption band due to ZnO, typically appearing at around 360 nm, was not observed for all Zn-containing zeolites. The Zn0.4 MOR and Zn0.6 MOR samples showed absorption bands below 200 nm and at 200–280 nm. Comparing with the spectrum of the Zn^{2+}-exchanged aluminosilicate MOR zeolite (Fig. 6 (d)), the absorption band below 200 nm can be assigned to the charge transfer transitions of framework Zn with lattice O^{2-}. All samples except for H-type aluminosilicate MOR showed the broad absorption bands at 200–280 nm, which is presumable arisen from extra-framework Zn^{2+} and Na^{+} present at ion-exchange sites.

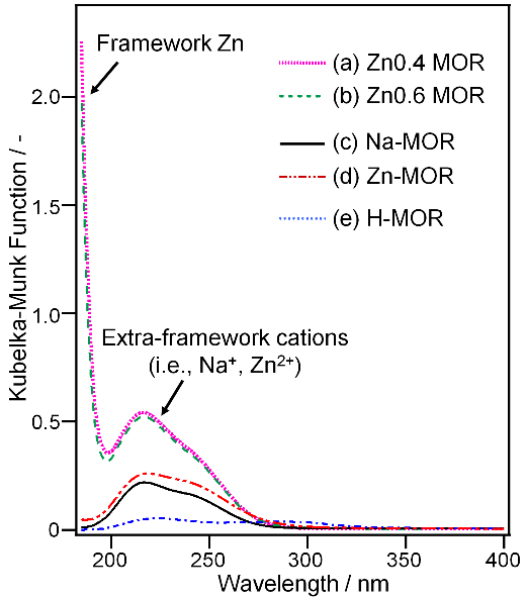

Figure 2-19 Deep UV spectra of (a) Zn0.4 MOR, (b) Zn0.6 MOR, (c) Na-type aluminosilicate MOR zeolite (used as seed crystal), (d) Zn^{2+}-exchanged aluminosilicate MOR zeolite, and (e) H-type aluminosilicate MOR zeolite (Tosoh, HSZ-640HOA).

Stability of the MOR prepared using zincoaluminosilicate gels against thermal treatment was tested by calcination at 400 ºC and 600 ºC for 10 h. It was confirmed that crystallinity of MOR zeolites prepared using zincoaluminosilicate gels (Zn0.4 MOR and Zn0.6 MOR) were decreased by the thermal treatment especially for Zn0.6 MOR (Figure 2-20). The MOR samples after the thermal treatment exhibited broad shoulder around 250 nm in UV-vis spectra (Figure 2-21). As is the case of Zn^{2+} exchanged MOR sample, this adsorption band around 250 nm may come from extraframework Zn species. It is suggested that, as Zn species in the zeolite framework are not thermally stable as Al in the framework, they come out from the tetrahedral position in the framework by the thermal treatment. This stability change can also be one indication of Zn incorporation in the zeolite framework.

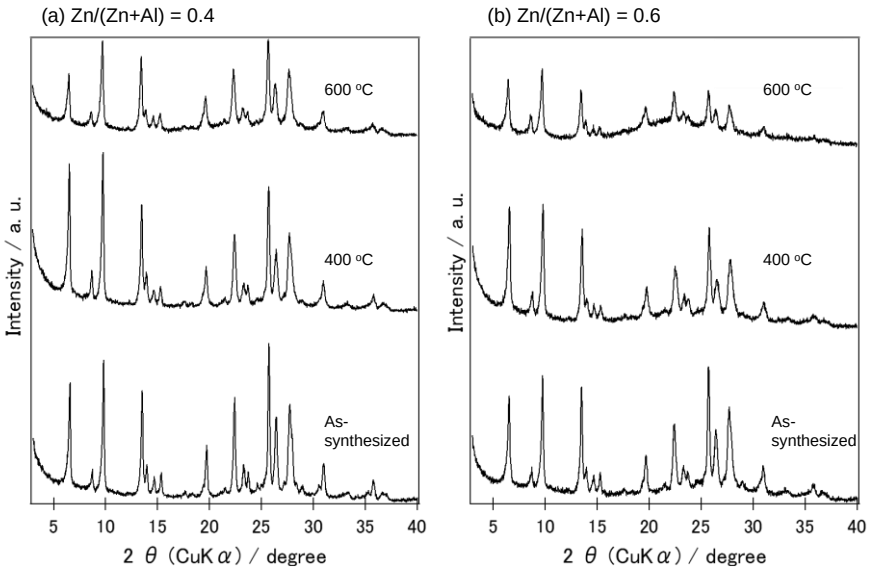

Figure 2-20 XRD patterns of MOR zeolites prepared with zincoaluminosilicate gels at the composition of (a) Zn/(Zn+Al) = 0.4 and (b) Zn/(Zn+Al) = 0.6 before and after thermal treatment at 400 ºC and 600 ºC for 10 h.

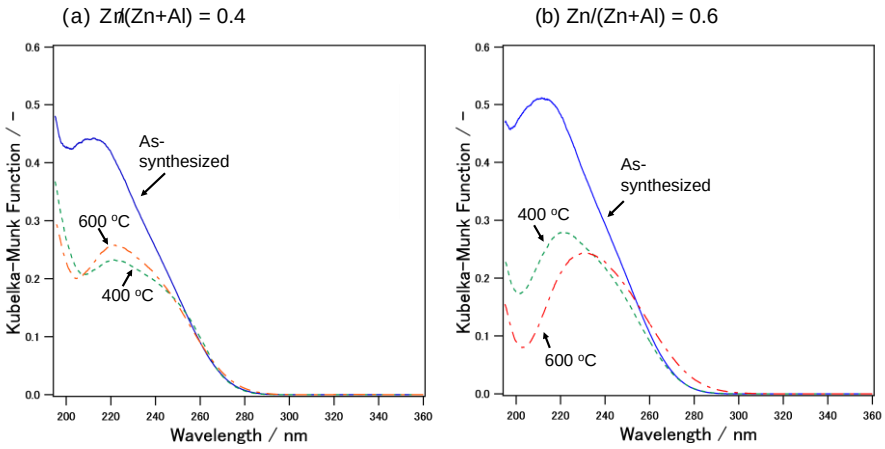

Figure 2-21 UV-vis spectra of MOR zeolites prepared with zincoaluminosilicate gels at the composition of (a) Zn/(Zn+Al) = 0.4 and (b) Zn/(Zn+Al) = 0.6 before and after thermal treatment at 400 °C and 600 °C for 10 h.

As reported recently, zincosilicate zeolites possess stronger Lewis acidity compared to other metal-substituted, Lewis acidic zeolites.[91] FT-IR spectroscopy of pyridine adsorbed at 80 °C and desorbed at 80–250 °C was used to characterize the acid sites of the H-type zincoaluminosilicate MOR zeolite (Zn0.4 MOR) in comparison with the H-type aluminosilicate analogue synthesized under the identical condition (Zn0 MOR). The characteristic vibrational modes of pyridine coordinated to a Lewis acid site and pyridinium ion generated from protonation of pyridine by a Brønsted acid site allow us to identify the presence of Brønsted and Lewis acid sites. Figure 2-22 compares pyridine adsorption onto the H-type Zn0 MOR and Zn0.4 MOR samples. The absorption bands at around 1450 and 1620 cm^{-1} are assigned to the pyridine coordinated to Lewis acid sites (labeled as “L” in Figure 2-22), while the bands at around 1545 and 1635 cm^{-1} are ascribed to the pyridinium ion adsorbed on Brønsted acid sites (labeled as “B” in Fig. 7).[177,178] The band at ca. 1490 cm^{-1} is due to the superposition of absorption signals arisen from both Lewis and Brønsted adsorbed species (“L+B” in Figure 2-22). In addition, the bands assigned to hydrogen-bonded pyridine (shown as “Py-H”) are also present in the samples before evacuation. The bands at ca. 1450 cm^{-1} and 1545 cm^{-1} are generally used for the quantitative identification of Lewis and Brønsted acid sites, respectively.[178] In the case of aluminosilicate Zn0 MOR, the band of Lewis acid sites (at 1452 cm^{-1}) was very weak and disappeared after evacuation at 150 °C. In

contrast, the characteristic band of Brønsted acid sites (at 1543 cm^{-1}) was clearly observed and maintained after evacuation at high temperatures up to 250 °C, revealing the strong Brønsted acidity of aluminosilicate MOR zeolite. On the contrary, the opposite trend was found in the zincoaluminosilicate Zn0.4 MOR, in which the band of Brønsted acid sites was hardly observed but the band at ca. 1451 cm^{-1} associated with Lewis acid sites was clearly seen and remained after evacuation at 250 °C. These results suggest the presence of strong Lewis acid sites in the obtained Zn0.4 MOR, akin to the previous report. [91] It can also be implied that Al in the Zn0.4 MOR sample (i.e., Brønsted acid sites) is located in the eight-ring pocket of the MOR zeolite framework, which is inaccessible to pyridine.

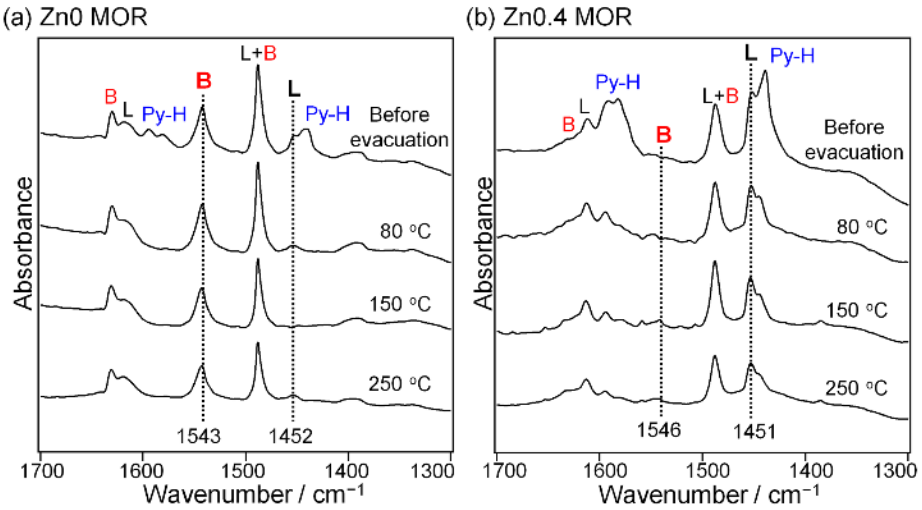

Figure 2-22 FT-IR spectra of (a) H-type Zn0 MOR and (b) H-type Zn0.4 MOR after pyridine adsorption at 80 °C (before evacuation), followed by evacuation at 80, 150, and 250 °C. L, B, L+B, and Py-H stand for Lewis acid, Brønsted acid, superposition of Lewis and Brønsted acids, and hydrogen-bonded pyridine, respectively.

To further characterize Lewis acid sites, similar FT-IR measurements were performed on the zincoaluminosilicate Zn0.4 MOR and Zn0.6 MOR samples (both in H-type) using deuterated acetonitrile (CD_3CN) as a probe molecule. The stretching frequency of CN is sensitive to the interaction strength with Lewis acid sites, making qualitative comparisons among different Lewis acid sites possible. FT-IR spectra of CD_3CN adsorbed onto the H-type Zn0.4 MOR and Zn0.6 MOR samples are shown in

Figure 2-23. In both samples, the absorption band due to physisorbed CD_3CN was observed at 2265 cm^{-1}, while the band present at ca. 2308 cm^{-1} was associated with CD_3CN coordinated to Lewis acid sites.[88] The additional band at 2319 cm^{-1} was seen only in the Zn0.4 MOR sample; the presence of this band became more noticeable after evacuation at high temperature, suggesting there are two different Lewis acid sites in the Zn0.4 MOR.

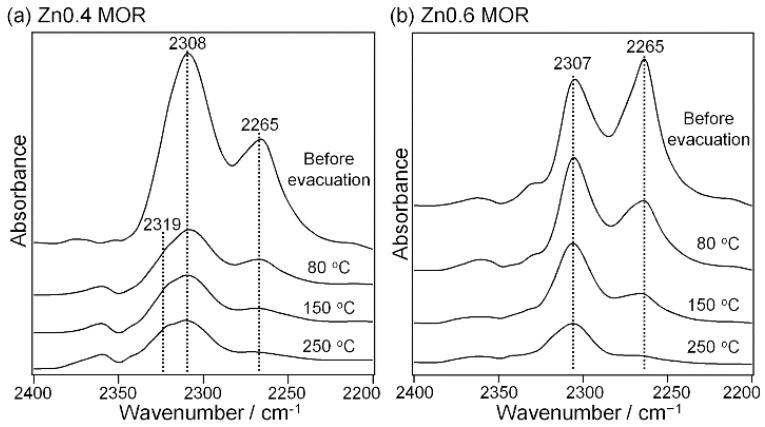

Figure 2-23 FT-IR spectra of deuterated acetonitrile adsorbed on (a) H-type Zn0.4 MOR and (b) H-type Zn0.6 MOR at 80 °C (before evacuation), followed by evacuation at 80, 150, and 250 °C.

As is well documented, in metal-substituted zeolites, particularly, Ti- and Sn-zeolites, there are two different metal sites, so-called "closed" and "open" sites.[88,179,180,181] The closed site is the defect-free metal center linking to four silicons via oxygen bridges whereas the open site is the defect metal site with a neighboring silanol group. The similar closed and open sites are also suggested to exist in the zincosilicate zeolites.[91] The closed Zn site creates two negative charges, while the opened Zn is monocation ion-exchangeable site (see Figure 2-24). The closed and open sites of Sn in stanosilicate *BEA zeolites show FT-IR bands of CD_3CN at *ca*. 2308 and 2317 cm^{-1}, respectively. [88179] The similar stretching frequencies observed in the obtained zincoaluminosilicate MOR zeolites (Figure 2-23) suggest that there were both closed and open Zn sites in the Zn0.4 MOR sample, while most of Zn in the Zn0.6 MOR sample was present in the closed sites.

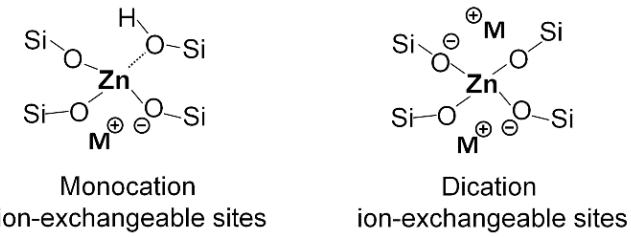

Figure 2-24 Local structures of two different Zn sites. M^+ is a monovalent cation. Monocation and dication ion-exchangeable sites represent the "open" and "closed" Zn sites, respectively.

The local environments of Zn sites in the MOR zeolite products were further verified by chemical analysis of Na^+ cations present in the as-synthesized products. The Na/(Zn+Al) molar ratio is equal to 1 if all Zn atoms are present in the open site, while the Na/(2Zn+Al) ratio is equal to 1 when all Zn are located in the closed site. As summarized in Table 3, the Na/Al ratio increased with increased Zn contents, again suggesting the successful incorporation of Zn into the zeolite frameworks. The Na/(Zn+Al) ratios were almost 1 in the case of Zn0.2 MOR and Zn0.4 MOR, while the Na/(Zn+Al) of Zn0.6 MOR was 1.4. In addition, the Na/(2Zn+Al) ratio of Zn0.6 MOR was close to 1. These results suggest that the Zn sites in Zn0.2 MOR and Zn0.4 MOR were dominated by the open sites, while the closed Zn sites were predominant in Zn0.6 MOR.

Table 3 Amounts of sodium cations and substituted metals of the as-synthesized (zinco)-aluminosilicate MOR zeolites[a]

Sample	Na/Al	Na/(Zn+Al)	Na/(2Zn+Al)
Zn0 MOR	1.0 ± 0.00	1.0 ± 0.00	1.0 ± 0.00
Zn0.2 MOR	1.1 ± 0.00	1.0 ± 0.00	0.80 ± 0.002
Zn0.4 MOR	1.7 ± 0.01	1.1 ± 0.0	0.79 ± 0.001
Zn0.6 MOR	3.1 ± 0.01	1.4 ± 0.02	0.93 ± 0.011

[a]Determined by ICP-AES.

Figure 2-25 shows changes in chemical compositions of the products prepared from the zincoaluminosilicate gel with Zn/(Zn+Al) of 0.6 for different periods of time.

The Zn/(Zn+Al) ratio only slightly decreased during the course of synthesis, suggesting that the contents of Zn and Al in the solid phase were almost constant throughout the synthesis. Interestingly, the Na/(Zn+Al) ratio was close to 1 at the initial stage and gradually increased as the formation of MOR zeolite proceeded. This suggests that Zn atoms in the initial solid created only one anionic charge per Zn. During the formation of zeolite, these Zn species evolved and condensed to form the closed Zn sites that can create two anionic charges per Zn as the Na/(2Zn+Al) approached 1 at the final stage.

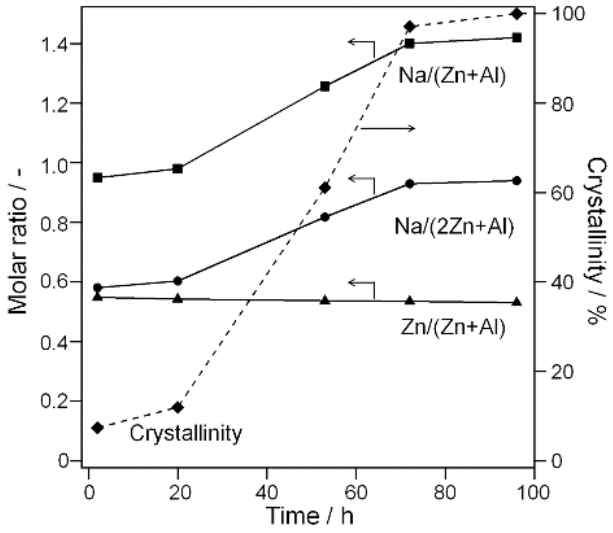

Figure 2-25 Changes in chemical compositions of the products obtained from the zincoaluminosilicate gel with Zn/(Zn+Al) of 0.6 along with the synthesis time.

The capability of the obtained zincoaluminosilicate MOR zeolites for ion-exchange of divalent cations was investigated using Ni^{2+} as a model cation because Ni^{2+}-exchanged zeolites show promising catalytic activity for dimerization and oligomerization of alkenes.[152,182,183] Chemical compositions of the products recovered after ion-exchange are summarized in Table 4. Compared with the compositions of the as-synthesized products, some leaching of Zn during ion-exchange was observed, probably due to slightly acidic conditions employed. The atomic ratios of Ni to Zn and Al increased as the contents of Zn were increased. The ion-exchange efficiency of the aluminosilicate sample (i.e., Zn0 MOR) was 64% whereas the efficiency of Zn0.6 MOR increased to 75%, calculated by assuming that all Zn in the sample are in the dication

ion-exchangeable sites (*i.e.*, the closed sites). This suggests that zincoaluminosilicate zeolites were efficient materials for hosting divalent cations.

Table 4 Chemical compositions of the products after ion-exchange with Ni^{2+} cations[a]

Sample	Zn/(Zn+Al)	Ni/(0.5Zn+0.5Al)	Ni/(Zn+0.5Al)
Zn0 MOR	0	0.64 ± 0.002	0.64 ± 0.002
Zn0.4 MOR	0.30 ± 0.002	0.95 ± 0.003	0.73 ± 0.002
Zn0.6 MOR	0.50 ± 0.001	1.2 ± 0.01	0.75 ± 0.003

[a]Determined by ICP-AES.

For the further investigation of the ion-exchange properties of the obtained MOR zeolites, ion-exchange isotherms describing mono-divalent ion exchange of Na^+ type MOR with Ni^{2+} was constructed. Ion-exchange isotherms exhibit selectivity of exchangeable cations toward ion-exchange sites in zeolites. The isotherms have been used to evaluate the affinity of cations to ion-exchange sites. For example, the high affinity of K^+ cations toward low silica X zeolites was shown to be the key of the selective growth of the zeolite.[184]

Here, mixture solutions of $Ni(NO_3)_2$ and $NaNO_3$ with total concentration of 0.1 mol equiv./L and various 2Ni:Na ratio were used to construct the ion-exchange isotherms. The ion-exchange period was determined by the long time exchange experiments up to 5 days to confirm that the system reached the exchange equilibrium. Figure 2-26 shows the time course change of 2Ni/(2Ni+Na) ratio in the zeolite, which corresponds to the ratio of Ni^{2+} species exchanged from Na^+. The 2Ni/(2Ni+Na) ratio became constant after 3h for Zn0 MOR, and after 3 days for Zn0.6 MOR when the solution with 2Ni/(2Ni+Na) of 1.0 was used, and 3h for Zn0 MOR, and after 2 days for Zn0.6 MOR when the solution with 2Ni/(2Ni+Na) of 0.1 was used. Therefore, the period to obtain the points of ion-exchange isotherms were determined to be 3 days to ensure the equilibrium of the system. Interestingly, the Zn0.6 MOR samples shows higher 2Ni/(2Ni+Na) ratio compared to Zn0 MOR sample, especially when the solution with 2Ni/(2Ni+Na) of 0.1 was used. The result suggested that the Zn0.6 MOR has stronger selectivity to Ni^{2+} compared to that of Zn0 MOR.

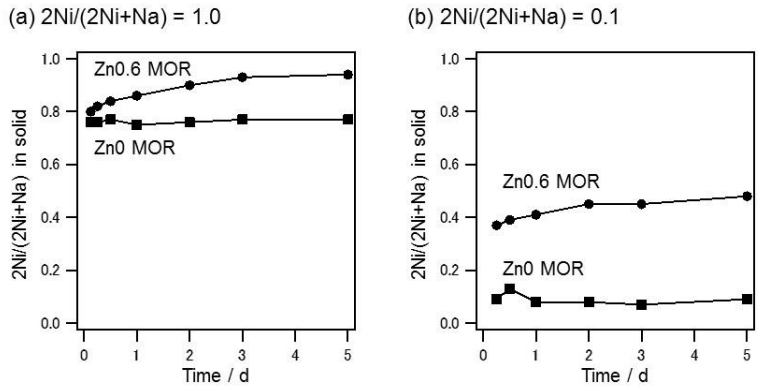

Figure 2-26 Changes in the chemical compositions of the solid products after ion-exchange using ion-exchange solutions with composition of (a) 2Ni/(2Ni+Na) = 1.0 and (b) 2Ni/(2Ni+Na) = 0.1.

The difference in selectivity for Ni^{2+} and Na^{+} was further evaluated from the shape of ion-exchange isotherms. As shown in Figure 2-27, the isotherm for Zn0.6 MOR shows a steep increase of 2Ni/(2Ni+Na) ratio in the solid with low 2Ni/(2Ni+Na) solution ratio, that is, small amount of Ni^{2+} in the solution is rapidly incorporated into the solid (zeolite) phase, suggesting the existence of ion-exchange sites with a strong affinity to Ni^{2+}. Then, the ion exchange selectivity became constant, and finally, a steep increase of Ni^{2+} exchange ratio in solid was again observed. This type of isotherm indicates the existence of two types of ion exchanged sites: the site with strong affinity to Ni^{2+}, and the site which is relatively difficult to be exchanged.[185] The former exchange site likely corresponds to the divalent ion-exchange sites generated by Zn in the frameworks, since the close divalent charges are expected to prefer one divalent cations to two monovalent cations due to the structure constrain. The latter exchange site is likely the ion-exchange sites generated by two Al atoms in the framework. The lower charge density of the two negative charges created by two Al atoms compared to that created by Zn atom might reduce the stabilizing effect of the divalent cations in the exchange site. The isotherm of Zn0.6 MOR crosses the dotted line at around (0.6, 0.6), which is in agreement with the elemental analysis that shows the Zn/(Zn+Al) ratio is 0.6. On the other hand, the ion-exchange isotherm on Zn0 MOR is almost linear; ion exchange ratio increases with increasing the concentration of Ni^{2+} ion in liquid, which

indicates that there is no site heterogeneity in the zeolite.

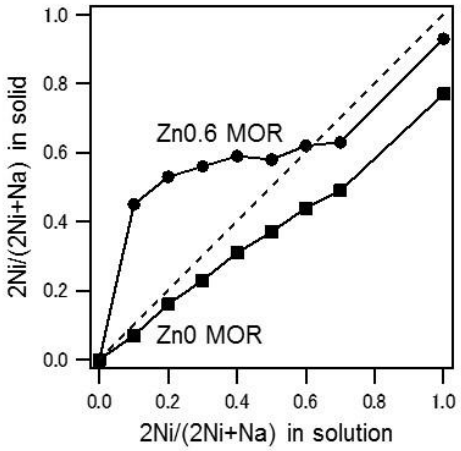

Figure 2-27 The ion-exchange isotherms of Zn0 MOR and Zn0.6 MOR

Figure 2-28 shows preliminary results showing time course change of 2Co/(2Co+Na) ratio in the Zn0.6 MOR and Zn0 MOR zeolites using ion-exchange solutions with composition of 2Co/(2Co+Na) = 1.0. As was the case of the ion-exchange with Ni^{2+}, the Zn0.6 MOR samples shows higher 2Co/(2Co+Na) ratio compared to Zn0 MOR sample. The result suggested that the Zn0.6 MOR has stronger selectivity to Co^{2+} compared to that of Zn0 MOR.

These results suggested that the ion-exchange sites generated by Zn in the framework have high affinity for divalent cations than that generated by Al. The high selectivity for divalent metals is desirable for several applications such as separation of divalent metal cations in low concentration from solutions.

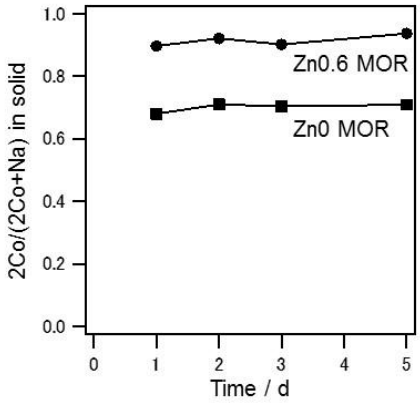

Figure 2-28 Changes in the chemical compositions of the solid products after ion-exchange using ion-exchange solutions with composition of 2Co/(2Co+Na) = 1.0.

The Ni^{2+} ion-exchanged MOR zeolites were tested in oligomerization reaction of propylene. The exchanged Ni^{2+} cations into FAU and MFI zeolites have been reported to catalyze oligomerization of light olefins (C2−C4) to higher molecular weight hydrocarbons.[186,187,188,189] Recently, Ni^{2+} exchanged zincosilicate zeolites with *BEA topology (CIT-6) have been demonstrated to have superior selectivity and stability in propylene oligomerization reaction compared to the Ni^{2+} exchanged aluminosilicate analogues of *BEA zeolite.[152] The high selectivity to C_{3n} products were attributed to the reduced acidity of zincosilicate zeolites.[152] Figure 2-29 shows typical reaction data for Ni^{2+} exchanged Zn0 MOR and Zn0.4 MOR at 200 °C. For each samples, propylene conversion decreased with increasing time on-stream as the catalyst deactivates. Formation of propane was observed for both samples probably because of hydration by Brønsted acid sites or hydride transfer reactions.[190] The Ni^{2+} exchanged aluminosilicate Zn0 MOR exhibited higher selectivity to C1 and C2 products formed by cracking reactions compared to Zn0.4 MOR, likely due to the high acidic strength of the aluminosilicate framework. With Zn0 MOR, the C6 selectivity was 5.3% when propylene conversion was 13.9%, on the other hand, Zn0.4MOR showed C6 selectivity of 21.3% when propylene conversion was 13.1%. The higher selectivity to C6 products is likely due to the high ion-exchange ratio and reduced Brønsted acidity of zincoaluminosilicate framework.

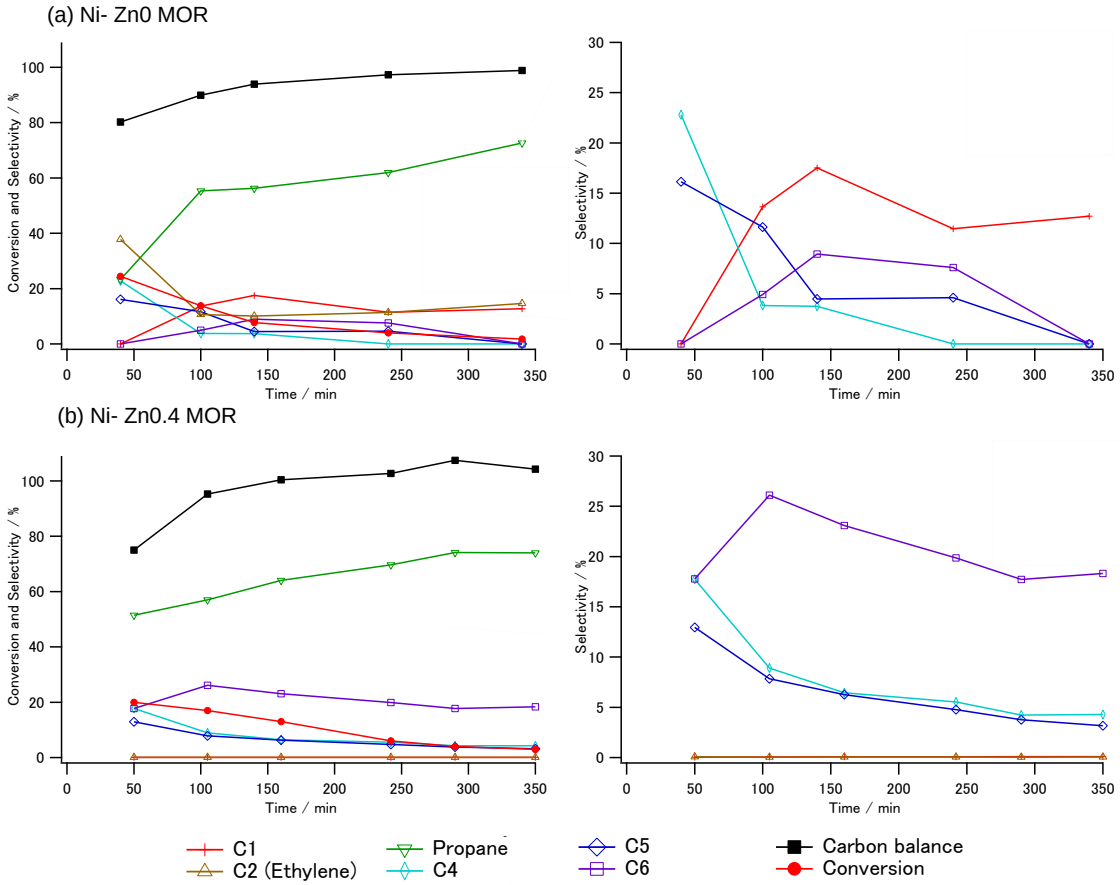

Figure 2-29 Time-on-stream profiles of conversion, carbon balance, and product selectivity for (a) Ni-Zn0 MOR and (b) Ni-Zn0.4 MOR catalysts.

2.4 Conclusions

Organic-free synthesis of zincoaluminosilicate MOR zeolites using homogeneous co-precipitated zincoaluminosilicate gels was demonstrated for the first time. In contrast to conventional synthesis of zeolites, in which separate sources of Si and other tetrahedral atoms such as Al and Zn are used, the co-precipitated gels containing all tetrahedral atoms were used as raw materials in the present method. Characterization of the zincoaluminosilicate gels suggested that both Zn and Al are homogeneously distributed in the silicate matrix. The use of such co-precipitated zincoaluminosilicate gels is a key for successful incorporation of both Zn and Al into the final MOR zeolite products because ZnO was formed separately from the zeolite

framework by using conventional Si, Zn and Al sources. Zincoaluminosilicate MOR zeolites were formed from the co-precipitated gels without using the seed crystal, however, the crystallization time significantly increased. It was found that there are two different local environments of Zn in the zeolite frameworks. The population of each site depended on the total contents of Zn in the zeolites. The obtained zincoaluminosilicate zeolites showed higher ion-exchange efficiency for nickel(II) cations compared to the aluminosilicate analog, thereby providing platforms for several important catalytic reactions.

2.5 Appendix

To broaden the applicable scope of the synthesis using the co-precipitated gels, a cobalt-aluminosilicate gel was prepared by the similar co-precipitation method and used for synthesis of cobalt-aluminosilicate MOR zeolite with Co atom substituted in the silicate framework.

The cobalt-aluminosilicate gel was prepared by mixing sodium silicate solution (8.25 wt% SiO_2) and acidic solution of aluminum sulfate and cobalt sulfate using peristaltic pumps. The mixing and the precipitation were performed in a vessel with an overflow tube under neutral pH at 40 °C. The amounts of aluminum sulfate and cobalt sulfate used for preparation of gels were calculated with Co/(Co+Al) molar ratios of 0.4, and Si/(Co+Al) of 8.0. The feed ratio of the sodium silicate solution and the sulfate solution was kept at 4:1 (by volume). The averaged residence time of the gel slurry (= vessel volume/total feed rate) was kept at around 15 min, so that the vessel volume and both of the feed rates were optimized. The neutralized suspension containing the cobalt-aluminosilicate gel was collected and recovered by a centrifugal separator. The gel was thoroughly washed with deionized water. The water content in the gel was measured from a weight loss after calcination at 600 °C for 4 h.

Cobalt-aluminosilicate MOR zeolites were synthesized using the co-precipitated gels. First, seed crystals of MOR zeolite (Tosoh, HSZ-640NAA, Si/Al = 9.0) were dispersed in sodium hydroxide aqueous solution. Then, the cobalt-aluminosilicate gel was added and mixed vigorously. The chemical compositions

of the reaction mixtures (without seed crystals) were 1.84 Na_2O: 0.3 Al_2O_3: 0.4 CoO: 8.0 SiO_2: 120 H_2O. The hydrothermal synthesis was carried out in a 60-mL autoclave at 150 °C for 96 h under a static condition. After completion, the solid product was recovered by filtration and washed with deionized water until the filtrate reached pH 7–8.

The obtained cobalt-aluminosilicate gel was colored light purple, and turned blue after calcination. The obtained product after hydrothermal treatment was also colored blue. Figure 2-30 compares the XRD patterns of the product and MOR zeolite used as the seed crystal. The product obtained from the co-precipitated gel showed high crystallinity comparable to the seed crystal. The high intensity of background around 5 degree is probably indicative for unknown impurities. As shown in Figure 2-31, absorption bands attributed to tetracoordinated Co-O bond were visible from UV-Vis spectroscopy, indicating the successful incorporation of cobalt to the zeolite framework. Co-substituted MOR zeolites have been prepared using complexing agent (EDMA).[191] The use of cobalt-aluminosilicate gel prepared by the co-precipitation enabled cobalt-aluminosilicate MOR zeolites without using any organics probably likely due to the highly dispersed cobalt in the silicate matrix.

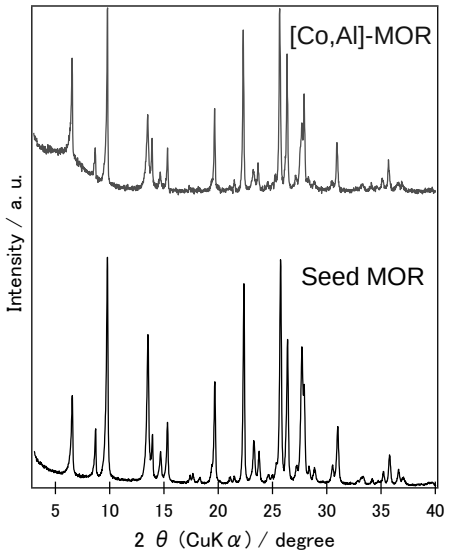

Figure 2-30 Powder XRD pattern of the MOR zeolite used as seed crystal and cobalt-aluminosilicate MOR zeolite obtained from the co-precipitated gel.

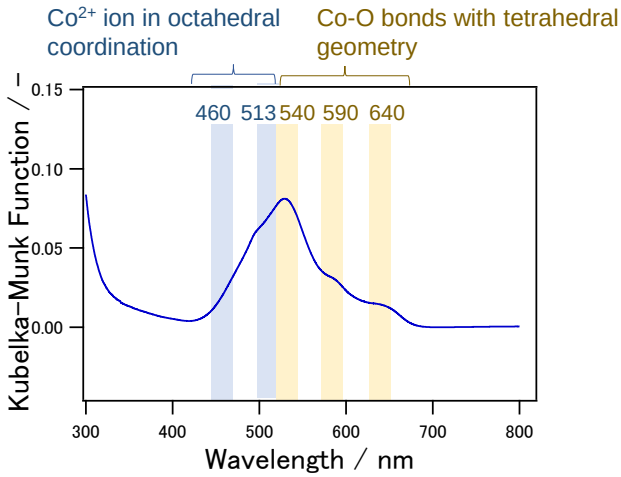

Figure 2-31 UV-Vis spectra of the cobalt-aluminosilicate MOR zeolite obtained from the co-precipitated gel.

Chapter 3.

Organic-Free Synthesis of Various Zincoaluminosilicate Zeolites from Co-precipitated Zincoaluminosilicate Gels by Applying Composite Building Unit Hypothesis

3.1 Introduction

As described in Chapter 2, one of the obstacles in the synthesis of zinc-containing zeolites is a use of organic structure-directing agents (OSDAs), because of the high cost and environmental burden. The high-zinc-containing zincosilicates, VPI-7,[137] VPI-9,[141] and RUB-17[149] are prepared in the presence of Na^+ Rb^+, mixture of Na^+ and K^+, respectively, without using OSDAs. Those zincosilicate zeolites have characteristic framework topologies rich in 3 membered-ring (3MR) with no pure-silica or aluminosilicate analogs. Expanding the number of available zinc-containing zeolite prepared in OSDA-free manner is necessary because desirable zeolite topology varies depending on required properties.

In the case of aluminosilicate zeolites, OSDA-free synthesis method have been established for zeolites with various topologies.[192,193,194] Recently, Itabshi *et al.* have reported versatile approach to achieve OSDA-free synthesis of various aluminosilicate zeolites based on building units of zeolite structures.[169] The framework structures of zeolites consist of secondary building unit (SBU), which are derived assuming that the entire framework is made up of one type of SBU only, and / or composite building unit (CBU), which are the units appear in several different framework structures, and can be useful in identifying relationships between framework types, as defined by the IZA-SC. The following hypothesis was proposed based on the CBUs to understand the various OSDA-free synthesis achieved by seed-assisted method. That is, when the seed crystal of target zeolite is added in the synthesis mixture that yields zeolite having common

CBU in an OSDA-free manner, the crystallization of target zeolite can be proceeded without addition of OSDAs.[169] This hypothesis explains various OSDA-free synthesis of zeolites. For example, as shown in Figure 3-1 (a), the *mor* CBU is common in *BEA and MOR structures, and OSDA-free synthesis of the *BEA zeolite was achieved by adding *BEA seed crystals to Na-aluminosilicate gel which yields MOR zeolite with the absence of seeds. MFI and MEL zeolites, which also contains the *mor* unit was also achieved by adding the seed crystals to the same Na-aluminosilicate gel which yields MOR zeolite with the absence of seeds (Figure 3-1(b)). It was also shown that synthesis conditions such as gel composition and temperature of hydrothermal treatment should be optimized to prevent spontaneous nucleation before the completion of crystallization of the targeted zeolites.

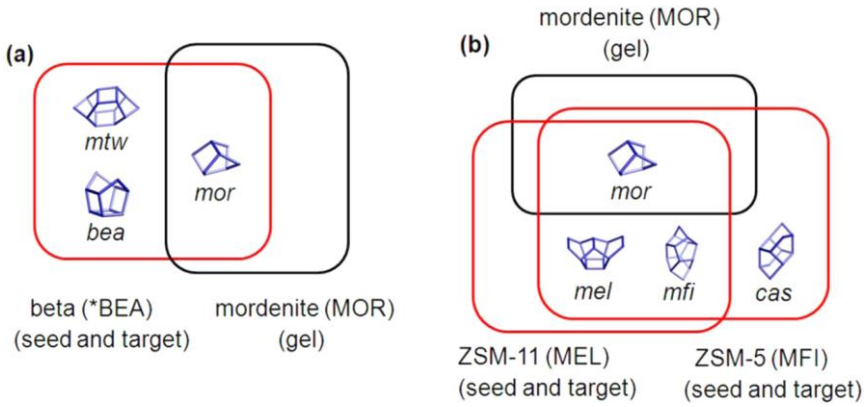

Figure 3-1 Correlation of common composite building unit between (a) MOR and *BEA, and (b) MOR, MFI, and MEL.[169]

With the assistance of seed crystals, synthesis of many aluminosilicate zeolites, including MTW,[171,195] MSE,[196] MAZ[197] and MWW[172] zeolites, was achieved based on the CBU hypothesis. It was also reported that zincosilicate *BEA zeolite can be used as a seed crystals to obtain aluminosilicate *BEA zeolite.[198] The obtained aluminosilicate zeolite *BEA possesses a hollow structure due to the dissolution of seed zincosilicate zeolite.[198] Recently, it was reported that the CBU hypothesis was further extended to replace complex OSDAs to the simple one for the synthesis of MSE zeolite.[199]

However, the only successful example for seed-assisted, OSDA-free synthesis of zincosilicate zeolite is VET.[173] It still remains a significant challenge to broaden the

types of zinc-containing zeolites that can be synthesized without using any OSDAs.

With the accomplishment of OSDA-free synthesis of zincoaluminosilicate MOR zeolite as described in Chapter 2, the OSDA-free synthesis of other zincosilicate zeolites having common CBU with MOR zeolite were targeted in this chapter to solve the abovementioned problem. The homogeneous zincoaluminosilicate gels, in which both Zn and Al atoms are substituted in silicate matrix, was used as starting materials to achieve successful zinc incorporation as described in Chapter 2. The *BEA and MFI zeolite, which has the common CBU with MOR was selected as the target zeolite (Figure 3-2).

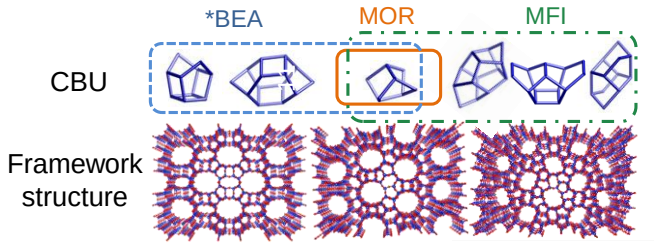

Figure 3-2 Framework structures and composite building units (CBU) of *BEA, MOR and MFI zeolites

3.2 Experimental Section

3.2.1 Materials

The following chemicals were used as received for synthesis of zeolites: sodium silicate solution (JIS No.3, Fuji Kagaku CORP), aluminum sulfate solution (Taimei Chemicals Co., Ltd.), zinc sulfate (Wako Pure Chemical Industries, Ltd.), sodium hydroxide solution (Wako Pure Chemical Industries, Ltd.), sulfuric acid solution (Wako Pure Chemical Industries, Ltd.), fumed silica (Cab-O-Sil M-5, Cabot Co.), sodium aluminate (Wako Pure Chemical Industries, Ltd.), and zinc acetate (Wako Pure Chemical Industries, Ltd.).

3.2.2 Preparation of Zincoaluminosilicate Gels

The zincoaluminosilicate gels were prepared by mixing sodium silicate solution (8.25 wt% SiO_2) and acidic solution of aluminum sulfate and zinc sulfate using peristaltic pumps. The mixing and the precipitation were performed in a vessel with an overflow tube under neutral pH at 40 °C. The desired amounts of aluminum sulfate and zinc sulfate used for preparation of gels were calculated with Zn/(Zn+Al) molar ratios of 0.1, 0.2, 0.4, 0.6, 0.8, and 1, while keeping Si/(Zn+Al) at 8.0. The feed ratio of the sodium silicate solution and the sulfate solution was kept at 4:1 (by volume). The averaged residence time of the gel slurry (= vessel volume/total feed rate) was kept at around 15 min, so that the vessel volume and both of the feed rates were optimized. The neutralized suspension containing the zincoaluminosilicate gel was collected and recovered by a centrifugal separator. The gel was thoroughly washed with deionized water. The water content in the gel was measured from a weight loss after calcination at 600 °C for 4 h.

3.2.3 Synthesis of *BEA and MFI Zeolites from Zincoaluminosilicate Gels

Zincoaluminosilicate zeolites were synthesized using the co-precipitated gels. First, seed crystals of target zeolite, MFI zeolite (Tosoh, HSZ-820NHA, Si/Al = 11.5) and *BEA zeolite (Tosoh, HSZ-931HOA, Si/Al = 13.6 or UniZeo, TEA023, Si/Al = 14.5), were dispersed in sodium hydroxide aqueous solution. Then, the zincoaluminosilicate gel was added and mixed vigorously. The typical chemical compositions of the reaction mixtures (without seed crystals) were 1.84 Na_2O: 0.5(1-x) Al_2O_3: x ZnO: 8.0 SiO_2: 120 H_2O, where x was varied as 0.1, 0.2, 0.4, 0.6, 0.8, and 1. The weight of seed crystals was fixed at 10 wt% (on a basis of SiO_2). The hydrothermal synthesis was carried out in a 60 mL autoclave at 150 °C for 20–96 h under a static condition. After completion, the solid product was recovered by filtration and washed with deionized water until the filtrate reached pH 7–8. The product was dried at 80 °C overnight before subsequent characterizations.

3.2.4 Characterization

Powder X-ray diffraction (XRD) analysis was conducted to determine the crystal structure of the products using a diffractometer (Rigaku Ultima IV) operated with Cu Kα monochromatized radiation at 40 kV and 40 mA. Elemental analysis of the products was performed by inductively coupled plasma-atomic emission spectrometry (ICP-AES, Thermo iCAP 6300) after dissolving the products in hydrofluoric acid or potassium hydroxide solutions. To observe crystal size and morphology, field-emission scanning electron microscopy (FE-SEM) images were obtained from JFM-7500FA (JEOL) at an accelerating voltage of 15 kV. Nitrogen adsorption–desorption measurements were performed on Quantachrome Autosorb-iQ2-MP at liquid nitrogen temperature. Prior to the measurements, the samples were degassed at 400 °C for 6 h under vacuum. Diffuse reflectance (DR) UV–vis spectra in the range over 190 nm were recorded on a JASCO V-670 spectrometer in the 190−800 nm wavelength range using barium sulfate as a reference. To obtain UV–vis spectra below 190 nm, a Shimadzu SolidSpec-3700DUV spectrometer was used. Solid-state magic-angle-spinning (MAS) nuclear magnetic resonance (NMR) experiments were conducted on a JNM-ECA 500 (JEOL). ^{27}Al MAS NMR spectra were recorded at 130.3 MHz with a pulse length (π/2) of 3.2 μs, a recycle delay of 5 s, and a spinning frequency of 14 kHz. ^{29}Si MAS NMR spectra were recorded at 99.3 MHz with a pulse length (π/2) of 5.0 μs, a recycle delay of 60 s, and a spinning frequency of 10 kHz. To characterize local environments of Zn in the obtained zeolites, ion-exchange with Ni(II) was performed. 0.01 M of nickel nitrate aqueous solution was prepared from nickel(II) nitrate hexahydrate (Wako Pure Chemical Industries, Ltd.). pH of the solution was adjusted to 6.0–6.5 by adding a few drops of ammonia aqueous solution (3 wt%). The solid samples (0.3 g) were dispersed in the nickel nitrate solution (100 mL) and then stirred at 500 rpm and room temperature. After stirring for 2 days, the samples were separated from the solution by centrifugation and re-dispersed in 100 mL of fresh nickel nitrate solution. The ion-exchange procedure was repeated for 3 times. Finally, the ion-exchanged products were thoroughly washed with deionized water and dried at 80 °C. The content of Ni was determined by ICP-AES (Thermo iCAP 6300).

3.3 Results and Discussion

3.3.1 Characterization of Zincoaluminosilicate Gels

The co-precipitated zincoaluminosilicate gels were formed with ratios of Zn/(Zn+Al) almost identical to the initial ratios of the solutions of zinc sulfate and aluminum sulfate used in the co-precipitation. Both Zn and Al are proved to be highly dispersed in the silicate structures. The detailed characterizations of the zincoaluminosilicate gels are described in Chapter 2.2.3.

3.3.2 Synthesis of *BEA Zeolites from Zincoaluminosilicate Gels

Powder XRD patterns of the products obtained by using *BEA seed crystals (Tosoh (HSZ931HOA)) and the zincoaluminosilicate gels with Zn/(Zn+Al) of 0, 0.1, 0.2, and 0.4 after hydrothermal treatment at 150 °C for 61 h are shown in Figure 3-3. The formation of highly crystalline *BEA zeolites was confirmed when the Zn/(Zn+Al) ratio was 0–0.2. As shown in Figure 3-4, well-defined crystals with truncated octahedral morphology that is typical for *BEA zeolites were observed. When the Zn/(Zn+Al) ratio was increased to 0.4, the crystallinity of the zeolite product was significantly decreased. To further improve its crystallinity, synthesis time was prolonged in the same conditions, but MOR zeolite was formed as a by-product. As shown in Table 3-1, the resulting *BEA zeolites had the contents of Zn comparable to those of initial zincoaluminosilicate gels used in the synthesis. Furthermore, the Na/(Zn+Al) ratio was about 1, suggesting that the Zn atoms generated one anionic charge per Zn in the zeolite frameworks.

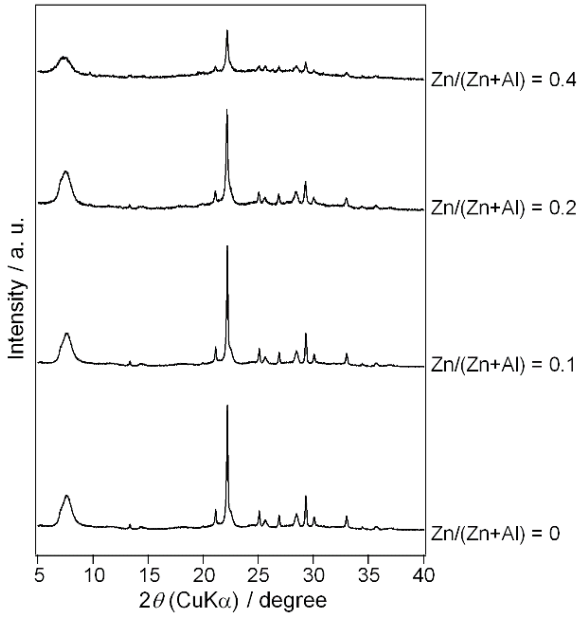

Figure 3-3 Powder XRD patterns of products synthesized from co-precipitated zoncoaluminosilicate gels with Zn/(Zn+Als) of 0, 0.1, 0.2, and 0.4 with the addition of seed crystals of *BEA zeolite (Tosoh (HSZ931HOA)).

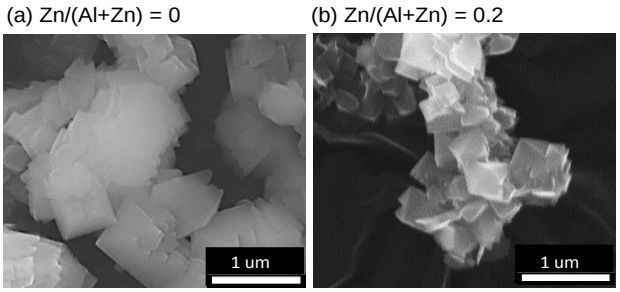

Figure 3-4 FE-SEM images of products synthesized from co-precipitated zoncoaluminosilicate gels with Zn/(Zn+Als) of (a) 0 and (b) 0.2 by using seed crystals of *BEA zeolite (Tosoh (HSZ931HOA)).

Table 3-1 Chemical compositions of the zincoaluminosilicate *BEA products[a]

Sample	Zn/(Zn+Al)	Si/(Zn+Al)	Na/Al	Na/(Zn+Al)
Zn0 *BEA	0	4.5 ± 0.00	1.0 ± 0.00	1.0 ± 0.00
Zn0.1 *BEA	0.08 ± 0.005	5.3 ± 0.01	1.1 ± 0.02	1.0 ± 0.01
Zn0.2 *BEA	0.17 ± 0.007	5.0 ± 0.02	1.3 ± 0.03	1.1 ± 0.02

[a]Determined by ICP-AES

Solid-state ^{27}Al MAS NMR measurements were conducted to investigate the local environments of Al species in the zincoaluminosilicate *BEA zeolites obtained after hydrothermal treatment of 61 h and 53 h, and aluminosilicate *BEA zeolite obtained after hydrothermal treatment of 53 h (Figure 3-5). In all samples, only one resonance at δ = 54.7 ppm, corresponding to tetrahedrally coordinated Al, was observed. ^{27}Al MAS NMR spectra of the *BEA zeolites with zinc have a shoulder peak in a range of chemical shifts at around 53–45 ppm compared to that of *BEA zeolite with no zinc (aluminosilicate *BEA zeolite). The lower chemical shift suggests increase in the average Al−O−Si angles.[176,200] Incorporation of zinc to aluminosilicate framework is expected to increase the angles because of the longer Zn–O bond length (ca. 2 Å), compared with Si–O (ca. 1.6 Å) and Al–O (ca. 1.8 Å). Therefore, the increase in the shoulder at lower chemical shifts is probably another evidence of zinc substitution in the zeolite framework.

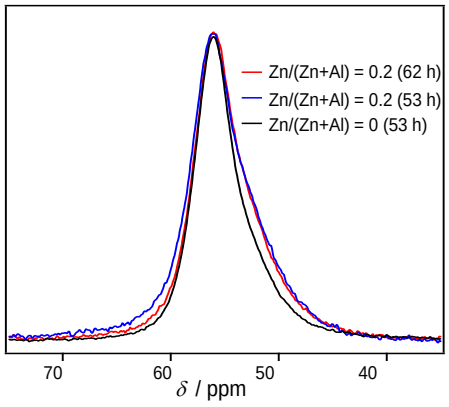

Figure 3-5 Solid-state 27Al MAS NMR spectra of (zinco)aluminosilicate *BEA zeolites with Zn/(Zn + Al) values of 0 and 0.2, obtained after hydrothermal treatment at 150 °C for 53 hour and 62 hour.

In the seed assisted OSDA-free synthesis, the seed crystals of target zeolite play a crucial role in the crystallization. When there is no seed crystals, other phases are formed instead of the targeted one.[169] The effect of the type of seed crystals were investigated using different seed. *BEA zeolites provided from Tosoh (HSZ931HOA) and UniZeo (TEA023) were used for the comparison. The Si/Al ratio (13.6 for

HSZ931HOA and 14.5 for TEA023) is comparable, while the crystal sizes are significantly different (ca. 4 um for HSZ931HOA and ca. 100 nm for TEA023). Figure 3-6 shows the XRD patterns of the products prepared using the zincoaluminosilicate gel with Zn/(Zn+Al) of 0.2 after hydrothermal treatment at 150 ^{o}C. When the XRD patterns of the products obtained from 53h of the hydrothermal treatment are compared, both product obtained using HSZ931HOA and TEA023 seed crystals contains amorphous phase. The intensity of diffraction peaks of the product obtained by using TEA023 was higher than that obtained by using HSZ931HOA. After 62 h, the amorphous phase almost disappeared and the intensity of diffraction peaks of the product obtained by using TEA023 was again higher than that obtained by using HSZ931HOA. It is suggested that the smaller particle sizes of TEA023 seed crystals is preferable for the crystal growth of *BEA zeolite, as reported in the synthesis of several aluminosilicate zeolites.[201]

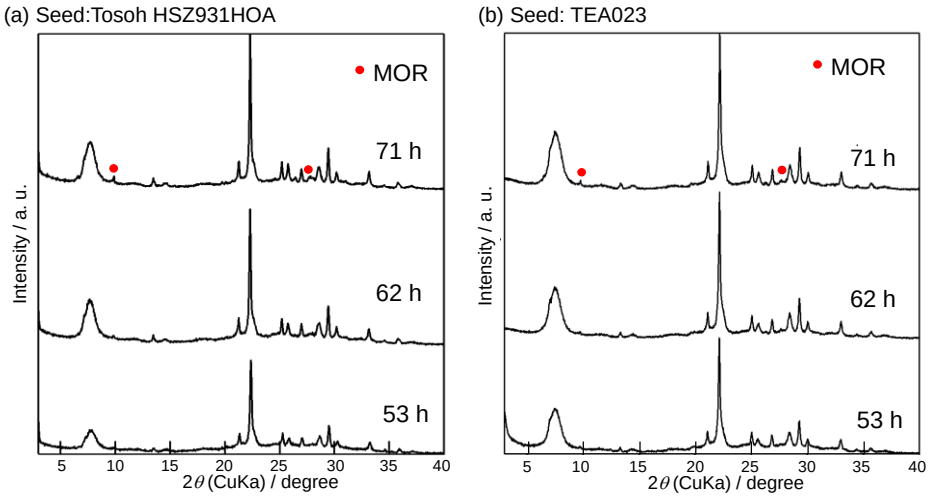

Figure 3-6 Powder XRD patterns of products synthesized from co-precipitated zincoaluminosilicate gels with Zn/(Zn+Al) of 0.2 with the addition of seed crystals of *BEA zeolite provided from (a) Tosoh (HSZ931HOA) and (b) UniZeo (TEA023) .

Figure 3-7 shows Nitrogen adsorption–desorption isotherms of *BEA seed crystals provided from (a) Tosoh (HSZ931HOA) and (b) UniZeo (TEA023), and the products synthesized from co-precipitated zincoaluminosilicate gel with Zn/(Zn+Al) of 0.2 using the seed crystals. The TEA023 seed crystals showed remarkably high uptake

at high partial pressure, suggesting large outer surface area due to the small particle sizes. As shown in Table 3-2, zincoaluminosilicate *BEA zeolites obtained by using TEA023 seed crystals exhibited higher micropore volumes compared to that obtained using HSZ931HOA seed crystals. It is again suggested that the smaller particle sizes of TEA023 seed crystals is effective for the crystal growth of *BEA zeolite.

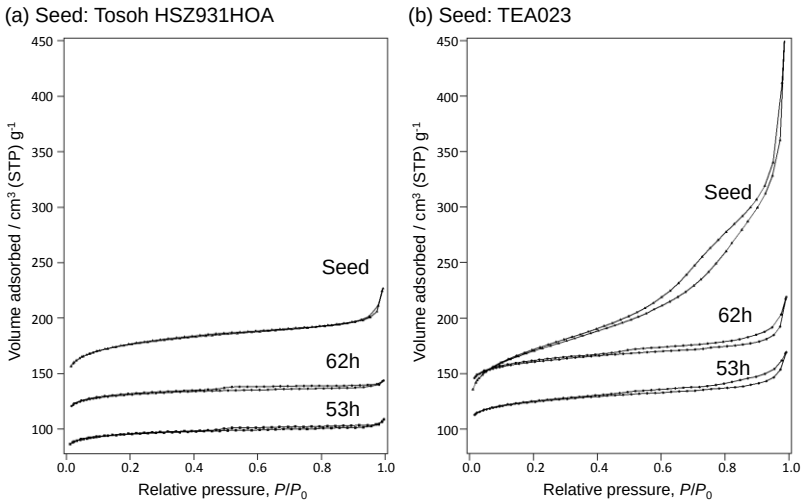

Figure 3-7 Nitrogen adsorption–desorption isotherms of products synthesized from co-precipitated zincoaluminosilicate gels with Zn/(Zn+Al) of 0.2 with the addition of seed crystals of *BEA zeolite from (a) Tosoh (HSZ931HOA) and (b) UniZeo (TEA023) .

Table 3-2 Micropore volumes and BET surface areas of the zincoaluminosilicate *BEA products[a]

	(a) Seed: Tosoh HSZ931HOA		(b) Seed: TEA023	
	S_{BET} [b]/m^2g^{-1}	V_{micro} [a] /cm^3g^{-1}	S_{BET} [b] /m^2g^{-1}	V_{micro} [a]/cm^3g^{-1}
seed	670	0.23	630	0.16
53h	370	0.13	470	0.15
62h	500	0.18	610	0.21

[a]Micropore volumes determined by a *t*-plot method. [b]BET surface area. [d]Not determined.

Even with the TEA023 seed crystals, when the Zn/(Zn+Al) ratio was increased to 0.4, the crystallinity of the zeolite *BEA product decreased and formation of MOR zeolite and layered silicate material was confirmed by XRD analysis and SEM observation, respectively (Figure 3-8). In this condition, amount of NaOH added to the mixture was varied from the initial ratio of NaOH/Si = 0.46 to 0.4 and 0.5. With the decreased alkalinity, NaOH/Si of 0.4, formation of MOR zeolite was enhanced. This is probably because the partial dissolution of seed crystal surface was suppressed due to the low alkalinity. And the speed for crystal growth of *BEA decreased in this conditions. With the increased alkalinity, NaOH/Si of 0.5, crystallinity of obtained zeolite *BEA was significantly decreased, and main product observed in SEM analysis was layered material. It is known that the synthesis of zincosilicate *BEA zeolites (i.e., CIT-6 zeolite)[145] with high contents of Zn is difficult and the Si/Zn ratio of CIT-6 is typically limited in a range of 30–50, regardless of synthesis conditions. Similarly, in our case, the Si/Zn of the zincoaluminosilicate *BEA products was 30–60. This may reflect the upper limit for Zn in the *BEA zeolite. It is noteworthy that Li^+ cations are required for conventional synthesis of CIT-6 but in this case only Na^+ was added as a cation for synthesis of zincoaluminosilicate *BEA zeolites.

Collectively, these results confirm the applicability of the co-precipitated zincoaluminosilicate gels as starting materials for the synthesis of *BEA zeolite with reasonable chemical compositions.

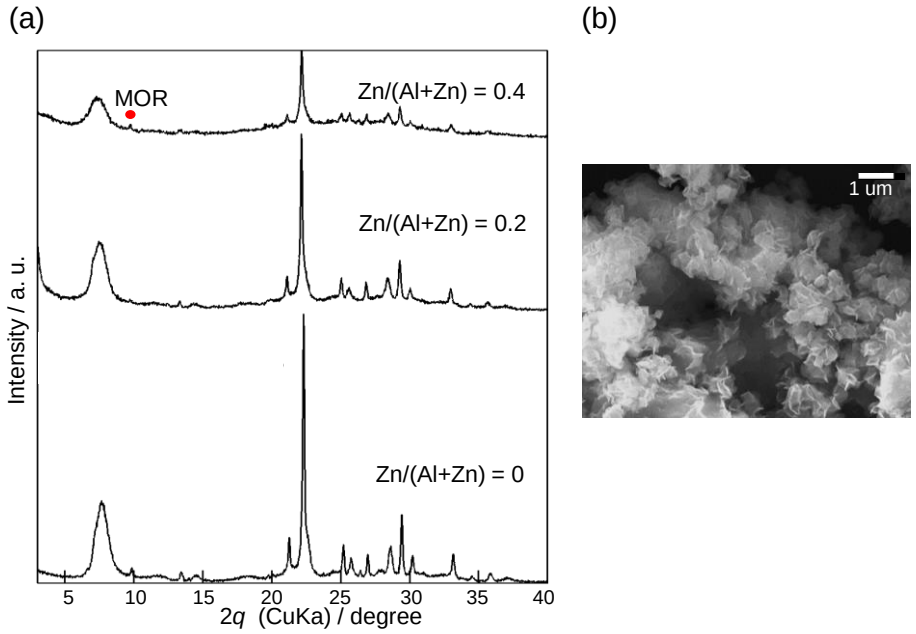

Figure 3-8 (a) Powder XRD patterns of products synthesized using co-precipitated zincoaluminosilicate gels with Zn/(Zn+Al) of 0, 0.2 and 0.4 with the addition of seed crystals of *BEA zeolite from UniZeo (TEA023) and (b) FE-SEM image of product synthesized from co-precipitated zincoaluminosilicate gels with Zn/(Zn+Al) of 0.4 with the addition of seed crystals of *BEA zeolite from UniZeo (TEA023).

3.3.3 Synthesis of MFI zeolites from Zincoaluminosilicate Gels

The synthesis of MFI zeolites was conducted at 170 ºC or 190 ºC according to the previous research which reported that, at 140 and 150 °C, the crystallization of MOR zeolites started prior to the crystallization of MFI zeolites because of its slower crystal growth rate in low temperature.[169]

Figure 3-9 shows powder XRD patterns of the products obtained from the zincoaluminosilicate gels with Zn/(Zn+Al) of 0.4 and 0.6 after hydrothermal treatment at 170 °C. When the amount of NaOH was same as that used in the synthesis of MOR zeolites in chapter 2 (*i.e.* NaOH/Si = 0.46), MOR phase appeared before completion of MFI crystallization both with Zn/(Zn+Al) of 0.4 (Figure 3-9 (a)(i)-(ii)) and 0.6 (Figure 3-9 (b)(i)-(iii)). These results suggest that zincoaluminosilicate MFI zeolites was obtained by the growth of seed crystals of MFI zeolites, in competition with the nucleation of MOR zeolites, as was the case of the synthesis of zincoaluminosilicate

*BEA zeolites described in the previous section. When the amount of NaOH was decreased to NaOH/Si of 0.3, highly crystalline MFI zeolites without MOR phase was obtained by using co-precipitated gel with Zn/(Zn+Al) of 0.4 after 3 days, probably because nucleation of MOR zeolite was suppressed in the low alkalinity (Figure 3-9(a)(iii)). When the hydrothermal treatment was prolonged to 6 days, trace amount of MOR phase was observed (Figure 3-9(a)(iv)). With the co-precipitated gel with Zn/(Zn+Al) of 0.6, MFI zeolite was obtained without MOR phase with NaOH/Si of 0.3, however, the crystallinity was low compared to that obtained with Zn/(Zn+Al) of 0.4 even after 8 days (Figure 3-9(b)(iv)). When the NaOH/Si ratio was further decreased to 0.25, the crystallinity of obtained products significantly decreased with both Zn/(Zn+Al) of 0.4 and 0.6, probably because partial dissolution of seed surface was suppressed due to the low alkalinity and crystal growth of MFI was prohibited (Figure 3-9(a)(v) and (b)(v)).

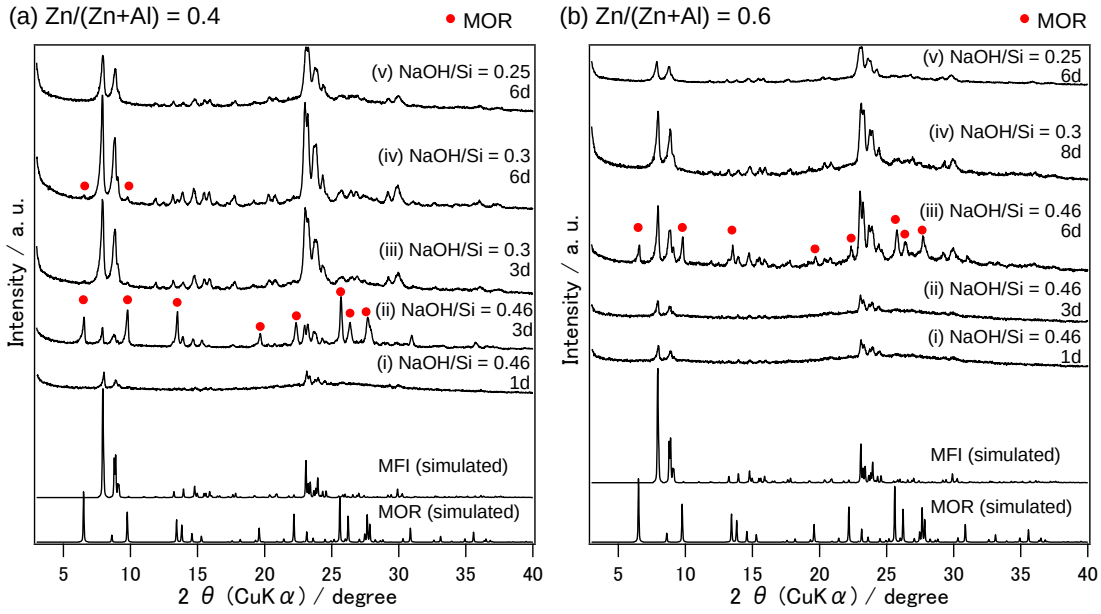

Figure 3-9 Powder XRD patterns of products synthesized from co-precipitated zincoaluminosilicate gels with Zn/(Zn+Al) of (a) 0.4 and (b) 0.6 with the addition of seed crystals of MFI zeolite by hydrothermal treatment at 170 °C. The ratio of NaOH/Si and duration of hydrothermal treatment time was varied.

To increase the crystallinity of MFI zeolite with high zinc content (Zn/(Zn+Al) = 0.6), the hydrothermal temperature was increased to 190 °C. By using the co-precipitated gel with Zn/(Zn+Al) of 0.4, highly crystalline MFI zeolite was obtained with NaOH/Si of 0.3 in 2 days, however, formation of trace amount of MOR zeolite was confirmed (Figure 3-10 (a)(ii)). When the NaOH/Si ratio was slightly decreased to 0.28, highly crystalline MFI zeolite was obtained without the formation of MOR zeolite (Figure 3-10 (a)(iii)). When the co-precipitated gel with Zn/(Zn+Al) = 0.6 was used, highly crystalline MFI zeolite was obtained with NaOH/Si of 0.3 (Figure 3-10 (b)(i)–(iii)). Formation of MOR zeolite was not observed even after 8 days (Figure 3-10 (b)(iii)), suggesting that crystal growth of MOR zeolite was suppressed in the condition with high zinc content.

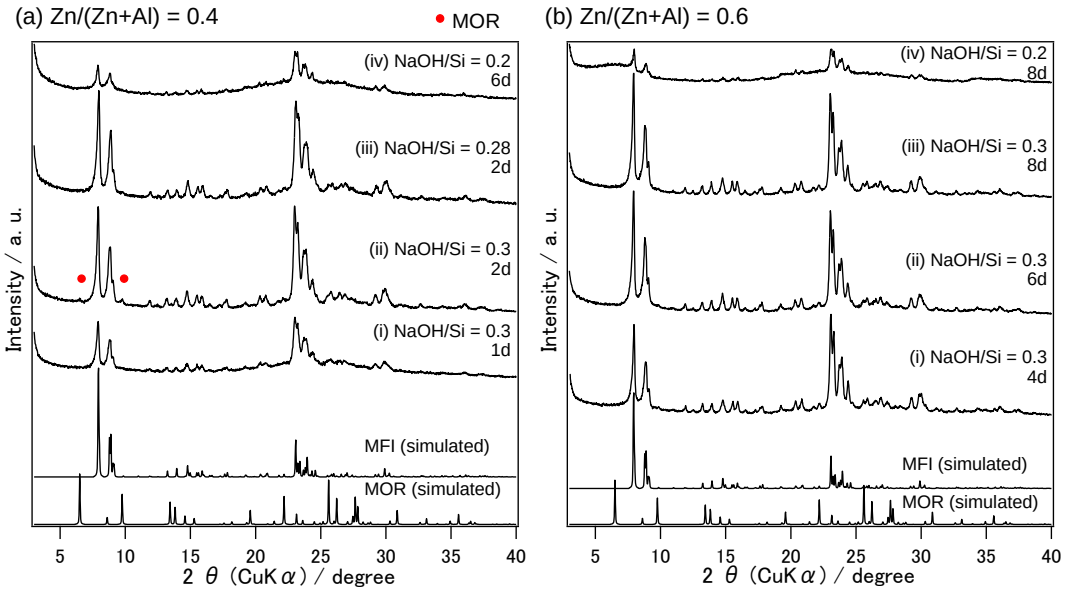

Figure 3-10 Powder XRD patterns of products synthesized from co-precipitated zincoaluminosilicate gels with Zn/(Zn+Al) of (a) 0.4 and (b) 0.6 with the addition of seed crystals of MFI zeolite by hydrothermal treatment at 190 °C. The ratio of NaOH/Si and duration of hydrothermal treatment time was varied.

Synthesis of MFI zeolites using co-precipitated gels with Zn/(Zn+Al) = 0.2 and 0.8 was also conducted. As shown in Figure 3-11(a), by using the gel with Zn/(Zn+Al) of 0.2, diffraction peaks attributed to MOR zeolites was observed with the NaOH/Si

ratio of 0.3 in both 170 and 190 °C (Figure 3-11(a)(i)–(iii) and (v)). When the NaOH/Si ratio was decreased to 0.2, the crystallization of MFI zeolite was not proceeded in both 170 and 190 °C (Figure 3-11(a)(iv) and (vii)). When the NaOH/Si ratio was adjusted to 0.28, highly crystalline MFI zeolite was obtained without MOR formation after hydrothermal treatment at 190 °C for 20 hours (Figure 3-11(a)(vi)). On the other hand, when the gel with Zn/(Zn+Al) of 0.8 was used, formation of MOR zeolite was not observed in any conditions, in agreement with the results described in Chapter 2. When the hydrothermal treatment was conducted at 170 °C, MFI zeolite with high crystallinity was not obtained after 9 days with NaOH/Si of 0.3 and 0.4 (Figure 3-11(b)(i) and (ii)), and when the synthesis time was prolonged to 12 days, unknown impure phase was observed (Figure 3-11(b)(iii)). When the temperature was increased to 190 °C, MFI zeolite was obtained after 6 days wih NaOH/Si of 0.3 (Figure 3-11(b) (vii)).

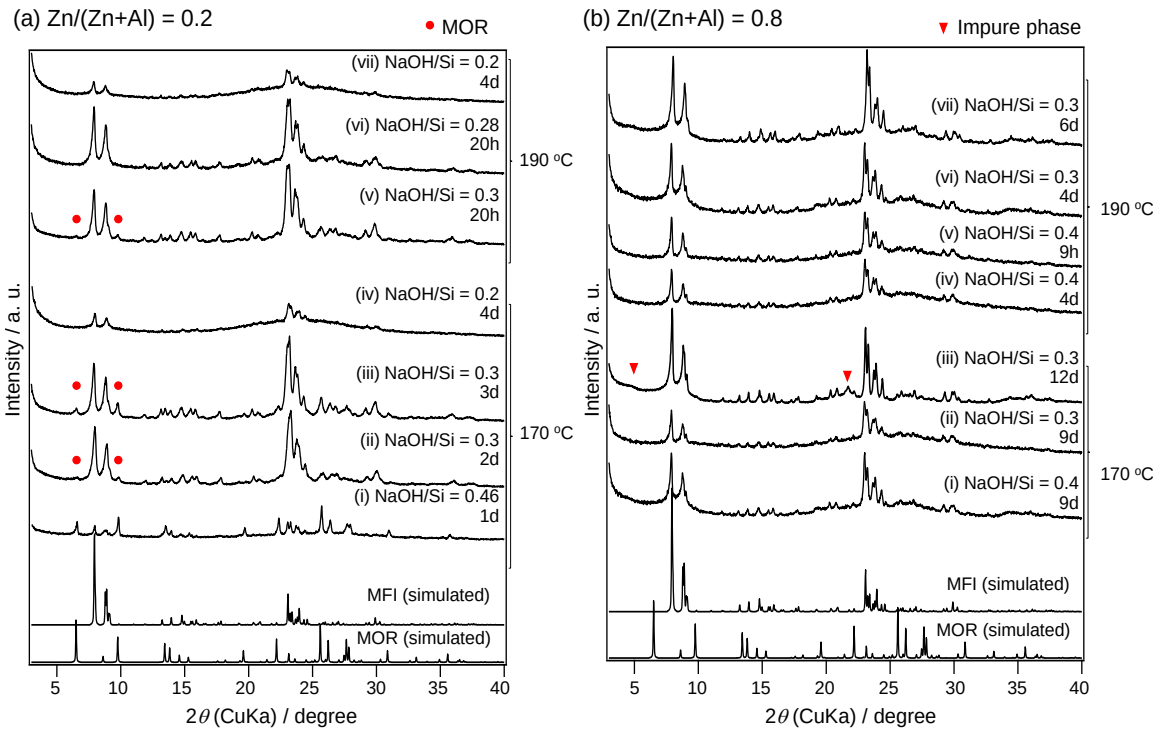

Figure 3-11 Powder XRD patterns of products synthesized from co-precipitated zincoaluminosilicate gels with Zn/(Zn+Al) of (a) 0.2 and (b) 0.8 with the addition of seed crystals of MFI zeolite by hydrothermal treatment at 170 °C and 190 °C. NaOH/Si ratio and duration of hydrothermal treatment time was varied.

Figure 3-12 shows FE-SEM images of zincoaluminosilicate MFI zeolites successfully prepared using co-precipitated gels with Zn/(Zn+Al) = 0.2 (NaOH/Si = 0.28, 190 ^{o}C, 20 hours), Zn/(Zn+Al) = 0.4 (NaOH/Si = 0.28, 190 ^{o}C, 2 days), Zn/(Zn+Al) = 0.6 (NaOH/Si = 0.3, 190 ^{o}C, 4 days) and Zn/(Zn+Al) = 0.8 (NaOH/Si = 0.3, 190 ^{o}C, 6 days) with the optimized conditions. Those samples are referred to as Zn0.2 MFI, Zn0.4 MFI, Zn0.6 MFI and Zn0.8 MFI. The obtained MFI zeolites with Zn/(Zn+Al) = 0.2 possess needle like structures with length of 3–5 μm (Figure 3-12(a)). When the zinc content was increased to Zn/(Zn+Al) = 0.4, the obtained crystals had morphology with needles aggregate at a center point and stretch to the around, forming snowflake-like clusters (Figure 3-12(b)). It is clear that with the increasing content of zinc, the thickness of the needles became thicker and number of needles aggregated around the same center increased, forming a larger cluster. These findings indicated that this novel morphology of crystals cluster depends on zinc amount. It has been reported that increase of twinned crystals is one evidence for substitution of isomorphous heteroatoms in the zeolite framework.[202,167] Therefore, this twined morphology is supposed to be correlated with the existence of zinc in zeolite frameworks.

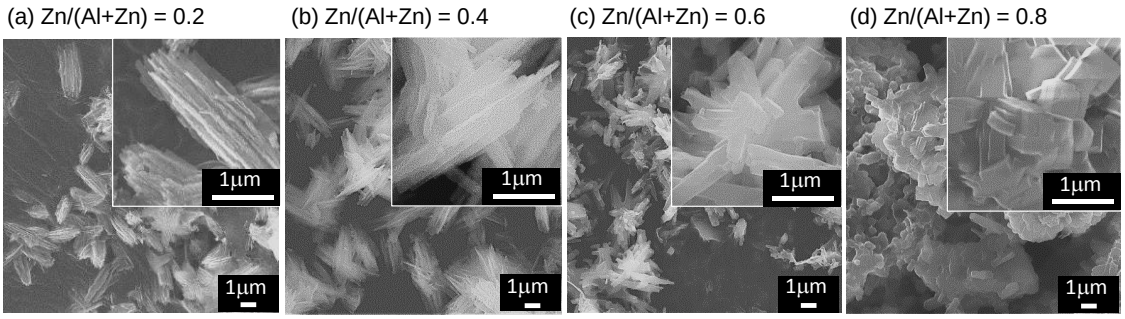

Figure 3-12 FE-SEM images of products synthesized from co-precipitated zincoaluminosilicate gels with Zn/(Zn+Al) of (a) 0.2, (b) 0.4, (c) 0.6 and (d) 0.8 with the addition of seed crystals of MFI zeolite .

Figure 3-13 compares the diffraction peaks in powder XRD patterns of those zincoaluminosilicate MFI zeolites. As is shown clearly in Figure 3-13(b), the diffraction peaks are shifted to lower angle with the increase in zinc content. These results suggest a lattice expansion due to the larger size of Zn atoms than that of Si.

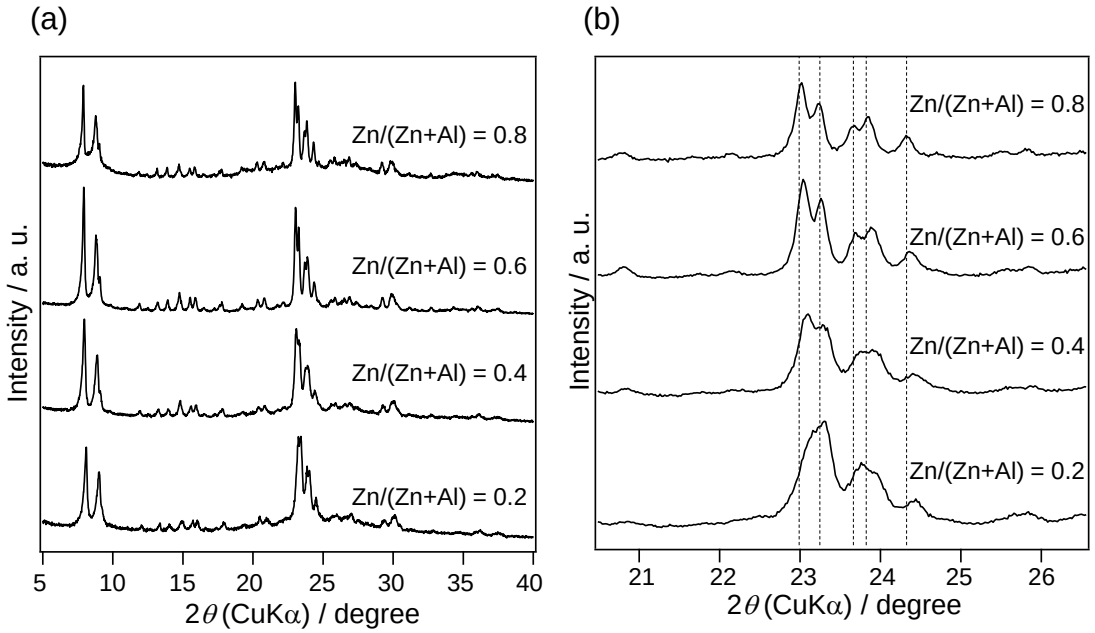

Figure 3-13 Powder XRD patterns of products synthesized from co-precipitated zincoaluminosilicate gels with Zn/(Zn+Al) of 0.2, 0.4, 0.6 and 0.8 with the optimized conditions using seed crystals of MFI zeolite.

Chemical compositions and micropore volumes of the obtained MFI zeolites are summarized in Table 3-3. The molar Zn/(Zn+Al) ratios of the zeolite products were almost the same as those of the initial zincoaluminosilicate gels. It was also confirmed that the obtained MFI zeolites had high micropore volumes. The micropore volumes were slightly decreased with the Zn/(Zn+Al) ratio of 0.8, probably because of the high content of sodium inside the pore, or higher atomic weight of zinc compared to aluminum. Since the Na/(Zn+Al) ratio is close to 1 for all samples, most of zinc species are expected to generate one negative charge per the atom.

Table 3-3 Chemical compositions and micropore volumes of the obtained zincoaluminosilicate MFI products

Zn/(Zn+Al) (Initial)	Si/(Zn+Al) [a]	Zn/(Zn+Al) [a]	Na/(2Zn+Al) [a]	Na/(Zn+Al) [a]	V_{micro} [b]/ cm^2g^{-1}	S_{BET} [c]/ m^2g^{-1}
0.2	6.69	0.17	0.76	0.89	n. d. [d]	n. d. [d]
0.4	7.03	0.37	0.75	1.03	0.08	220
0.6	7.20	0.55	0.73	1.13	0.08	250
0.8	7.69	0.74	0.62	1.08	0.06	200

[a]Determined by ICP-AES. [b]Micropore volumes determined by a *t*-plot method. [c]BET surface area. [d]Not determined.

Solid-state ^{27}Al MAS NMR measurements were conducted to investigate the local environments of Al species in the zincoaluminosilicate MFI zeolites. As shown in Figure 3-14, no octahedrally coordinated Al species, generally appearing at a chemical shift (δ) of ca. 0 ppm, were observed in the zincoaluminosilicate MFI zeolites prepared using zincoaluminosilicate gels with Zn/(Zn+Al) of 0.4, 0.6 and 0.8 in the optimized conditions. In all samples, only one resonance at around δ = 54.2–54.7 ppm, corresponding to tetrahedrally coordinated Al, was observed. This suggests that all Al species are incorporated in the silicate structures in a four-coordination.

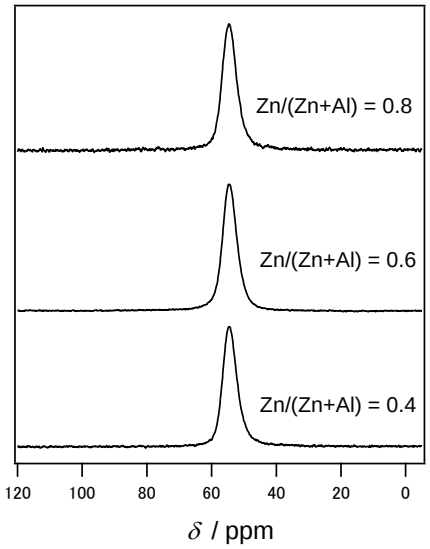

Figure 3-14 Solid-state ^{27}Al MAS NMR spectra of zincoaluminosilicate MFI zeolites obtained from gels with of Zn/(Zn+Al) of 0.4, 0.6 and 0.8.

Figure 3-15 shows solid-state ^{29}Si MAS NMR spectra of Zn0.2 MFI, Zn0.4 MFI and Zn0.6 MFI. The spectra were deconvoluted to three signals attributed to Q^4(0T) silicon species (*Si*$(OSi)_4$) at δ around −110 ppm, Q^4(1T) silicon species (*Si*(OT)$(OSi)_3$) at δ of ca. −105 ppm, and Q^4(2T) silicon species (*Si*$(OT)_2(OSi)_2$) at δ of ca. −95 ppm, where T stands for substituted Zn or Al atoms. The peak shifts derived from substituted Zn and Al are calculated together here because it has been difficult to distinguish Q^4(1Zn) and Q^4(1Al). The broader peak in low shift range is probably due to contribution from Zn species. Si/(Zn+Al) ratio was calculated for each samples from the peak areas of the three peaks using following formula.

$$\left(\frac{\mathrm{Si}}{\mathrm{T}}\right)\mathrm{NMR} = \sum_{n=0}^{4} I_{\mathrm{Si}(n\mathrm{T})} \Big/ \sum_{n=0}^{4} \left(\frac{n}{4}\right) I_{\mathrm{Si}(n\mathrm{T})}$$

The Si/(Zn+Al) ratios calculated from the ^{29}Si MAS NMR spectra are close to the ratios obtained by ICP-AES analysis. The concurrence of the chemical compositions calculated from ^{29}Si MAS NMR and ICP-AES results suggests the successful incorporation of Zn and Al atoms into the zeolite frameworks. The Zn0.6 MFI exhibited slightly smaller Si/(Zn+Al) ratios calculated from NMR spectra compared to those of ICP-AES results, likely indicating the presence of some silanol defects in the zeolites.

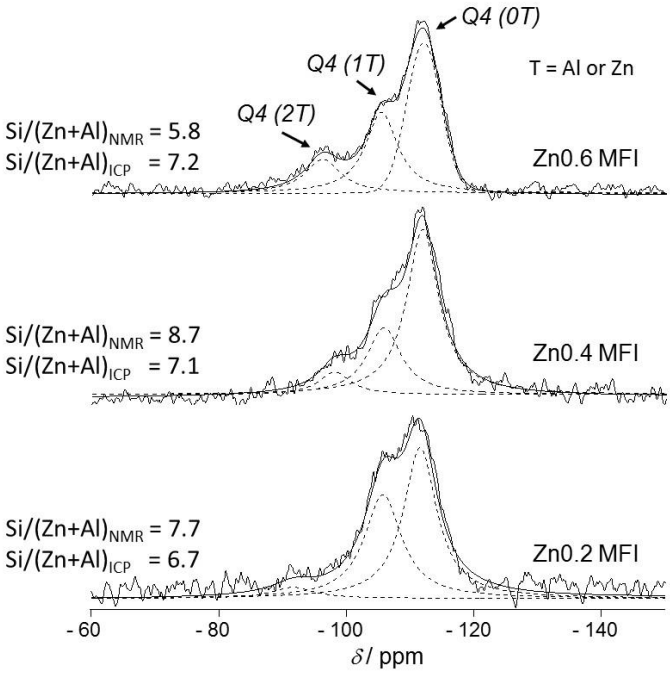

Figure 3-15 Solid-state ^{29}Si MAS NMR spectra and their peak deconvolution of MFI zeolites obtained from gels with of Zn/(Zn+Al) of 0, 0.4, and 0.6 (i.e., Zn0.2 MFI, Zn0.4 MFI and Zn0.6 MFI).

3.3.4 Environments of Zn in Zincoaluminosilicate Zeolites

The environment of zinc species in the obtained zincoaluminosilicate MFI zeolites was investigated in the view of ion-exchange capability for a divalent cation. Ni^{2+} was used as a model cation of divalent cations because Ni-exchanged zeolites show promising catalytic activity for dimerization and oligomerization of alkenes.[152,182,183] The aluminosilicate MFI zeolite used as seed crystals and zincoaluminosilicate MFI zeolites obtained from zincoaluminosilicate gels with Zn/(Zn+Al) of 0.4, 0.6 and 0.8 was tested in the ion- exchange experiments. Chemical compositions of the products recovered after ion-exchange are summarized in Table 3-4. The Ni/(Zn+0.5Al) ratio was almost 1 for the aluminosilicate MFI and zincoaluminosilicate MFI obtained from zincoaluminosilicate gels with Zn/(Zn+Al) of 0.4 and 0.6. This results suggest that the ion-exchange ratio reached 100% when all Zn species in the sample are assumed to generate two negative charges per the atom, being dication ion-exchangeable sites.

Considering that Si/Al ratio in aluminosilicate MFI is limited,[169] the zincosluminosilicate MFI zeolites are expected to achieve higher amount of Ni^{2+} introduced to zeolite than aluminosilicate MFI zeolites on the basis of weight ratio. As shown in Table 3-4, the weight percent of introduced nickel increased with the increasing content of zinc. These results suggested that zincoaluminosilicate MFI zeolites would be efficient materials for hosting divalent cations.

Table 3-4 Chemical compositions of the products after ion-exchange with Ni^{2+} cations[a]

	Si/(Al+Zn)	Zn/(Al+Zn)	Ni/(Zn+0.5Al)	Ni/(0.5Zn+0.5Al)	Ni wt%
Ni_MFI (Seed)	10.129	0.000	1.044	1.044	4.1
Ni_MFI (Zn/(Al+Zn) = 0.4)	7.437	0.326	1.041	1.381	6.9
Ni_MFI (Zn/(Al+Zn) = 0.6)	7.285	0.519	1.065	1.619	8.2
Ni_MFI (Zn/(Al+Zn) = 0.8)	7.524	0.735	0.894	1.552	8.0

[a]Determined by ICP-AES.

3.4 Conclusion

By using the zincoaluminosilicate gels prepared by co-precipitation, organic free synthesis of zincoaluminosilicate *BEA and MFI zeolites was achieved by seed assisted method. The synthesis was conducted by adding the seed crystals of target zeolite to the synthetic mixture which yields MOR zeolite with the absence of seeds. It was also shown that synthesis conditions such as NaOH/Si ratio and temperature of hydrothermal treatment should be optimized to prevent spontaneous nucleation of MOR zeolites before the completion of crystallization of the targeted zeolites. These results can be understood by the CBU hypothesis which established for aluminosilicate zeolites, since the MOR, *BEA and MFI zeolites have a common CBU in their topologies. This achievement showed the possibility to prepare various zinc containing zeolites in an

OSDA-free manner by applying the CBU hypothesis as have been achieved with various aluminosilicate zeolites. The *BEA and MFI zeolites were obtained by using zincoaluminosilicate gels with Zn/(Zn+Al) = 0.1–0.2, and 0.2–0.8, respectively, while the MOR zeolites were prepared by using the gels with Zn/(Zn+Al) of 0.1–0.6. These results suggested that the limitation in zinc introduction differs depending of the structures of zeolites. Distortion in the structures caused by the longer Zn-O bonds can be the one reason of the existence of upper limit. Both zinc and aluminum in the zeolite structure were proved to be ion exchange sites.

Chapter 4. Synthesis of Zincosilicate Zeolites from Zincosilicate gels prepared by an Organic Structure-Directing Agent Involved Co-precipitation Method

4.1 Introduction

As described in Chapter 2 and 3, preparation of co-precipitated zincoaluminosilicate composite gels is quite important to form zinc-containing zeolites by preventing precipitation of zinc species. To further extend the applicable scope of the method toward various zeolite structures and compositions, co-precipitation involving organic structure-directing agents (OSDAs) is conducted.

It has been reported that silicate species in OSDA-containing environment form structures relevant to final zeolite structures prior to hydrothermal treatment. For example, formation of silicate structures upon gradual addition of TEOS to concentrated tetrapropylammoniumoxide (TPAOH), which crystallizes MFI, and tetrabutyllammoniumoxide (TBAOH), which crystallizes MEL was investigated. It was revealed that the small particles having relevant structures of final zeolite formed by the respective OSDA.[203,204,205,206] Dry gel conversion (DGC) techniques are the method for synthesizing zeolites that hydrogel is dried and crystallized to zeolites in the presence of steam (*e.g.* high-silica *BEA[207], high-silica MOR[208] and methylene-bridged MOR[209] synthesis in steam) or in a mixed vapor of steam and OSDAs (*e.g.* MFI and FER synthesis in Et_3N and EDA vapor[210]).[211] This method have accomplished various zeolites with compositions which had been previously not available.[211] In the steam-assisted crystallization method, dried aluminosilicate gel containing OSDAs was investigated during the course of crystallization.[212] The effect of OSDAs in the initial structure of dried gel to form "4-2"-type unit which plays a significant role in the crystallization of *BEA-type zeolite was confirmed.[212] Changes in distribution of tetraethylammonium cation (TEA^+) in dry gels during crystallization period was also

investigated by temperature programmed decomposition and NMR technique.[213] It has been also shown that the DGC method is useful to form metallosilicates, such as, Ti-*BEA,[214] B-*BEA, B-MFI and B-MWW.[215] Synthesis of Zn-*BEA was also attempted, but it was succeeded only in very low initial zinc content (Si/Zn = 100 – 200).[211]

As described above, interaction of OSDAs and silicate species (and other metal sources) prior to hydrothermal treatment significantly affects the resulting zeolites. The co-precipitation method can be considered as a promising method to achieve well-mixed metallosilicate material with charge-balancing organic cations. In contrast to Chapter 2 and 3, in which sodium cation was used as the counter cation, tetraethylammonium (TEA^+) cation was occluded in co-precipitated zincosilicate gels as charge-balancing cations in this chapter. TEA^+ is a common OSDA for *BEA zeolite, therefore the prepared TEA-zincoaluminosilicate gels are expected to be suitable precursors for zinc-containing *BEA zeolite.

4.2 Experimental

4.2.1 Materials

The following chemicals were used as received for zeolite synthesis: Fumed silica (Cab-O-Sil M-5, Cabot Co.), zinc acetate (Wako Pure Chemical Industries, Ltd.), Lithium hydroxide monohydrate (Wako Pure Chemical Industries, Ltd.), tetraethylammonium hydroxide (TEAOH) solution (35 wt%, Sigma-Aldrich) and Ludox-HS (Sigma-Aldrich Co. LLC.).

4.2.2 Preparation of Zincosilicate Gels Using an Organic Structure-Directing Agent

The zincosilicate gels were prepared by organic structure-agent involved co-precipitation method. To prepare silicate solution, fumed silica and TEAOH solution (35 wt%) was mixed in a plastic vessel and heated at 80 °C in oven with tumbling at 20 rpm. The molar ratio of the solution was SiO_2 : TEAOH : H_2O = 1 : 0.75 : 11.6. After

the heating for 2 hours, fumed silica was totally dissolved and clear solution was obtained. Zinc solutions were prepared by mixing zinc sulfate and sulfuric acid. The molar ratio of these two solutions was, in total, SiO_2 : TEAOH : Zn : SO_4 = 1 : 0.75 : *x* : 0.38, where the *x* was varied from 10 to 30. The volume ratio of the silicate solution and the zinc solution was adjusted to be 3:1 by addition of distilled water. For example, in a typical procedure to prepare the zincosilicate gel with Si/Zn of 10 (*x* = 0.1), 25 g of fumed silica was added to 130 g of TEAOH solution (35 wt%) and heated at 90 ºC in an oven. Note that the amount of solution should be less than 10 % of the maximum capacity of the plastic vessel, otherwise the plastic vessel will not stand the pressure rise. After the dissolution of fumed silica and subsequent cooling of the solution, 786 g of distilled water was added to the solution and mixed well. In another vessel, 6.7 g of zinc sulfate was dissolved in 262 g of distilled water, and sulfuric acid (1mo/L) 137 g was added to the solution. The prepared silicate solution and zinc sulfate solutions were gradually mixed by using two peristaltic pumps. The mixing and the precipitation were performed in a vessel with an overflow tube under neutral pH at 40 °C. The feed ratio of the sodium silicate solution and the sulfate solution was kept at 3:1 (by volume). The averaged residence time of the gel slurry (= vessel volume/total feed rate) was kept at around 15 min, so that the vessel volume and both of the feed rates were optimized. The neutralized suspension containing the zincoaluminosilicate gel was collected and recovered by a centrifugal separator. The gel was thoroughly washed with deionized water. The water content in the gel was measured from a weight loss after calcination at 600 °C for 4 h. To remove the occluded TEA cations in the zincosilicate gels while retaining the silicate structure, two-step calcination was conducted as shown in Figure 4-1.[176] In the first step, the samples were heated in nitrogen flow to carbonize the organic species in the samples. Subsequently, the samples were heated in air flow to remove the carbon from the samples.

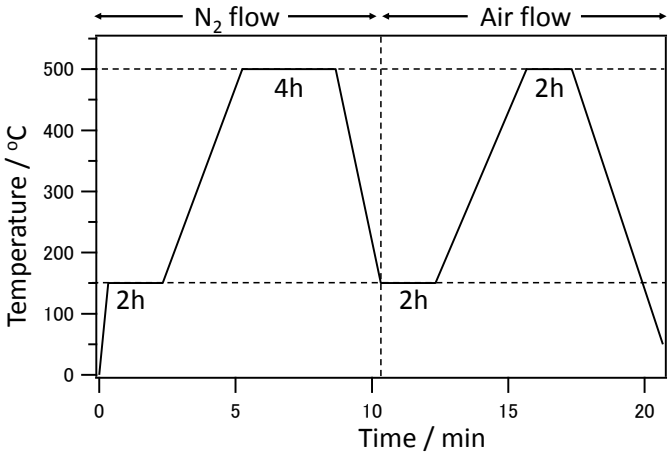

Figure 4-1 A calcination profile to remove TEA^+ from zincosilicate gels. The ramping rate was 2 K min^{-1}.

4.2.3 Synthesis of *BEA Zeolites from Zincosilicate Gels

Synthesis of zincosilicate *BEA zeolites were conducted using the zincosilicate gels prepared by the OSDA involved co-precipitation. First, lithium hydroxide monohydrate was dissolved to distilled water and subsequently, 35 wt% TEAOH solution was mixed to the solution. Then, seed crystals of *BEA zeolite (UniZeo, TEA023) were dispersed in the solution. Finally, the zincosilicate gel was added and mixed vigorously. In a typical procedure, the chemical compositions of the reaction mixtures (without seed crystals) were 0.02 LiOH : 0.45 : TEA : *x* ZnO: 1.0 SiO_2: 30 H_2O, where *x* was varied as 30–10 according to the composition of the prepared zincosilicate gels. The weight of seed crystals was 10 wt% or 20 wt% (on a basis of SiO_2). The hydrothermal synthesis was carried out in a 60 mL autoclave or 23 mL Teflon-lined stainless autoclave at 150 °C–210 °C for 20–96 h under a static condition. After completion, the solid product was recovered by filtration and washed with deionized water until the filtrate reached pH 7–8. The product was dried at 80 °C overnight before subsequent characterizations.

For comparison, synthesis of *BEA zeolites using conventional sources of Si and Zn, namely, colloidal silica (Ludox) and zinc acetate, respectively, was also carried out. Typically, lithium hydroxide was dissolved in TEAOH aqueous solution and subsequently, zinc acetate was added to the solution. After the dissolution of zinc

acetate, colloidal silica (Ludox HS-40) was added drop wise. Then, the resultant mixture was stirred at 500 rpm at room temperature for 1 day. Finally seed *BEA crystals were dispersed in the resulting solution and the mixture was stirred vigorously. The resulting homogeneous mixture was transferred to an autoclave and hydrothermal synthesis was conducted similarly as described above.

4.2.4 Characterization

Powder X-ray diffraction (XRD) analysis was conducted to determine the crystal structure of the products using a diffractometer (Rigaku Ultima IV) operated with Cu Kα monochromatized radiation at 40 kV and 40 mA. Elemental analysis of the products was performed by inductively coupled plasma-atomic emission spectrometry (ICP-AES, Thermo iCAP 6300) after dissolving the products in hydrofluoric acid or potassium hydroxide solutions. To observe crystal size and morphology, field-emission scanning electron microscopy (FE-SEM) images were obtained from JFM-7500FA (JEOL) at an accelerating voltage of 15 kV. Nitrogen adsorption–desorption measurements were performed on Quantachrome Autosorb-iQ2-MP at liquid nitrogen temperature. Prior to the measurements, the samples were degassed at 350 °C for 6 h under vacuum. Diffuse reflectance (DR) UV–vis spectra in the range over 190 nm were recorded on a JASCO V-670 spectrometer in the 190−800 nm wavelength range using barium sulfate as a reference. CHN elemental analyses were carried out on a CE-440 elemental analyser (Exeter Analytical) to measure the carbon, hydrogen, and nitrogen percentage of the samples which are related to the amount of organic substance in zeolite pores. Raman spectra of the solid products were collected on an NRS-5100 (JASCO) by using a laser of 532 nm. High-energy X-ray total scattering (HEXTS) measurements were conducted to elucidate the zincosilicate structures in the gels at the beam line of BL04B2 (SPring-8, Japan) with a horizontal two-axis diffractometer, dedicated to glass and liquid amorphous materials. The powder sample was introduced to a quartz capillary with an alumina ball and vacuum grease on top. The incident photon energy was 61.43 keV (λ= 0.2018 Å). The maximum Q ($Q = 4\pi \sin \theta / \lambda$; where θ is scattering angle, λ is the wavelength of the photons), Q_{max}, collected in this study was 25 $Å^{-1}$.[216] The obtained data were subjected to well-established analysis procedures, such as absorption,

background, and Compton scattering corrections, and then normalized to give the Faber−Ziman total structure factor, S(Q).[217] Then, the pair distribution function, G(r), was calculated from S(Q) by using the following equation:

$$G(r) = 4\pi r[\rho(r) - \rho_0] = \frac{2}{\pi}\int_{Q\,\mathrm{min}}^{Q\,\mathrm{max}} Q[S(Q) - 1]\sin(Qr)\,\mathrm{d}Q$$

where ρ_0 is the atomic number density.

.

4.3 Results and Discussion

4.3.1 Characterization of Zincosilicate Gels

The chemical compositions of the co-precipitated zincosilicate gels are shown in Table 4-1. The ratios of Si/Zn of the gels were measured by ICP analysis. It was found that the Si/Zn ratio was almost identical to the initial ratios of zinc sulfate and fumed silica used in the co-precipitation, suggesting that most of zinc and silicon species in the solutions precipitated as the gels during the co-precipitation processes. When zinc species are introduced to silicate framework, negative charge will be generated to compensate the difference in the atomic valence. Therefore, positively charged TEA^+ ions are expected to be occluded in the gels to balance the charge. The amount of TEA^+ in the gels were calculated from CHN analysis. In the analysis, by complete combustion of the samples in oxygen flow, C is detected as CO_2, N is detected as N_2 (after reduction process), and the amount of H is detected as H_2O. As shown in the table, the C/N ratio detected in the analysis was 7.8–8.2, suggesting that almost all of the organics occluded in the gels are TEA^+ cations (C8H20N) which should give the C/N ratio of 8.0. Assuming that obtained zincosilicate gels were composed of oxides (zincosilicate), TEA^+ and water, molar composition of the zincosilicate gels were calculated from the results of ICP analysis and CHN analysis. The ratio of oxides/TEA^+ was calculated from the results of CHN analysis, and ratio of Zn/Si was calculated from the values measured in the ICP analysis. As shown in the Table 4-1, the value of TEA^+/Zn was 1.74 when the Si/Zn was 32.7, and TEA^+/Zn was 0.78 when the Si/Zn was 10.9. Zn species in silicate frameworks are expected to have various structures as shown in Figure 4-2. With Zn

species that datively coordinate an oxygen of two neighboring silanols (Figure 4-2(a)), no extra cations are occluded in the ion-exchange sites. On the other hand, with the Zn site with a neighbouring silanol group (Figure 4-2(b)) and defect-free Zn site linking to four silicons *via* oxygen bridges (Figure 4-2(c)), one negative charge and two negative charges are generated to silicate framework, respectively, with charge-balancing cations in the ion-exchange sites. According to the observation of TEA/Zn ratio, which should be 0, 1 and 2 when all zinc species are in the structures of (a), (b) and (c) in Figure 4-2, respectively, in the zincosilicate gels with low zinc content (Si/Zn = 32.7) the site (c) exists dominantly, and with increasing content of zinc, the zinc site (a) and (b) increased.

Table 4-1 Chemical Compositions of the zincosilicate gels prepared by co-precipitation with TEAOH

Initial Si/Zn	ICP results	CHN results					Composition (mol)		
	Si/Zn	C(wt%)	H(wt%)	N(wt%)	R[a](wt%)	C/N (mol)	TEA	ZnO	SiO_2
10	10.9	6.11	2.37	0.91	90.6	7.8	0.78	1	10.9
15	16.5	6.09	2.33	0.87	90.7	8.2	0.83	1	16.5
20	18.4	7.25	2.58	1.05	89.1	8.1	1.16	1	18.4
25	26.7	7.21	2.51	1.07	89.2	7.9	1.41	1	26.7
30	32.7	6.84	2.35	0.98	89.8	8.1	1.74	1	32.7

[a] : The residue remained after complete combustion

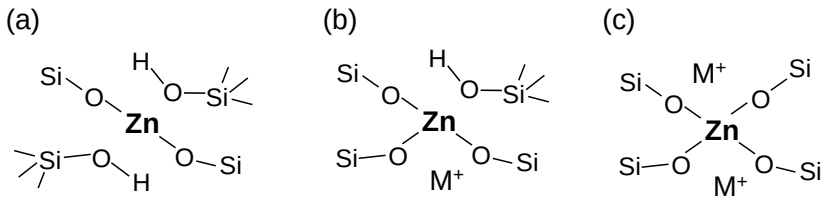

Figure 4-2 Local structures of Zn sites. M^+ is a monovalent cation.

To further verify the state and dispersity of zinc in the zincosilicate gels, DR UV–vis spectra of the obtained zincosilicate gels were measured. As shown in Figure 4-3, three major absorption bands were observed at around 250 nm, 210 nm and below 200 nm. No absorption band assigned to ZnO, which is observed at around 360–380 nm due to the $O^{2-} \rightarrow Zn^{2+}$ ligand-to-metal charge transfer transition,[173] was observed for all samples in spite of the high content of zinc. It has been reported that the absorption peak at around 250 nm is attributed to the interaction of Zn^{2+} ion with the zeolite framework.[218] The absorption band around 210 nm are ascribed to TEA cations.[219] The absorption band observed below 200 nm can be assigned to the charge transfer transitions of Zn in the silicate structure with lattice O^{2-}. From the observation that the absorption band below 200 nm is more distinct compared to the band around 250 nm, it is suggested that isolate zinc species in silicate structure is the major component in the zincosilicate gels. To verify the stability of zincosilicate structure, two-step calcination of the gel was conducted at 500 °C for 2 h in nitrogen flow, and subsequently, 500 °C for 2 h in air flow (Figure 4-1). Even after the calcination, absorption band assigned to ZnO was not observed, suggesting that Zn in the gels was stable against the formation of ZnO, providing additional evidence of the high dispersity of Zn in the silicates. After the calcination, the sharp absorption band observed below 200 nm, which attributed to zinc in silicate structure, decreased. On the other hand, absorption band around 250 nm which attributed to Zn^{2+} species out of silicate structure, increased. Additionally, absorption band around 285 nm was observed. The additional absorption band observed at around 285 nm is probably assigned to Zn-O-Zn bridging species formed in the zeolite pores which have been observed at around 275 nm.[220,221,131] These results suggested that some of the zinc species in the silicate structures were removed from the silicate structure by thermal treatment, though significant amount of ZnO was not formed.

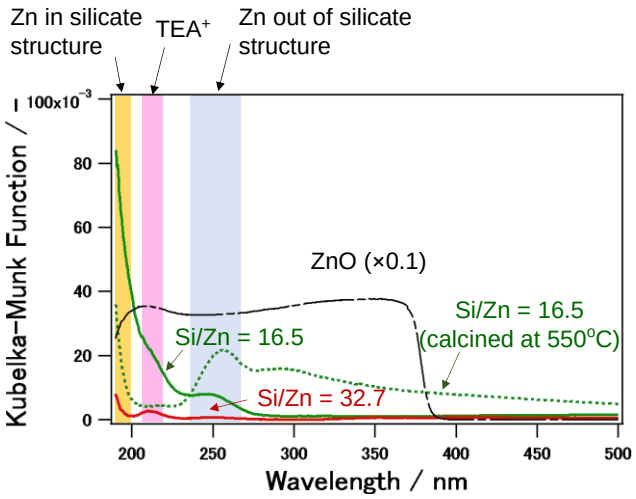

Figure 4-3 DR UV-Vis spectra of obtained zincosilicate gel (Si/Zn = 16.5 and 32.7) dried at 80 °C and zincosilicate gel (Si/Zn = 16.5) after two step calcination (Figure 4-1, 500 °C for 2 h in nitrogen flow, and subsequently, 500 °C for 2 h in air). A spectrum of ZnO is shown for comparison.

Raman spectroscopy was employed to obtain information about the confirmation of TEA^+ occluded in the zincosilicate gels. Figure 4-4 shows the Raman spectra of zincosilicate gels with Si/Zn ratio of 10.9, 19.8, and 26.7 prepared by the co-precipitation using TEAOH. TEA^+ cation in aqueous solution consisted of two stable conformers with all-trans (*tt.tt*, D_{2d}) and trans-gauche (*tg.tg*, S_4) arrangements in a ratio of 1:1.[222,223,224] The two conformers exhibited two different Raman bands of different C_4N tetrahedral symmetric stretching mode. As shown in Figure 4-4, the Raman spectrum of the prepared zincosilicate gels presented both peaks assigned to *tt.tt* and *tg.tg* conformers, respectively. From two bands centered at 662 and 673 cm^{-1}, fractions of *tg.tg* and *tt.tt* conformers, respectively, can be estimated by deconvolution of the spectra. Ratios of the peak areas of two Raman bands attributed to *tt.tt* and *tg.tg* was calculated to be 1.7:1 for the zincosilicate gel with Si/Zn ratio of 26.7. The fraction of *tg.tg.* is higher than that in the aqueous solution phase. It has been reported that the conformational changes occur to fit TEA^+ by minimizing unoccupied free space and simultaneously to maximize the interaction with substituted metal atoms.[225] The TEA^+ cations probably interact with the formed zincosilicate structure and occluded in the gels with the conformational changes.

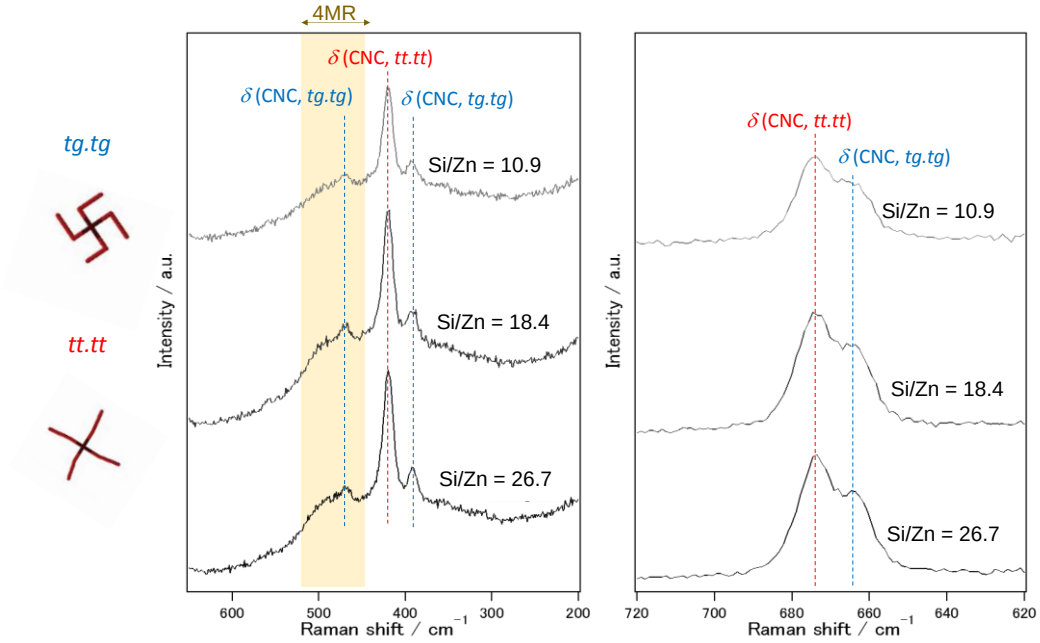

Figure 4-4 Raman spectra of TEA-zincoaluminosilicate gels with Si/Zn ratio of 10.9, 19.8, and 26.7.

After the calcination at 300 ºC for 4 hours or 500 ºC for 5 hours, the obtained zincosilicate gels showed high microporosity (Table 4-2). For comparison, the micropore volumes of Na-zincoaluminosilicate gel (Si/(Zn+Al) = 8.0, Zn/(Zn+Al) =0.6) prepared by the co-precipitation without TEAOH was also shown in Table 4-2. In contrast to the zincosilicate gels prepared with TEAOH, the Na-zincoaluminosilicate gel possessed almost no micro porosity. Figure 2-15 shows nitrogen adsorption–desorption isotherms of co-precipitated TEA-zincoaluminosilicate gel with Si/Zn of 15 and Na-zincoaluminosilicate gels with Zn/(Zn+Al) of 0.6. The zincosilicate gels prepared using TEAOH showed type I isotherms indicative for microporous solids.[2] On the other hand, the Na-zincoaluminosilicate gels showed likely type II isotherms generally given by physisorption of gases on nonporous or macroporous solids.[2] The micropores are likely formed by the removal of TEA^+ in the zincosilicate gels.

From these results, it is suggested that the TEA^+ cation is occluded in the silicate structure of the gel forming the microporous structure.

Table 4-2 Micropore volumes and BET surface areas zincosilicate gels prepared by co-precipitation with TEAOH

Initial Si/Zn	Initial Zn/(Zn+Al)	Calcination	S_{BET}[b] /m^2g^{-1}	V_{micro}[a] /cm^3g^{-1}
10		300 °C, 4h	420	0.136
15		300 °C, 4h	430	0.143
15		550 °C, 5h	350	0.105
13.3[c]	0.6	300 °C, 4h	80	0.002
13.3[c]	0.6	550 °C, 5h	60	0.002

[a]Micropore volumes determined by a *t*-plot method. [b]BET surface area. [c]The Na-zincoaluminosilicate gel prepared by co-precipitation without TEAOH as described in chapter 2 and 3.

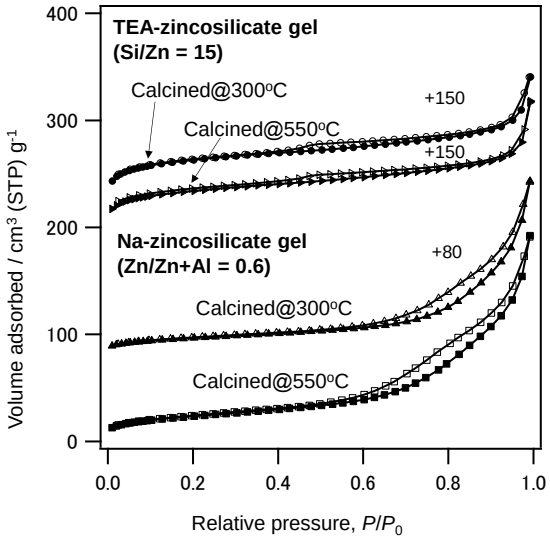

Figure 4-5 Nitrogen adsorption–desorption isotherms of co-precipitated TEA-zincoaluminosilicate gel with Si/Zn of 15 and Na-zincoaluminosilicate gels with Zn/(Zn+Al) of 0.6.

Structural evolution of zincosilicate gels in an intermediate range order was investigated by HEXTS measurements.[216] For comparison, the co-precipitation using NaOH was conducted to prepare zincosilicate gels with similar Si/Zn ratio but without occluded TEA^+. The chemical compositions of the zincosilicate gels used for the HEXTS analysis are summarized in Table 4-3. Figure 4-6 shows the total structural

factors, S(Q), of the zincosilicate gels. The S(Q) of the zincosilicate gels exhibited the oscillation typically observed in amorphous aluminosilicates without sharp peaks. Figure 4-7 shows the pair distribution functions, G(r), of the zincosilicate gels. The peaks at 1.60, 1.98, 2.63, and 3.11 Å correspond to the distances of the first nearest Si−O, Zn−O, O−O, and Si−Si(Zn) and O−Zn−O, respectively.[151] These peaks are commonly seen regardless of sizes and structures of silicate rings.[216,176,151] G(r) above 3.5 Å gives useful information on medium-range structures of silicates. Figure 4-7(a) compares zincosilicate gels with Si/Zn of around 20. There is no significant difference between the zincosilicate gel prepared by co-precipitation using NaOH and that prepared by co-precipitation using TEAOH. The small peak at 2.25 Å seen in the zincosilicate gel prepared by co-precipitation using NaOH likely corresponds to the distances of Na−O. Note that the peak observed at 3.73 Å, which is assigned to the second nearest T−O distances (T: tetrahedral atoms, in these cases, Si and Zn) of 4Rs and 5Rs, is more distinct compared to that observed in amorphous silica.[151] Figure 4-7(b) compares zincosilicate gels with Si/Zn of around 10. Correlation of the second nearest neighbor of T-O in 3MR is around 3.3 Å which appears as a tail of the peak of 3.1 Å.[151] This tail peak is slightly pronounced for the zincosilicate gel prepared by co-precipitation using NaOH compared with that prepared by co-precipitation using TEAOH. This result suggested that the high content of zinc in the sodium silicate has an effect on formation of 3MR, while the addition of TEA^+ as a counter cation suppress the 3MR formation likely because of the low charge density.

Table 4-3 Chemical compositions of the zincosilicate gels used for HRXTS analysis

Gels	Gel Compositions (mol)			
	Na[c]	TEA[d]	ZnO[c]	SiO_2[c]
Na-zincosilicate-20[a]	1.08	n. a.	1.0	19.2
Na-zincosilicate-8[a]	0.98	n. a.	1.0	7.5
TEA-zincosilicate-20[b]	0.00	0.9	1.0	18.4
TEA-zincosilicate-10[b]	0.00	0.8	1.0	10.9

[a]prepared by co-precipitation using NaOH [b]Prepared by co-precipitation using TEAOH
[c]Calculated by ICP-AES analysis [d]Calculated by CHN analysis

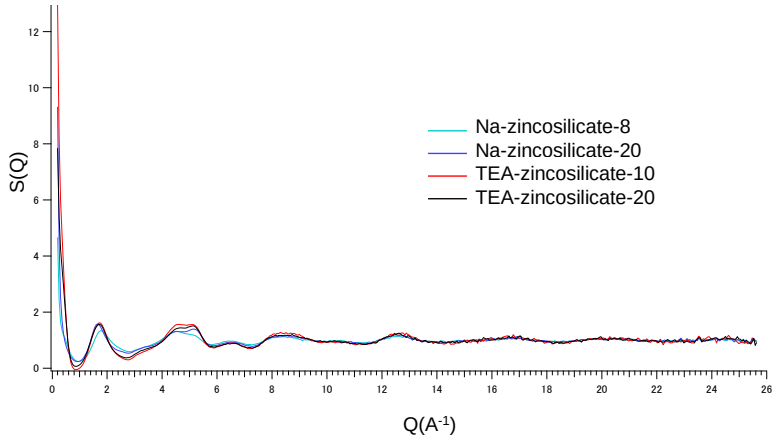

Figure 4-6 Total structural factors S(Q) of the zincosilicate gels prepared by co-precipitation.

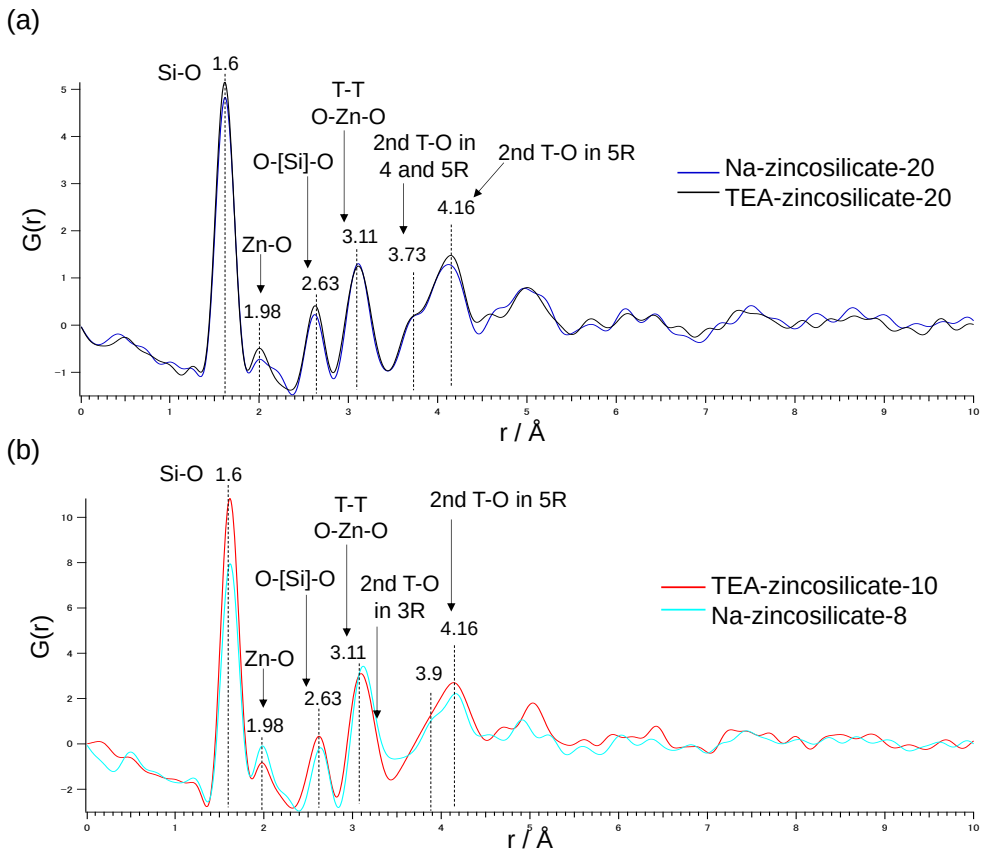

Figure 4-7 Pair distribution functions, G(r), of the zincosilicate gels prepared by co-precipitation with Si/Zn ratio of around (a) 20 and (b) 10.

4.3.2 Synthesis of *BEA Zeolites from the Zincosilicate Gel

In the previous studies, the synthesis of zincosilicate *BEA zeolite was conducted with the Si/Zn ratio of around 33. The range of the composition in which the zincosilicate *BEA phase can be obtained is very limited because the other phases such as VPI-8 is very easy to form in the same conditions.[147] To increase the zinc content introduced to the *BEA zeolites, the zincosilicate gels prepared by the OSDA-involved co-precipitation were used in the synthesis. For the synthesis of zincosilicate *BEA zeolites with high content of zinc, the use of seed crystals is very important. Figure 4-8 shows powder XRD patterns of the products obtained using the TEA-zincosilicate gels with Si/Zn = 18.4 with different amount of seed crystals. After the hydrothermal treatment was conducted at 150 °C for 4 days, the product prepared using 10 wt% of seed crystals on the basis of SiO_2 was highly crystalline *BEA zeolite. The Si/Zn ratio of the product determined by ICP-AES analysis was 21.0. However, the product prepared using 5 or 1 wt% of seed crystals showed a broad peak at around 7 degree. These results suggested that, only with the enough amount of seed crystals, pure zincosilicate *BEA can be obtained without formation of impure phase.

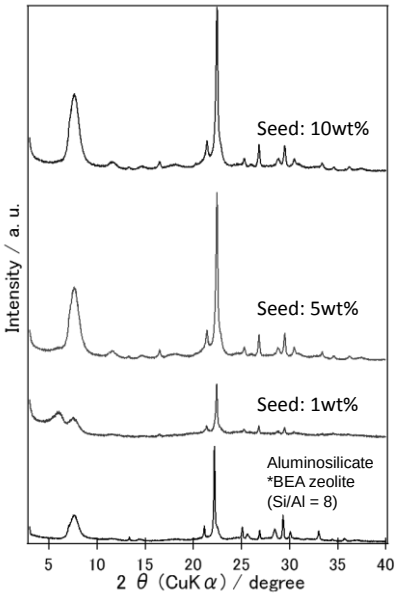

Figure 4-8 Powder XRD patterns of the products obtained using the TEA-zincosilicate gels with Si/Zn = 18.4 with different amount of seed crystals. The hydrothermal treatment was conducted at 150 °C for 4 days.

For comparison, the synthesis of zincosilicate *BEA zeolites was conducted using conventional raw materials, that is, colloidal silica and zinc acetate, while keeping other conditions the same as described above. As shown in Figure 4-9, diffraction patterns of *BEA zeolite with decreased crystallinity and distinct peak from unknown impure phase were observed. This is probably because the high concentration of Zn species with less homogeneity in the reaction mixture caused formation of impure phase. These results suggest that zincosilicate *BEA zeolites with high contents of Zn incorporated into the zeolite framework cannot be obtained using conventional Si and Zn sources. It is also indicated that the zincosilicate gels prepared *via* co-precipitation are appropriate precursors for the synthesis of *BEA zeolites with high content of Zn in the framework.

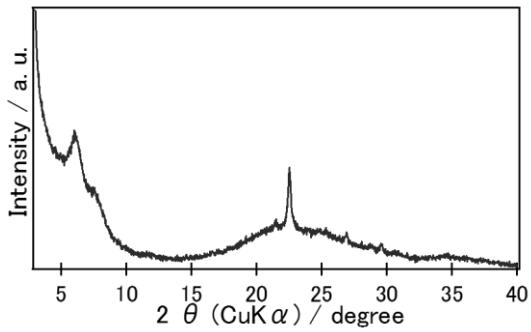

Figure 4-9 Powder XRD patterns of the product obtained using the TEA-zincosilicate gels with Si/Zn = 18.4 with different amount of seed crystals. The hydrothermal treatment was conducted at 150 ^{o}C for 4 days.

To further increase the zinc content in *BEA zeolites, zincosilicate gels prepared by co-precipitation with increased content of zinc was used in the synthesis. As shown in Figure 4-10 (a), when the zincosilicate gel with Si/Zn of 16.5 was used, pure *BEA zeolite was not obtained by hydrothermal treatment at 150 ^{o}C because the impure phase was formed with *BEA zeolite. When the temperature was increased to 170 ^{o}C, highly crystalline *BEA zeolite without the impure phase was obtained, probably because the crystal growth of *BEA zeolite became faster at the higher

temperature and the crystallization was completed before the formation of the impure phase. The obtained *BEA zeolite retained its crystallinity after calcination conducted in the way as described in Figure 4-1. The Si/Zn ratio of the sample after calcination was 17.8 and exhibited high micropore volume (Table 4-4). When the zinc content of the zincoaluminosilicate gel is further increased to Si/Zn ratio of 10.9, even at 170 °C, the impure phase could not be totally eliminated. After hydrothermal treatment at 170 °C for 1 day, the Si/Zn ratio of the product was 15.6 (Table 4-4).

It has been reported that zincosilicate *BEA zeolite (CIT-6) is synthesized from clear solutions that contain TEA^+, Li^+ and Zn^{2+}. The crystallization proceeds through the formation of a homogeneous amorphous solid that incorporates all the initial Zn species.[147] Nucleation of the *BEA phase is effected by re-organization of the amorphous phase, whereas crystal growth involves the incorporation of soluble species also.[147] In the method described here provides homogeneous zincosilicate gels incorporates zinc, silicon and TEA^+, therefore, crystallization of the *BEA phase probably occurred by re-organizing the amorphous phase of zincoaluminosilicate gels.

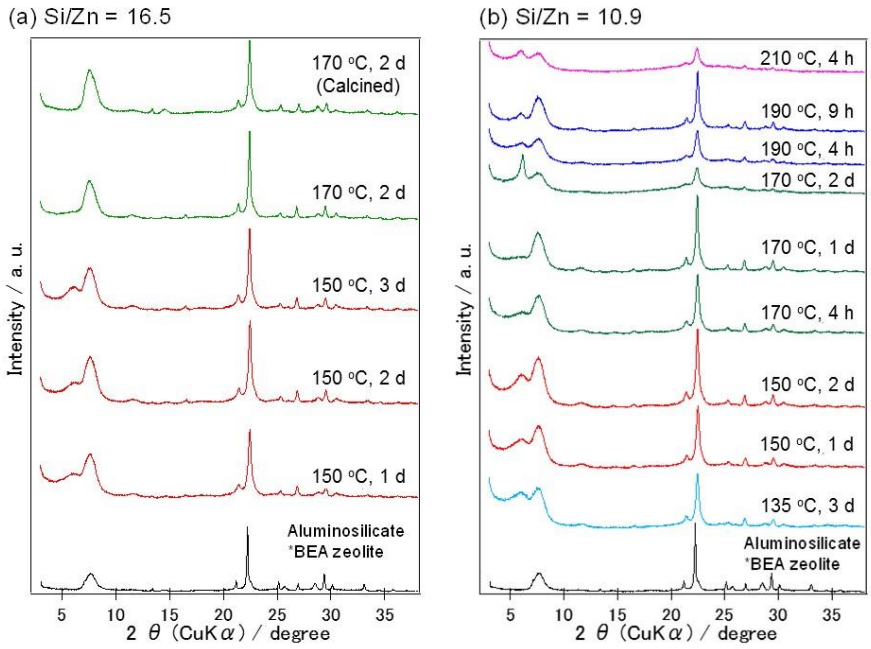

Figure 4-10 Powder XRD patterns of the products obtained using the TEA-zincosilicate gels with Si/Zn of (a) 16.5 and (b) 10.9 using 20 wt% of seed crystals on the basis of SiO_2 after hydrothermal treatment at various temperature.

Table 4-4 Chemical Compositions and micropore volumes of zincosilicate *BEA zeolites obtained by using zincoaluminosilicate gels prepared by co-precipitation with TEAOH.

Si/Zn in co-precipitation	Zincosilicate gel	Zincosilicate *BEA zeolite	
	Si/Zn [a]	Si/Zn [a]	V_{micro} [b] /cm^{3}g^{-1}
10	13.6	15.6 [c]	*n. d.*
15	16.5	17.8	0.22
20	18.4	21.0	0.22

[a] Determined by ICP-AES analysis

[b] Micropore volumes determined by a *t*-plot method after calcination

[c] The product contains small amount of layered silicate as impurity

Figure 4-11 shows XRD patterns of the products obtained using zincosilicate gel with Si/Zn of 16.5 with different hydrothermal duration and different seed crystals. When the aluminosilicate *BEA zeolite was used as seed crystals, the formation of impure phase was not observed through the hydrothermal treatment up to 5 days. However, when the zincosilicate *BEA, which was obtained using the zincosilicate gel by 2 days of hydrothermal treatment (shown as (b) in Figure 4-11), the cyrstallinity of obtained zeolite decreased and impure phase was observed. The zincosilicate *BEA added as the seed was likely dissolved during the hydrothermal treatment because of the low stability of the zincosilicate framework compared to the aluminosilicate.

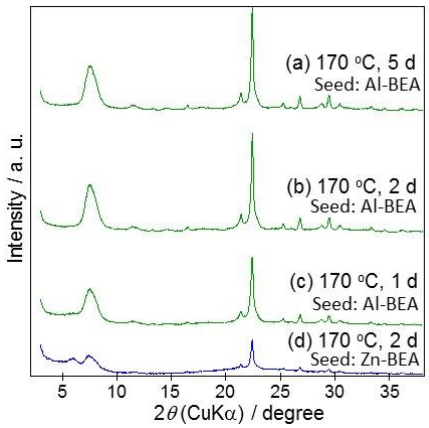

Figure 4-11 Powder XRD patterns of the products obtained using the TEA-zincosilicate gels with Si/Zn of 16.5 using 20 wt% of seed crystals on the basis of SiO_2 after hydrothermal treatment at various temperature.

4.3.3 Environments of Zn in the Zincosilicate *BEA Zeolites

To analyze zinc coordination states in the obtained *BEA zeolite, DR UV–vis spectra of the zincosilicate *BEA zeolite prepared using the co-precipitated gel with Si/Zn of 16.5 were obtained as depicted in Figure 4-12. The as-synthesized sample exhibited a distinct peak below 200 nm, which is assigned to the charge transfer transitions of Zn in the silicate structure with lattice O^{2-}. Other absorption band is not observable; therefore, it is suggested that isolate zinc species in silicate structure is the major component in the obtained zincosilicate *BEA zeolite. To remove TEA^{+} cations in the zeolite, calcination of the zeolite was conducted at 500 °C for 2 h in nitrogen flow, and subsequently, 500 °C for 2 h in air flow (Figure 4-1). As shown in Figure 4-10, no significant change was observed in the XRD pattern, however, the UV-vis spectra indicated that state of some zinc species was changed after the calcination. No absorption band assigned to ZnO, which is observed at around 360–380 nm due to the $O^{2-} \rightarrow Zn^{2+}$ ligand-to-metal charge transfer transition[173], was not observed, however, the sharp absorption band observed below 200 nm, which attributed to zinc in silicate structure, decreased, and adsorption band around 250 nm which attributed to Zn^{2+} species out of silicate structure, increased. These results suggests that some of the zinc species in the silicate structures were removed from the silicate structure by thermal treatment.

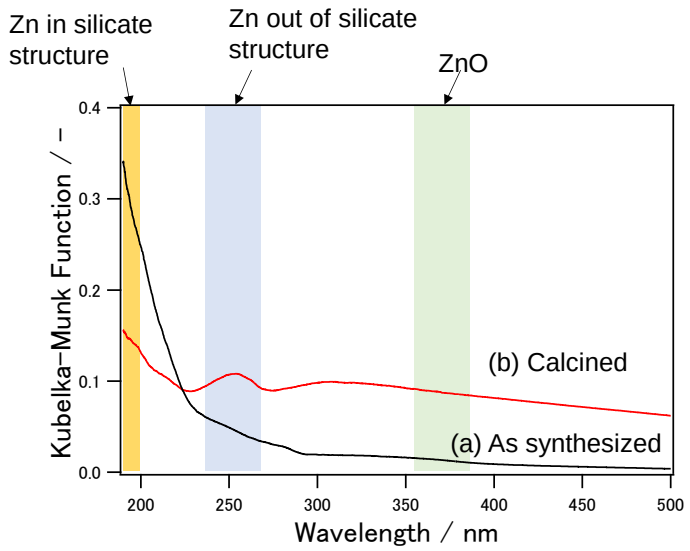

Figure 4-12 DR UV-Vis spectra of obtained zincosilicate *BEA zeolite using zincosilicate gel (Si/Zn = 16.5), (a) before and (b) after the calcination.

4.4 Conclusion

The co-precipitation method to prepare homogeneous zincosilicate gels was further extended to obtain the zincosilicate gel with occluded OSDA in the silicate structure by conducting the co-precipitation in the presence of the OSDA.

In contrast to the co-precipitation using NaOH which yielded zincosilicate gels containing sodium cation as counter cation, tetraethylammonium (TEA) cation was occluded in zincosilicate gels prepared by the co-precipitation in the presence of TEAOH. Characterization of the zincosilicate gels suggested that Zn species were homogeneously distributed in the silicate matrix. TEA^+ cations were occluded in the zincosilicate structure and the existence of TEA^+ probably inhibit 3MR formation which have been reported to occur in the conditions with high-zinc content without OSDAs.

By using the zincosilicate gels formed with TEA^+, synthesis of *BEA zeolites, which have been synthesized by using TEA^+ as an OSDA, was conducted. Zincosilicate *BEA zeolites with higher zinc content compared to the previous reports were obtained with the assistance of seed crystals. When conventional zinc and silica sources were used, highly crystalline *BEA zeolite was not obtained in the same conditions. The zinc species in the obtained zincosilicate *BEA zeolite (Si/Zn = 17.8) were shown to be located in the zeolite silicate framework, although after calcination, some of the zinc species were removed from the silicate structure.

Chapter 5. Synthesis of New Zincosilicate Zeolites with CHA Topology by Focusing on Mixing Procedures of Raw Materials in Liquid Phase

5.1 Introduction

Small pore zeolites defined as the zeolites having the pore openings limited by 8 tetrahedral atoms (8 membered-ring, 8MR) have received particular attention recently because they have exhibited excellent performances in several important applications, for example, as catalysts for methanol-to-olefin (MTO) and ethene-to-propene (ETP) reactions, and as adsorbents and membranes for gas separations.[226,227,228] Among several small pore zeolites, CHA-type zeolites with three-dimensional network built by stacking layers of double 6MR has been intensively studied. The CHA-type zeolites possess large *cha* cage cavities with transportation limited by 8MR windows formed by interconnection of the 6MR. Because of the characteristic structure, they have remarkable applications. For example, SSZ-13, a high-silica aluminosilicate zeolite with CHA topology have been used for, for example, selective catalytic reduction (SCR) of NO_x, methane conversion, MTO and gas separation.[226,229,230,231] Silicoalumino phosphate SAPO-34 with CHA topology also has remarkable activity in MTO to produce ethylene and propylene.[232] Both SSZ-13 and SAPO-34 have been commercialized or close to be commercialized for those applications.[233]

CHA zeolites exchanged with divalent metal cations are of particular interest because of the great promise in several new applications relevant to energy and environment. For example, Cu(II) and Fe(II) exchanged zeolites have proven to have high activity especially in selective catalytic reduction (SCR) of NO_x and methane conversions.[231,229,153,234] For the application, the local environments of the counter metal cation species remarkably affect the catalytic activity.[153,234,154,235,236] For example, mono-copper sites in small pore zeolites were reported to be active sites for SCR of NO_x.[153,235] It has been reported that only bare divalent metal cations are key in the

several catalytic cycles, such as Cu^{2+} for outstanding NO_x conversion and Fe^{2+} for N_2O decomposition.[237,238] Note that in larger pore zeolites metal dimers and trimers can also catalyze such reactions through different catalytic mechanisms.[234,236,239]

For aluminosilicate zeolites, to stabilize the active monomeric sites of divalent metals, two Al with close proximity (*e.g.* Al pair, which are defined here as two Al atoms separated by one or two Si atoms in 6MR, Al–O–(Si–O)$_n$–Al (n = 1 or 2)) are needed since isomorphous substitution of Al(III) for Si(IV) in the zeolite framework creates only one negative charge per the atom.[165] On the other hand, isolated framework Al configuration (n > 2) suitable for stabilization of oxo-species of divalent cations or monovalent cations, which are sometimes undesired for several applications.[238,240] In addition, isolated Al sites can remain unchanged as Brønsted acid sites when counterbalanced by protons and cause side reactions or catalyst deactivation.[152] It has been reported that in the case of high-silica zeolites, such as SSZ-13, the isolated framework Al exists dominantly.[165,239] The fraction of Al in pairs can be increased by using equimolar amount of Na^+ together with *N*,*N*,*N*-trimethyl-1-adamantylammonium cation ($TMAda^+$), which is an organic structure directing agent occluded within *cha* cavities, but the paired Al densities cannot be increased more than that in random Al distribution (*e.g.* fraction of Al in pairs is reported to be ca. 17% for SSZ-13 with Si/Al = 15).[165]

In contrast to aluminosilicate zeolites, isomorphous substitution of Si(IV) by Zn(II) can generate two negative charges per one Zn atom. Therefore, the Zn atom in framework can stabilize a divalent cation in one by one ratio and zincosilicate zeolites have been considered as an efficient platform for stabilization of extra-framework divalent cations.[152] However, Zn in synthesis gels is known to favor formation of only a few frameworks (*e.g.* VET and some frameworks rich in 3MR such as RSN) or inhibit zeolite formation by precipitation as oxide or hydroxide form.[140,151,147,149] Therefore, a number of available zincosilicate zeolites is quite limited to few structures. Recently, zincoaluminosilicate CHA zeolites with both Al and Zn in their frameworks are reported to be achieved by using FAU zeolite as an Al source.[166] In this case, a large amount of Al is needed for direct crystallization of CHA zeolites. Still, synthesis of pure zincosilicate zeolites with CHA topology is a challenge and it is desired because Al

species in the frameworks can cause undesired side reactions as is described above.[152]

In Chapter 2–4, it was found that the use of homogeneous gels of zinc and silicate species is crucial for introduction of zinc to zeolite structures. In this chapter, to prevent formation of extraframework Zn species, particular attention was paid to the mixing procedures of the raw materials in liquid phase prior to hydrothermal synthesis of zeolites. For the successful synthesis of zincosilicate CHA, initial state of Zn species in a basic solution is probed to be very crucial.

5.2 Experimental

5.2.1 Materials

The following chemicals were used as received for synthesis of the organic structure directing-agent: Potassium carbonate (Wako Pure Chemical Industries), 1-adamantylamine (Wako Pure Chemical Industries, Ltd.), 0.01 M hydrocholoric acid (Wako Pure Chemical Industries, Ltd.) and iodomethane (Wako Pure Chemical Industries, Ltd.). The following chemicals were used as received for synthesis of zeolites: anhydrous zinc acetate (Wako Pure Chemical Industries, Ltd.), Lithium hydroxide monohydrate (Wako Pure Chemical Industries, Ltd.), zinc sulfate (Wako Pure Chemical Industries, Ltd.), aluminium hydroxide (Wako Pure Chemical Industries, Ltd.), sodium hydroxide (Wako Pure Chemical Industries, Ltd.), sodium silicate (Wako Pure Chemical Industries, Ltd.), tetraethoxysilane (Wako Pure Chemical Industries, Ltd.), hydrofluoric acid (Wako Pure Chemical Industries, Ltd.) and fumed silica (Cab-O-Sil M-5, Cabot Co.).

5.2.2 Synthesis of Zincosilicate CHA Zeolites

Synthesis of *N,N,N*-trimethyl-1-adamantamonium hydroxide (TMAdaOH)

Potassium carbonate (2.5 equiv) and 1-adamantylamine (1 equiv) were added into an oven-dried three-necked flask equipped with a condenser and a magnetic stirrer. This flask was evacuated and refilled with nitrogen gas for three times. After the addition of dehydrated chloroform, iodomethane (3.5 equiv) was slowly added to the mixture while

stirring. Then, this reaction mixture was kept in dark and stirred for 7 days at room temperature. After 7 days, this mixture was filtered to remove the solid. The filtrate was evaporated to remove chloroform by a rotary evaporator. The recovered solid was recrystallized in hot ethanol. The recrystallized solid was washed with acetone and dried under atmospheric condition, yielding *N*,*N*,*N*-trimethyl-1-adamantamonium iodide (TMAdaI). The solid product was characterized by ^{1}H and ^{13}C NMR spectroscopy. TMAdaI was ion-exchanged to the hydroxide form (TMAdaOH) using hydroxide ion exchange resin (OH^- exchange resin, Dowex). After ion-exchange, the concentration of OH^- was determined by titration with 0.01 M hydrocholoric acid.

Synthesis of Zincosilicat CHA zeolite

In all procedures, the chemical compositions of the final mixture was SiO_2: *x* ZnO: 0.42 TMAdaOH: 0.08 LiOH: 30 H_2O, *x* = 0.02–0.06.

Procedure (i)

Lithium hydroxide monohydrate was dissolved in distilled water. Fumed silica (Cab-O-Sil M-5) was added in the LiOH solution and stirred for 2 h at room temperature to obtain a semitransparent suspension. In another vessel, anhydrous zinc acetate was added to a TMAdaOH aqueous solution (*ca.* 27 wt%) and stirred for 5 min to complete dissolve zinc acetate, resulting in a clear Zn solution. The Zn solution was then added to the silica suspension and further stirred for 5 min. The obtained mixture was then subjected to hydrothermal treatment at 150 °C under a static condition for 7 days. The solid product was recovered by filtration and washed with deionized water until the filtrate reached pH 7–8. The product was dried at 80 °C overnight. The calcination was conducted, if need, at 600 °C.

Procedure (ii)

A TMAdaOH aqueous solution was mixed with distilled water. Then, lithium hydroxide monohydrate was dissolved in the solution. Subsequently, anhydrous zinc acetate was added to the clear solution containing TMAdaOH and LiOH, and stirred for several minutes until complete dissolution. Then, fumed silica was added in the solution and stirred for 2 h at room temperature. The obtained mixture was then subjected to hydrothermal treatment at 150 °C under a static condition for 7 days. The solid product

was recovered by filtration and washed with deionized water until the filtrate reached pH 7–8. The product was dried at 80 °C overnight.

Procedure (iii)

A TMAdaOH aqueous solution was mixed with distilled water. Then, fumed silica was added in the solution and stirred for 2 h at room temperature to obtain a semitransparent suspension. In another vessel, lithium hydroxide monohydrate was dissolved in distilled water. Anhydrous zinc acetate was then added to the LiOH solution. The resulting mixture was stirred for 5 min. The Zn solution was then added to the silica suspension and further stirred for 5 min. The obtained mixture was then subjected to hydrothermal treatment at 150 °C under a static condition for 7 days. The solid product was recovered by filtration and washed with deionized water until the filtrate reached pH 7–8. The product was dried at 80 °C overnight.

Procedure (iv)

A TMAdaOH aqueous solution was mixed with distilled water and lithium hydroxide monohydrate. Then, fumed silica was added to the clear solution containing TMAdaOH and LiOH and stirred for 2 h at room temperature to obtain a semitransparent suspension. In another vessel, anhydrous zinc acetate was dissolved in distilled water and stirred for 5 min to obtain a clear solution. The Zn solution was then added to the silica suspension and further stirred for 5 min. The obtained mixture was then subjected to hydrothermal treatment at 150 °C under a static condition for 7 days. The solid product was recovered by filtration and washed with deionized water until the filtrate reached pH 7–8. The product was dried at 80 °C overnight.

Synthesis of SSZ-13 (aluminosilicate CHA zeolite)

SSZ-13 (aluminosilicate CHA zeolite) was synthesized for comparison in ion-exchange experiments. First, aluminium hydroxide was dispersed in a TMAdaOH aqueous solution and then heated at 80 ^{o}C to completely dissolve. After cooling to room temperature, distilled water and fumed silica were added to the dissolved aluminate solution. The chemical composition of the final mixture was SiO_2: 0.025 Al_2O_3: 0.4 TMAdaOH: 16 H_2O. The obtained mixture was then subjected to hydrothermal treatment at 150 °C under a static condition for 7 days.

Synthesis of zincoaluminosilicate CHA zeolite

Zincoaluminosilicate CHA zeolite with both Zn and Al in the framework (Zn,Al-CHA) was synthesized according to the previous report[166] for comparison in ion-exchange experiments. First, sodium hydroxide was dissolved in a TMAdaOH aqueous solution. Then, sodium silicate was added. Zinc acetate and FAU zeolite (as Al source; Tosoh, HSZ320NAA) was added to the mixture and stirred vigorously. The chemical composition of the final mixture was SiO_2: 0.033 ZnO: 0.034 Al_2O_3: 0.17 TMAdaOH: 0.5 NaOH: 20 H_2O. The resulting homogeneous mixture was then transferred to an autoclave and hydrothermal synthesis was conducted at 150 ^oC for 7 days in a static condition.

Synthesis of pure silica CHA zeolite

Pure silica CHA zeolite was used as seed crystals. Tetraethoxysilane was added dropwise to a TMadaOH solution aqueous while stirring. After stirring for 5 h at room temperature, the resulting mixture was heated on a hot plate (*ca*. 80 °C) while stirring to evaporate an excess amount of water. Then, hydrofluoric acid (Wako Pure Chemical Industries, Ltd.) was added and the mixture was mixed by a spatula for about 15 min. The chemical composition of the final mixture was SiO_2: 0.5 TMAdaOH: 0.5 HF: 8 H_2O. The obtained mixture was then subjected to hydrothermal treatment at 150 °C under a tumbling condition (60 rpm) for 8 days. The solid product was recovered by filtration, washed thoroughly with deionized water and dried at 80 °C overnight.

Preparation of proton-form zeolites

Proton-form zeolite samples were prepared for ion-exchange experiments. SSZ-13 was synthesized without using alkali metal cations; therefore, its proton-form was obtained after calcination to remove $TMAda^+$. For the zincosilicate and zincoaluminosilicate zeolites, their proton-form samples were prepared by ion-exchange with ammonium nitrate, following by calcination. The ion-exchange was performed using a 0.1 M ammonium nitrate (Wako Pure Chemical Industries, Ltd) aqueous solution. pH of the solution was adjusted to 7.0 by adding a few drops of ammonia aqueous solution (3 wt%). The calcined zeolite samples (0.3 g) were dispersed in the ammonium nitrate

solution (100 mL) and then stirred at 500 rpm and room temperature. After stirring for 1 day, the solid samples were recovered, thoroughly washed with deionized water and dried at 80 °C, resulting in NH^{4+}form zeolites. The samples was calcined at 400 °C for 2 h under a nitrogen flow to obtain proton-type CHA zeolites.

Ion exchange experiments with K^+

Ion-exchange with potassium, as a model monovalent cation, was performed using a 0.1 M potassium chloride aqueous solution prepared from potassium chloride (Wako Pure Chemical Industries, Ltd.). The solid samples (0.05 g) were dispersed in the potassium chloride solution (150 mL) and then stirred at 500 rpm and room temperature. After a few days, the solid samples were separated from the solution by centrifugation, thoroughly washed with deionized water and dried at 80 °C. The content of potassium was determined by atomic absorption spectroscopy (Hitachi Z-2000).

Ion exchange experiments with Ni^{2+}

Ion-exchange with nickel(II), as a model divalent cation, was performed using a 0.005 M nickel nitrate aqueous solution prepared from nickel(II) nitrate hexahydrate (Wako Pure Chemical Industries, Ltd.). The solid samples (0.05 g) were dispersed in the nickel nitrate solution (500 mL) and then stirred at 500 rpm and room temperature. After a few days, the solid samples were separated from the solution by centrifugation, thoroughly washed with deionized water and dried at 80 °C. The content of Ni was determined by inductively coupled plasma-atomic emission spectrometry (Thermo iCAP 6300).

5.2.3 Characterization

Powder X-ray diffraction (XRD) analysis was conducted to determine the crystal structure of the products using a diffractometer (Rigaku Ultima IV) operated with Cu Kα monochromatized radiation at 40 kV and 40 mA. Elemental analysis of the products was performed by inductively coupled plasma-atomic emission spectrometry (ICP-AES, Thermo iCAP 6300) after dissolving the products in hydrofluoric acid or potassium hydroxide solutions. The ICP-AES analyses were repeated 3 times for each sample. In addition, a Hitachi Z-2000 atomic absorption spectrometer equipped with a heated

graphite tube atomizer was used for the determination of potassium contents of samples after ion-exchange. To observe crystal size and morphology, field-emission scanning electron microscopy (FE-SEM) images were obtained from JFM-7500FA (JEOL) at an accelerating voltage of 15 kV. Nitrogen adsorption–desorption measurements were performed on a Quantachrome Autosorb-iQ2-MP at liquid nitrogen temperature. Prior to the measurements, the samples were degassed at 400 °C for 6 h under vacuum. Diffuse reflectance (DR) UV–vis spectra were recorded on a JASCO V-670 spectrometer in the 190–800 nm wavelength range using barium sulfate as a reference. Solid-state magic-angle-spinning (MAS) nuclear magnetic resonance (NMR) experiments were conducted on a JNM-ECA 500 (JEOL). ^{29}Si MAS NMR spectra were recorded at 99.3 MHz with a pulse length ($\pi/2$) of 5.0 μs, a recycle delay of 60 s, and a spinning frequency of 10 kHz. FT-IR spectra using acetonitrile-d_3 (CD_3CN) as a probe molecule were corrected using a JASCO FT-IR 4100 spectrometer equipped with a mercury cadmium telluride (MCT) detector. Spectra in a range of 4000–700 cm^{-1} were acquired with a resolution of 4 cm^{-1}. The samples (15–18 mg) were pressed at around 30 MPa for 5 min to form self-standing pellets with a diameter of 2 cm. The pellets were placed in a vacuum cell. While evacuating, the samples were heated to 500 °C at a heating rate of 10 °C min^{-1} and held at this temperature for 1 h. Then, the samples were cooled to 80 °C and CD_3CN (Sigma-Aldrich Co. LLC, 99.8% D atoms) was dosed to the samples until the spectra became unchanged. After collecting the first spectra, the cell was evacuated at 80 °C and FT-IR spectra were recorded after 1 h. Then, the cell was heated to 150 °C and subsequently to 250 °C under vacuum. After holding at each targeted temperature for 30 min, the cell was cooled to 80 °C and FT-IR spectra were then recorded. The resulting spectra were subtracted with the spectra obtained at 80 °C but without dosing probe molecules. Thermogravimetric and differential thermal analyses (TG-DTA) were performed on a PU 4K (Rigaku) at a heating rate of 10 °C min^{-1} under a flow (200 mL min^{-1}) of 10% O_2/90% He mixed gas.

5.3 Results and Discussion

5.3.1 Synthesis of Zincosilicate CHA zeolites

TMAdaOH is a common organic structure-directing agent and successfully prepared without impurities as was confirmed by ^{1}H and ^{13}C NMR spectroscopy (Figure 5-1).

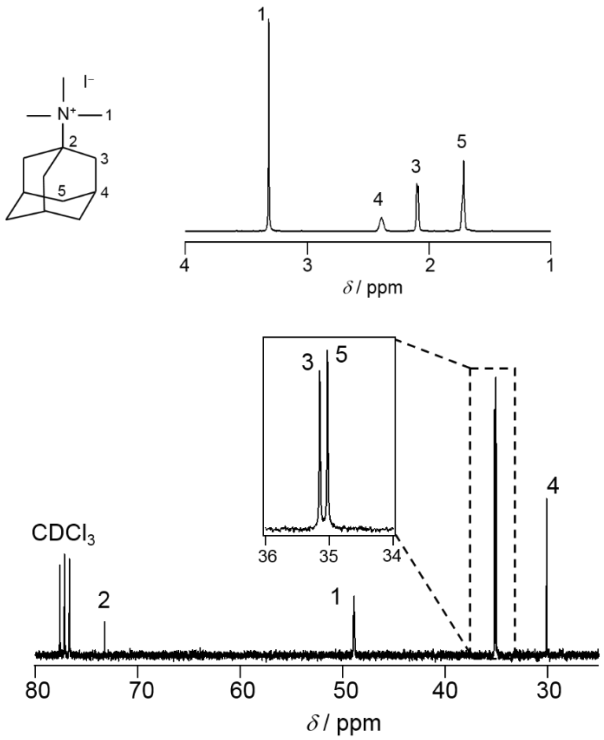

Figure 5-1 Solution-state 1 H and 13C NMR spectra of synthesized TMAdaI.

For the successful synthesis of zincosilicate zeolite with CHA topology, 4 different procedures were investigated to prepare synthetic mixtures prior to hydrothermal treatment as shown in Figure 5-2. Even though the difference is only the order of mixing of chemicals, the products obtained after hydrothermal treatment was quite different.

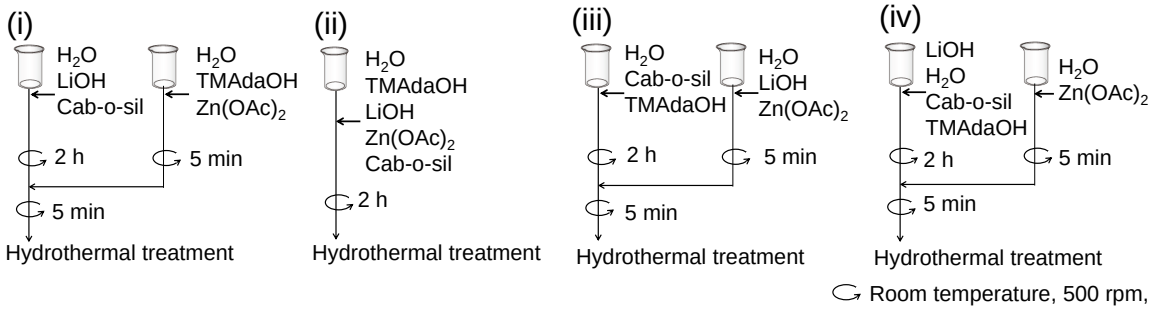

Figure 5-2 Scheme of mixing procedures of synthetic mixtures prior to hydrothermal treatment.

Only the procedure (i), in which zinc acetate and TMAdaOH aqueous solution were mixed separately from LiOH and fumed silica, highly crystalline CHA zeolite was obtained after hydrothermal treatment at 150 °C under a static condition for a week (Figure 5-3 (i)). On the other hand, when the synthetic mixtures were prepared in different ways (procedures (ii)–(iv) in Figure 5-2), the products were either amorphous solid or the mixture of layered silicate and CHA zeolite (Figure 5-3 (ii)-(iv)).

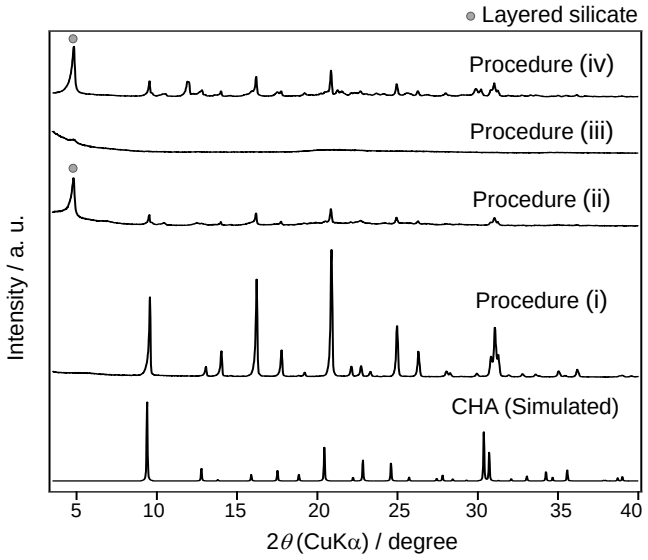

Figure 5-3 Powder XRD patterns of the products synthesized from the mixture solutions prepared by procedure (i)-(iv) after hydrothermal treatment at 150 °C for 7 days in a static condition.

Figure 5-4 shows SEM images of the product obtained from the different procedures (i)–(iv). The zeolite product obtained from the procedure (i) was uniform, cubic particles with a size of ca. 6 μm. On the other hand, the layered material-like

particles were observed in the product prepared by the procedure (ii) with only a small portion of cubic particles. For the procedure (iii), irregularly shaped particles, likely amorphous solid, were observed without any cubic particles. The product obtained from the procedure (iv) was the mixture of layered materials and cubic zeolite particles.

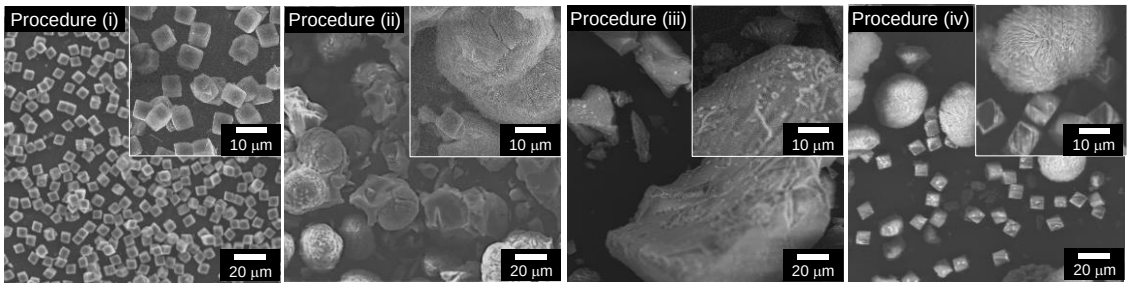

Figure 5-4 Powder XRD patterns of the products synthesized from the mixture solutions prepared by procedure (i)-(iv) after hydrothermal treatment at 150 °C for 7 days in a static condition.

As was shown in Chapter 2–4, for the synthesis of zeolites with Zn in the frameworks, the formation of the homogeneous mixture of Zn and Si species is crucial to form the zincosilicate structures while preventing the precipitation of zinc oxides/hydroxides during hydrothermal treatment. In the procedure (i), Zn species are totally dissolved as $[Zn(OH)_4]^{2-}$ or $[Zn(OH)_3]^-$ in the clear solution because of the high alkalinity of TMAdaOH solution (pH > 14).[241] The negatively charged Zn species can interact with $TMAda^+$, thereby preventing the precipitation of Zn even in such a highly alkaline solution. Separately, fumed silica particles are dispersed in the LiOH solution, yielding a semitransparent suspension (pH 12.5). When the Zn solution is mixed with the silica suspension, pH of the mixture drops to ca. 13, in which the solubility of Zn decreases.[241] Similar to aluminosilicates,[176] it is surmised that the dissolved Zn species react with dissolved silicate, forming zincosilicate, and/or precipitate on the surface of dispersed silica particles. As a result, Zn and Si species are well mixed before hydrothermal treatment. In the procedure (ii), fumed silica is not dispersed beforehand; therefore, when it is added to the Zn solution, the reactions between dissolved Zn species and silica occur only at the outer surface of agglomerated silica particles. The large amount of the unreacted silica would hence lead to the formation of layered silicate after hydrothermal treatment.

To further explain the difference between the procedures (i) and (ii), the intermediate products during hydrothermal treatment were recovered and characterized by UV–vis spectroscopy. Figure 5-5 shows diffuse reflectance (DR) UV–vis spectra of the products obtained via the procedures (i) and (ii) after hydrothermal treatment for 2 and 7 days. Only the product prepared via the procedure (ii) collected after 2 days exhibited an absorption band assigned to ZnO, which is observed at around 360 nm due to the $O^{2-} \rightarrow Zn^{2+}$ ligand-to-metal charge transfer transition. The ZnO observed in the initial stage is probably due to the formation of Zn-rich species precipitated apart from the silicate species in the procedure (ii).

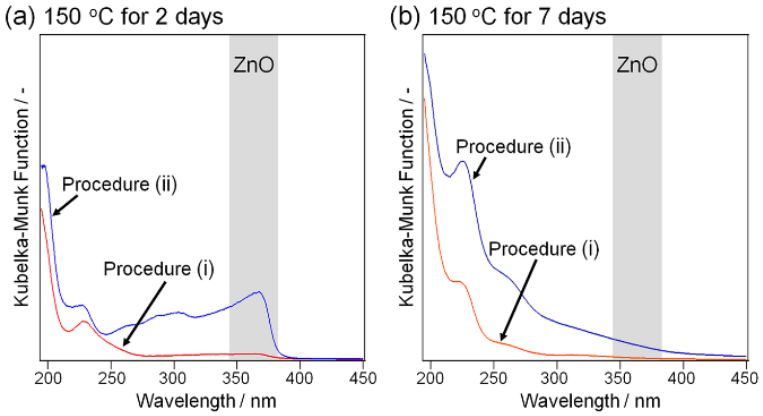

Figure 5-5 DR UV-Vis spectra of products collected after hydrothermal treatment at 150 °C for (a) 2 and (b) 7 days following procedures (i) and (ii).

In the procedure (iii), ZnO is formed immediately after addition of zinc acetate into the LiOH solution, as is confirmed by XRD measurement, because the solubility of Zn is somewhat low in the relatively weak basic solution of LiOH (pH 13).[241,242] As a result, the reactions between Zn and Si species are limited. The procedure (iv) provides a weakly acidic, clear aqueous solution of Zn, in which zinc is present in the cationic Zn^{2+} form. When the acidic Zn solution is added to the highly basic silica suspension (pH > 14), Zn is precipitated readily because of the rapid change in pH, yielding the inhomogeneous mixture of Zn and Si species. As a result, layered silicate and CHA zeolite are formed after hydrothermal treatment.

As shown in Figure 5-6, by applying the successful procedure (i), effect of the

types of alkali metal cation was investigated. When LiOH was replaced by NaOH or KOH, CHA zeolite was not obtained, even with the addition of seed crystals (pure silica CHA zeolite, 5 wt% based on SiO_2). In the absence of alkali metal cation (*i.e.*, only $TMAda^+$), CHA zeolite was formed together with layered silicate when the seed crystals were added, while no crystalline product was observed without seed addition. These results suggest the important role of Li^+ on the formation of zincosilicate CHA zeolites, similar to the previous reports of *BEA and VET zeolites.[147,139]

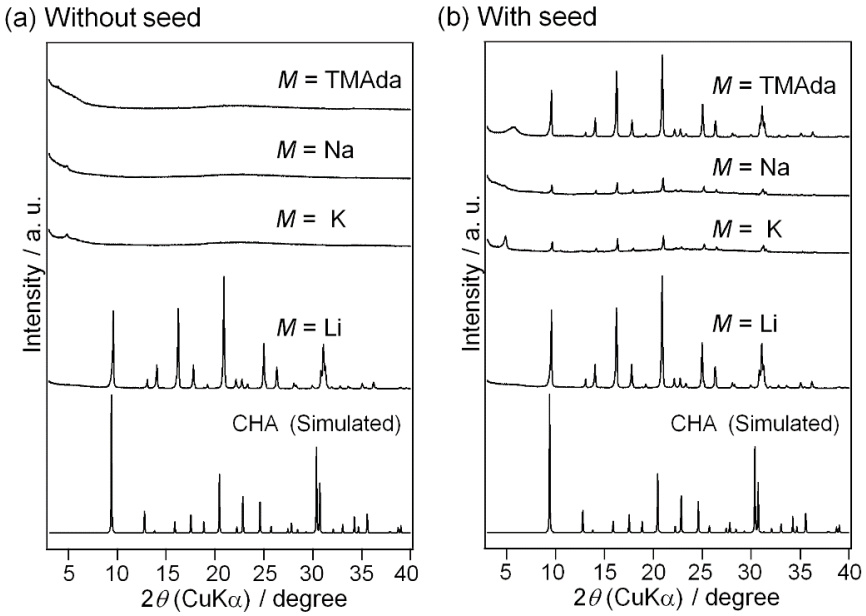

Figure 5-6 Powder XRD patterns of products synthesized (a) without and (b) with pure silica CHA seed crystals (5 wt% on a basis of SiO_2) with the composition of SiO_2: 0.03 ZnO: 0.42 TMAdaOH: 0.08 *M*OH: 30 H_2O, where *M* is varied as Li, K, Na and TMAda.

Several synthetic parameters were varied to obtain CHA zeolites with various Zn contents. As shown in Figure 5-7, when the amount of Zn in the synthetic mixture was decreased to Si/Zn = 40, distinct XRD peak from layered silicate was observed, while peaks from CHA zeolite were hardly seen. However, when pure silica CHA zeolite was added as seed crystals, the formation of CHA zeolite was confirmed at Si/Zn = 40. When the amount of Zn was further decreased to Si/Zn = 50, highly crystalline CHA zeolite was not formed.

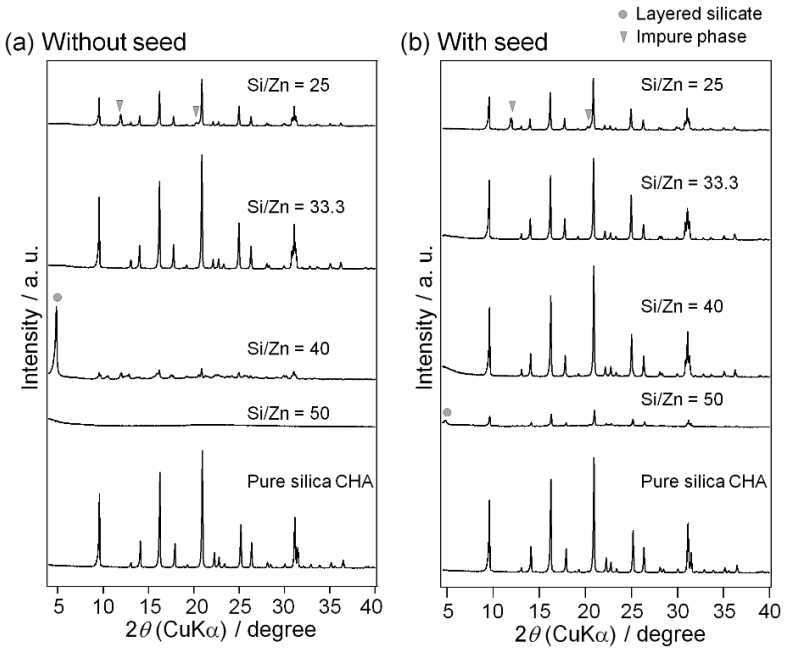

Figure 5-7 Powder XRD patterns of products synthesized (a) without and (b) with pure silica CHA seed crystals (5 wt% on a basis of SiO_2) at different Si/Zn ratios in the synthetic mixtures. Other composition is SiO_2: 0.42 TMAdaOH: 0.08 LiOH: 30 H_2O.

Given the expected use of zincosilicate zeolites for stabilization of multivalent cations, the Zn content in the synthetic mixture was increased to Si/Zn = 25. The formation of CHA zeolite was observed together with the unknown phase both with and without seed crystals (Figure 5-7). However, as shown in Figure 5-8, the formation of such impurity can be suppressed by carrying out the hydrothermal treatment under a tumbling condition at 20 rpm.

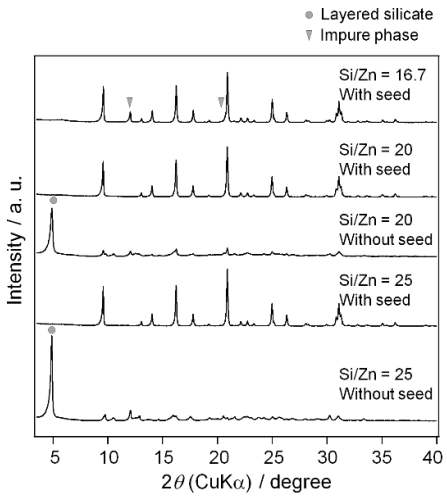

Figure 5-8 Powder XRD patterns of products synthesized under a tumbling condition (20 rpm) with or without pure silica CHA seed crystals (5 wt% on a basis of SiO_2) at different Si/Zn compositions.

Chemical compositions of the selected zincosilicate CHA zeolite products are summarized in Table 1. The molar Si/Zn ratios of the zeolite products were lower than those of the initial synthetic mixture, especially in the case of Zn-CHA1, which is likely because the solid product had low yield due to the absence of seed crystals. Nitrogen adsorption–desorption analysis confirms that all of the obtained zeolites had high micropore volumes. Thermogravimetric analysis shows that 2.8 $TMAda^+$ cations were occluded in a unit cell of CHA zeolite, equivalent to 0.93 $TMAda^+$ per *cha* cage (Figure 5-9). Note that the sharp weight loss due to $TMAda^+$ cation was not observed in the product synthesized by the procedure (ii).

Table 1 Chemical compositions and micropore volumes of the obtained zincosilicate CHA products.

Sample	Seed[a]/wt%	Condition	Si/Zn (Initial)	Si/Zn (Product)[b]	V_{micro}[c] /cm^3 g^{-1}
Zn-CHA1	0	Static	33	12.8	0.24
Zn-CHA2	5	20 rpm	25	18.2	0.25
Zn-CHA3	5	20 rpm	20	14.5	0.25

[a]Pure silica CHA zeolite. [b]Determined by ICP-AES. [c]Calculated by a *t*-plot method

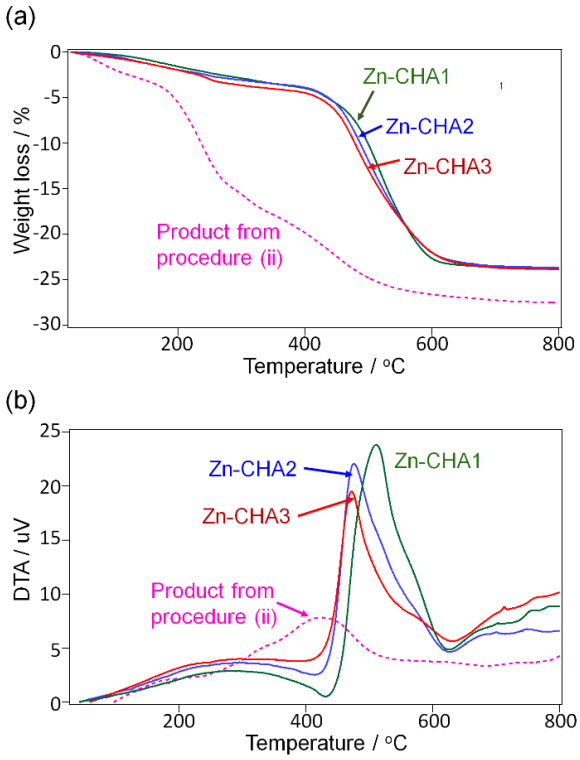

Figure 5-9 (a) TGA and (b) DTA curves of products synthesized from different conditions (see Table 1 for details of products).

Figure 5-10 shows solid-state ^{29}Si MAS NMR spectra of Zn-CHA1, Zn-CHA2 and Zn-CHA3. The spectra were deconvoluted to three signals attributed to $Q^4(0T)$ silicon species ($Si(OSi)_4$) at δ around −110 ppm, $Q^4(1Zn)$ silicon species ($Si(OZn)(OSi)_3$) at δ of ca. −100 ppm. Si/Zn ratio was calculated for each samples from the peak areas of the three peaks using following formula.

$$\left(\frac{\mathrm{Si}}{\mathrm{Zn}}\right)\mathrm{NMR} = \sum_{n=0}^{4} I_{\mathrm{Si}(n\mathrm{Zn})} \Big/ \sum_{n=0}^{4} \left(\frac{n}{4}\right) I_{\mathrm{Si}(n\mathrm{Zn})}$$

The Si/Zn ratios calculated from the ^{29}Si MAS NMR spectra are close to the ratios obtained by ICP-AES analysis. The concurrence of the chemical compositions calculated from ^{29}Si MAS NMR and ICP-AES results suggests the successful incorporation of Zn atoms into the zeolite frameworks. The slightly smaller Si/Zn ratios calculated from NMR spectra compared to those of ICP-AES results are likely indicating the presence of some silanol defects in the zeolites.

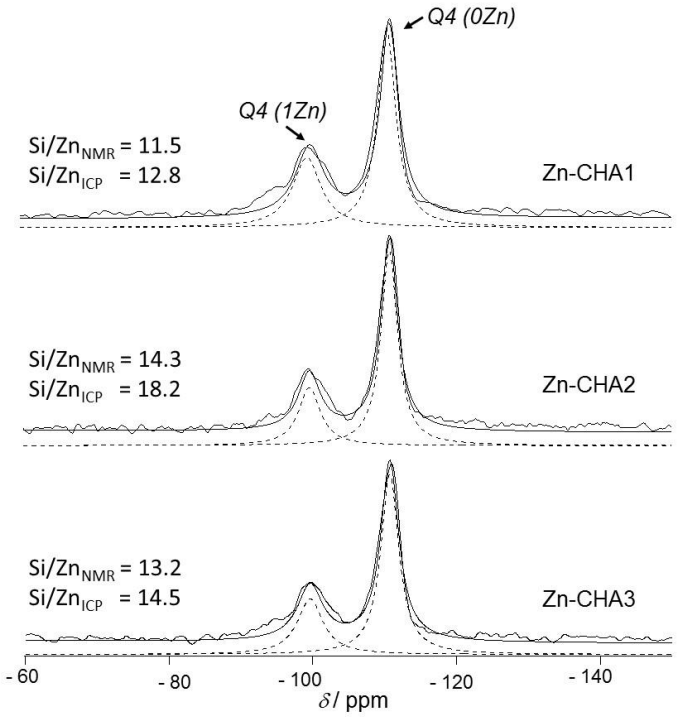

Figure 5-10 Solid-state ^{29}Si MAS NMR spectra and their peak deconvolution of Zn-CHA1, Zn-CHA2 and Zn-CHA3.

The incorporation of Zn into the zeolite framework was confirmed by the peak shifting toward lower angles in XRD patterns, compared to pure silica CHA (Figure 5-11). By assuming all products possess the same space group of $R\bar{3}m$, the cell parameters are calculated to be $a = b$ = 13.49 Å and c = 14.82 Å for pure silica CHA (Rwp = 0.109, Rp = 0.0854), and $a = b$ = 13.55 Å and c = 14.97 Å for Zn-CHA1 (Rwp = 0.116, Rp = 0.0857). As the Zn–O bond length (*ca*. 2 Å) is longer than the Si–O (ca. 1.6 Å), the lattice expansion clearly suggests the successful formation of CHA zeolite with Zn in the framework. The refinement was performed using the PDXL software (Rigaku).

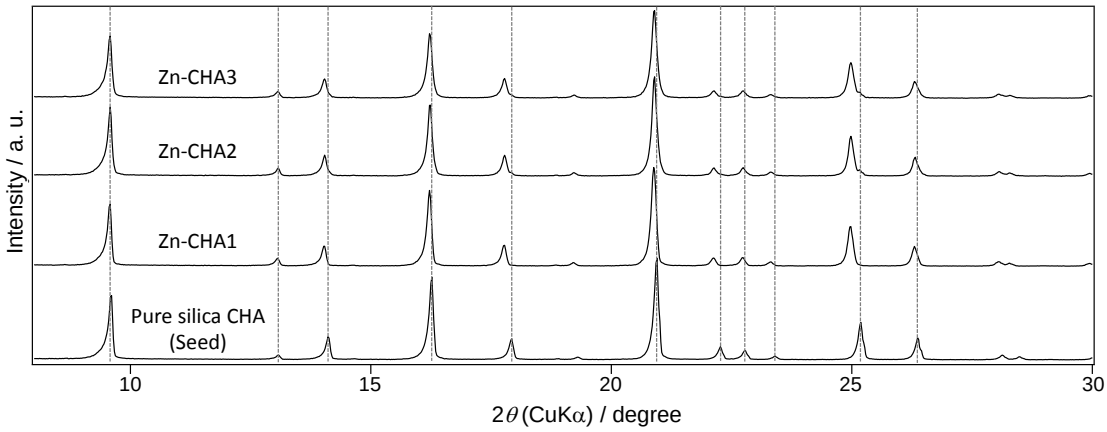

Figure 5-11 Comparison of powder XRD patterns of CHA products with various Zn contents.

As is reported recently, zincosilicate zeolites show strong Lewis acidity.[91] FT-IR analysis of the zeolite product after adsorption of deuterated acetonitrile (CD_3CN) at 80 °C and then desorbed at 80–250 °C was performed to characterize the acid sites of the zincosilicate CHA zeolite in comparison with zincoaluminosilicate CHA[166] (Zn,Al-CHA; Si/Al = 10.5, Si/Zn = 15.3). The stretching frequency of C≡N is sensitive to the interaction strength with Lewis acid sites, making qualitative comparisons among different Lewis acid sites possible. As shown in Figure 5-12 (a), the absorption band due to physisorbed CD_3CN was observed at 2267 cm^{-1}, while the band at 2284 cm^{-1} is probably associated with Li-bearing Zn sites.[91] The bands present at 2308 and 2319 cm^{-1} are associated with CD_3CN coordinated to Lewis acid sites.[91] The existence of these two absorption bands suggests that there are two different Lewis acid sites in the zincosilicate CHA product, as is well documented that the metal-substituted zeolites have different metal sites, so-called "closed" and "open" sites.[91,88,181] The closed Zn site (observed at 2308 cm^{-1}) creating two negative charges is suitable for stabilization of bare divalent metal cations, [152,91] while the open Zn site (observed at 2319 cm^{-1}), a monocation ion-exchangeable site, has been considered as an active Lewis acid (Figure 5-12 (c)). The Zn,Al-CHA sample also showed similar spectra; however, the band assigned to the Li-bearing sites at 2284 cm^{-1} observed in Zn-CHA2 was shifted to 2277 cm^{-1}, which is likely associated with Na^+ present in the Zn,Al-CHA sample (Figure 5-12 (b)).[91] While in the case of relating stannosilicates (well known as a Lewis acid

catalyst), most of adsorbed CD_3CN is desorbed upon evacuation at room temperature,[88] in both Zn-containing CHA samples CD_3CN remains on samples even after evacuation at 250 °C, suggesting the stronger Lewis acidity of zincosilicate materials.

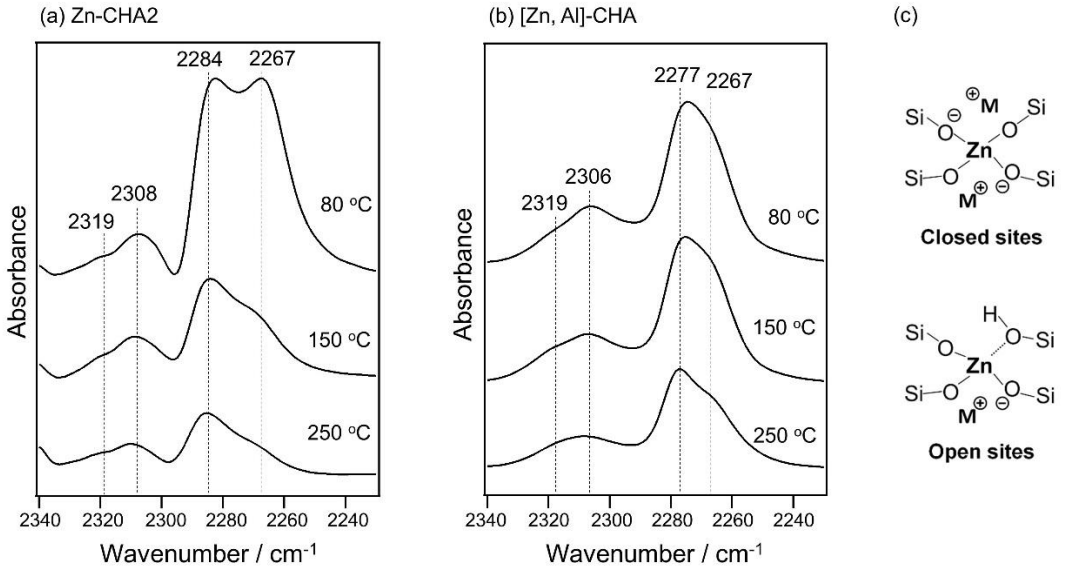

Figure 5-12 FT-IR spectra of deuterated acetonitrile adsorbed on (a) Zn-CHA2 and (b) Zn,Al-CHA followed by evacuation at 80, 150, and 250 °C, respectively. (c) Local structures of two different Zn sites (M^+ is a monovalent cation).

The ion-exchange ability of the obtained zincosilicate CHA zeolites was investigated for both monovalent and divalent cations. Aluminosilicate (SSZ-13) and zincoaluminosilicate[166] (Zn,Al-CHA) CHA zeolites were prepared to compare the ion-exchange abilities (Figure 5-13, Figure 5-14 and table 2).

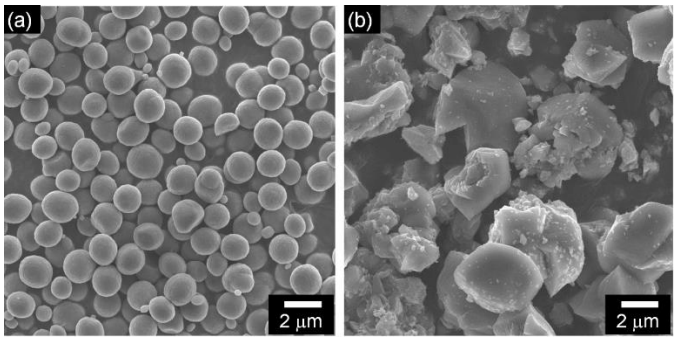

Figure 5-13 FE-SEM images of (a) SSZ-13 and (b) zincoaluminosilicate CHA zeolites.

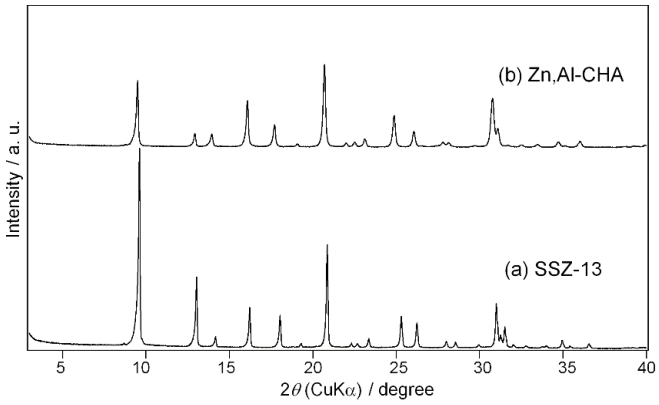

Figure 5-14 Powder XRD patterns of (a) SSZ-13 and (b) zincoaluminosilicate CHA zeolites.

Table 2 Chemical compositions, micropore volumes and particle sizes of SSZ-13 and Zn,Al-CHA samples used for comparison in the ion-exchange experiments

	Si/(Al+Zn)[a]	Si/Al[a]	Si/Zn[a]	Zn/(Al+Zn)[a]	V_{micro}[b]/cm^3 g^{-1}	Particle size[c]/μm
SSZ-13	13.2	13.2	n.a.[d]	n.a.[d]	0.28	1–2
Zn,Al-CHA	6.2	10.5	15.3	0.41	0.19	1–6

[a]Determined by ICP-AES. [b]Micropore volumes calculated by a *t*-plot method. [c]Observed by SEM. [d]Not applicable.

K^+ and Ni^{2+} cations were used as model monovalent and divalent cations, respectively. As shown in Figure 5-15(a), the aluminosilicate SSZ-13 zeolite reached 86% ion-exchange efficiency after 48 h. In contrast, the zincosilicate CHA zeolites exhibited slower ion-exchange rate and the ion-exchange efficiency became 31% for Zn-CHA1 (Si/Zn = 12.8) and 52% for Zn-CHA2 (Si/Zn = 18.2) after 48 h. Note that the ion-exchange efficiency was calculated by assuming that Zn in the framework generates two negative charges per Zn atom (*i.e.*, closed Zn sites). This slower ion-exchange rate may be due to the larger particle sizes of the zincosilicate CHA zeolites and the structure constrain arising from the high density of the negative charges in the structures.

The benefit of Zn in the zeolite framework for ion-exchange of divalent cations was demonstrated using Ni^{2+} because Ni^{2+}-exchanged zeolites are promising catalysts for dimerization and oligomerization of olefins.[152,182] As shown in Figure 5-16(b), the

SSZ-13 sample showed very low ion-exchange efficiency (only 6% after 96 h). The formation of the paired Al sites is known to be unfavorable in the case of SSZ-13 zeolite due to the high charge density of $TMAda^+$ employed for its synthesis.[165] As a result, the SSZ-13 sample used here is not suitable for ion-exchange of divalent cations. On the contrary, the zincosilicate CHA products exhibited higher ion-exchange efficiency (80% and 62% after 96 h for Zn-CHA1 and Zn-CHA2, respectively) despite the fact that the zincosilicate CHA products have comparable substitution contents to that of aluminosilicate SSZ-13 (i.e., similar Si/Zn and Si/Al ratios). The zincoaluminosilicate CHA zeolite[166] has intermediate ion-exchange efficiency (39% after 96 h), suggesting that Zn in the zincoaluminosilicate framework can stabilize Ni^{2+}, while the content of the paired Al sites is insufficient for the divalent cation-exchange.

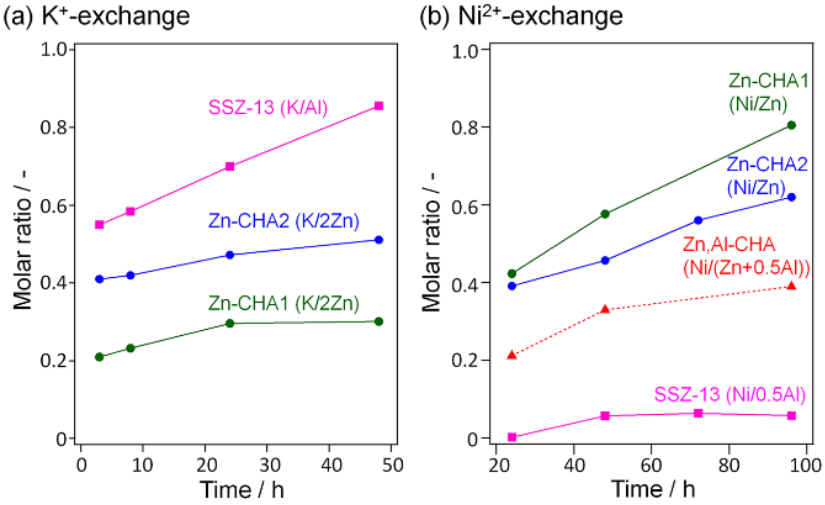

Figure 5-16 Contents of ion-exchange versus time of (a) K^+ and (b) Ni^{2+} cations for zincosilicate, aluminosilicate (SSZ-13) and zincoaluminosilicate CHA zeolites.

FT-IR spectra of Zn-CHA2 before and after ion-exchange with Ni^{2+} are depicted in Figure 5-17. The disappearance of the broad band centered at 3630 cm^{-1}, presumably assigned to the bridging SiOHZn groups, after ion-exchange confirmed the ion-exchange from protons to Ni^{2+}. In addition, no marked absorption band due to the Ni–OH vibration, typically appearing at around 3640 cm^{-1},[243,244,245] was observed, suggesting that no significant amount of $Ni(OH)^+$ species was formed after ion-exchange.

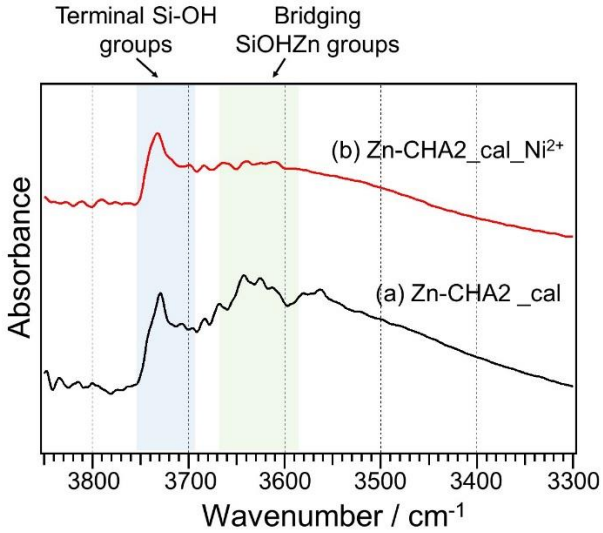

Figure 5-17 FT-IR spectra in the region of hydroxyl groups of (a) Zn-CHA2 and (b) Zn-CHA2 after the ion-exchange with Ni^{2+}.

Effect of thermal treatment on the environment of Ni^{2+} species was investigated. After ion-exchange for 96 h, DR UV–vis spectra of the Ni^{2+}-exchanged Zn-CHA2 and Zn,Al-CHA samples showed characteristic adsorption bands correlated to Ni^{2+} cations in octahedral symmetry,[246] suggesting the presence of $[Ni(H_2O)_6]^{2+}$ complexes in the zeolite samples (Figure 5-18(a)). After thermal treatment under dried air at 600 °C for 6 h, both Zn-CHA2 and Zn,Al-CHA samples exhibited additional bands at around 260 nm (Figure 5-18(b)), attributed to an electronic transition with charge transfer (CT) in NiO.[32] The position of this $O^{2-} \rightarrow Ni^{2+}$ CT band is related to the degree of agglomeration of NiO species (note that the CT band for bulk NiO is observed at 320 nm).[247] The blue shift of this band observed in both samples suggests the formation of small NiO clusters.[247] The band observed in Zn,Al-CHA was stronger than that in Zn-CHA2 and had a broad shoulder between 260 and 350 nm, suggesting the higher degree of NiO agglomeration. Collectively, these results suggest that the zincosilicate CHA zeolites are superior to the aluminosilicate and zincoaluminosilicate counterparts for ion-exchange and stabilization of divalent cations such as Ni^{2+}.

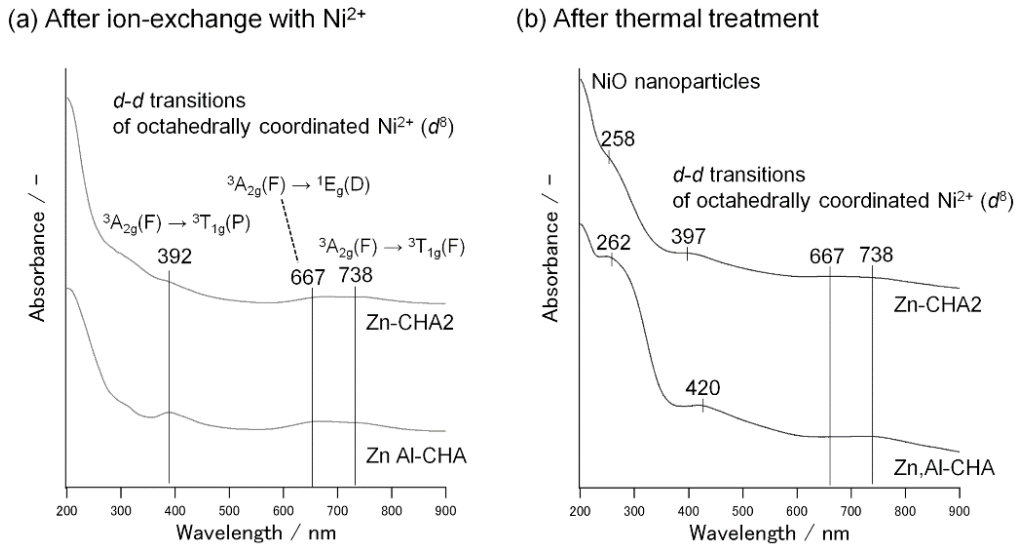

Figure 5-18 DR UV-Vis spectra of Zn-CHA2 and Zn,Al-CHA samples (a) after the ion-exchange with Ni^{2+} and (b) subsequent calcination at 600 °C for 6 h.

As shown in Figure 5-19, the prepared Zn-CHA2 (after removal of $TMAda^{+}$) decreased crystallinity by calcination at 600 °C for 6 hours in air, because some of the zinc atoms can be removed from the CHA framework. However, when the zincosilicate CHA was calcined after the ion-exchange with Ni^{2+}, the crystallinity was almost unchanged. This improved thermal stability is attributed to divalent cation (Ni^{2+} here) placed onto the ion-exchange site of zincosilicate sample, which can protect the framework zinc.[152]

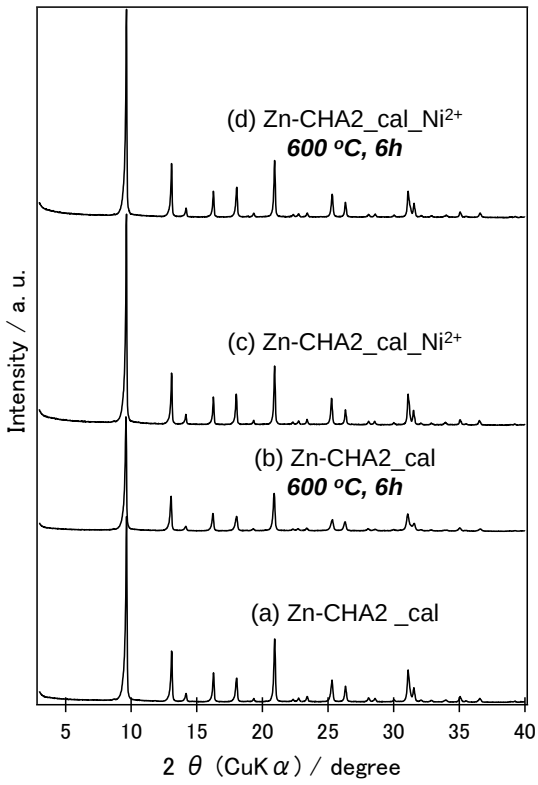

Figure 5-20 Powder XRD patterns of products pf (a) Zn-CHA2 zeolite after removal of $TMAda^+$, (b) Zn-CHA2 calcined at 600°C for 6 hours in air after removal of $TMAda^+$, (c) Zn-CHA2 zeolite after removal of $TMAda^+$ and subsequent ion-exchange with Ni^{2+}, (d) zincosilicate CHA zeolite after removal of $TMAda^+$ and subsequent ion-exchange with Ni^{2+} and calcination at 600°C for 6 hours in air.

5.4 Conclusions

Zincosilicate CHA zeolites were synthesized for the first time by controlling the initial state of Zn in the synthetic mixture. Only the mixture with high homogeneity of zinc and silicate species, pure CHA zeolite was obtained, otherwise amorphous phase or layered silicate materials are formed. By controlling several synthetic factors, such as additional seed crystals, zincosilicate CHA zeolites with various Zn contents (Si/Zn = 12.8–18.2) were obtained. For the synthesis of zincosilicate CHA zeolite, Li cation is needed for the nucleation, but crystal growth can proceed with only TMAdaOH. The

obtained zincosilicate CHA zeolites possessed remarkably higher ion-exchange ability for divalent cations, demonstrated using Ni^{2+}, compared to that of aluminosilicate and zincoaluminosilicate analogs. The thermal stability of zincosilicate CHA zeolite was improved by Ni^{2+} cation in the ion exchange position.

It is noteworthy that the approach to prepare homogeneous mixture of zinc and silicate for the synthesis of zinc-containing zeolites can be achieved not only by the co-precipitation method but by simply adjusting the mixing procedure of raw materials.

Chapter 6. General Conclusions and Future perspectives

New classes of zeolites with partial substitution of various heteroatoms other than aluminum in their frameworks has realized many new applications or shown greatly improved properties compared to conventional zeolites. Therefore, synthesis of those metal substituted zeolites have continued to be a significant research field. However, to achieve the synthesis of metal substituted zeolites, complex procedures and/or compounds with high cost and environmental burden are sometimes needed to overcome several obstacles such as low solubility of the metal in basic media. Even though the product shows remarkable properties, it would be difficult to industrialize those methods for commercialization because of the obstacles.

Zinc-containing zeolites are promising materials with characteristic Lewis acidity and ion-exchange capacity. However, available zeolite topologies and content of zinc-containing zeolites is quite limited due to, for example, the different reactivity from silicon and aluminum and longer Zn–O bond length compared to Si–O and Al–O. For the synthesis, sometimes expensive organic compound as organic structure-directing agent or complexing agent to stabilize zinc is needed. In this dissertation, synthesis methods for zinc-containing zeolites were developed in various conditions with a focus on mixing method of raw materials. This dissertation describes the important factors to accomplish zinc introduction to zeolite frameworks in various conditions and broaden available zeolite topologies and content of zinc-containing zeolites. The synthesis was achieved by focusing on mixing procedures of commonly used raw materials without using additional complex compounds.

In Chapter 1, a general background of porous materials was described. Then, researches about various metal containing zeolites, especially zinc-containing zeolites, were summarized. The two main remarkable properties of zincosilicate zeolites, *i.e.* ion-exchange ability and Lewis acidity are described in detail in relation to the different zinc sites. Other attempts targeting to introduce Lewis acidity (*e.g.* Ti and Sn containing

zeolites) or increase ion-exchange ability of zeolites (*e.g.* aluminosilicate zeolites with increased paired Al sites) are also summarized and superiority of zincosilicate zeolites in some features are described.

In Chapter 2, co-precipitation method is demonstrated to be an alternative method to prepare zincoaluminosilicate gel with highly dispersed zinc species in silicates. The homogeneous zincoaluminosilicate gels were used for the synthesis of MOR zeolites and organic-free synthesis of zincoaluminosilicate MOR zeolites was demonstrated for the first time. In contrast to conventional synthesis of zeolites, in which separate sources of Si and other tetrahedral atoms such as Al and Zn are used, the co-precipitated gels contained all tetrahedral atoms, therefore the reaction between zinc and silicate species was expected to be promoted to form zincoaluminosilicate zeolite frameworks. The successful zinc introduction to MOR frameworks without using any organic substances revealed the importance to prepare the homogeneous gels before hydrothermal treatment. Importance of aluminum species in the synthesis was also suggested.

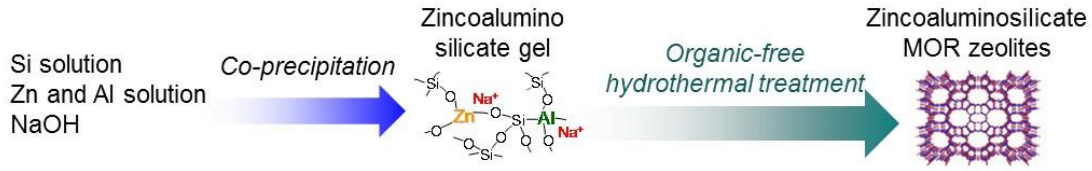

Figure 6-1 Schematic images for organic-free synthesis of zincoaluminosilicate MOR zeolites by using homogeneous gels prepared by co-precipitation method

In Chapter 3, based on the success in the synthesis of zincoaluminosilicate MOR zeolites using the co-precipitated zincoaluminosilicate gels, the applicable scope of the synthesis of zinc-containing zeolites using the gels was aimed to be broaden using ‘composite-building unit (CBU)’ hypothesis which has been developed as a strategy to achieve OSDA-free synthesis of aluminosilicate zeolites. Based on the hypothesis, *BEA and MFI zeolites which have same CBU as MOR zeolite were selected as target zeolites. The synthesis was conducted by adding the seed crystals of target zeolites to the synthetic mixture which yield MOR zeolite with the absence of seeds. The *BEA and MFI zeolites were obtained by using zincoaluminosilicate gels

with Zn/(Zn+Al) = 0.1–0.2, and 0.2–0.8, respectively, while the MOR zeolites were prepared by using the gels with Zn/(Zn+Al) of 0.1–0.6. These results suggested that the limitation in zinc introduction differs depending of the structures of zeolites. It was shown that synthesis conditions such as NaOH/Si ratio and temperature of hydrothermal treatment should be optimized to prevent spontaneous nucleation of MOR zeolites before the completion of crystallization of the targeted zeolites. This achievement showed the possibility to prepare various zinc containing zeolites in an OSDA-free manner by applying the CBU hypothesis as OSDA-free synthesis of various aluminosilicate zeolites have been achieved.

Figure 6-2 Schematic images for organic-free synthesis of various zincoaluminosilicate zeolites from co−precipitated zincoaluminosilicate gels by applying composite building unit hypothesis

In Chapter 4, the co-precipitation method to prepare homogeneous zincosilicate gels was further extended to obtain the zincosilicate gels with occluded OSDA in the silicate structure by conducting the co-precipitation in the presence of the OSDA. In contrast to the co-precipitation using NaOH which yielded zincosilicate gels with sodium cation as counter cation, tetraethylammonium (TEA) cation was occluded in zincosilicate gels prepared by the co-precipitation in the presence of TEAOH. Characterization of the zincoaluminosilicate gels suggested that Zn species were homogeneously distributed in the silicate matrix. TEA^+ cations were occluded in the zincosilicate structure and the existence of TEA^+ probably inhibit 3MR formation which have been reported to occur in the conditions with high-zinc content. By using the zincosilicate gel formed with TEA^+, synthesis of *BEA zeolites, which have been synthesized by using TEA^+ as an OSDA was conducted. Zincosilicate *BEA zeolites with higher zinc content compared with the previous reports were obtained with the assistance of seed crystals.

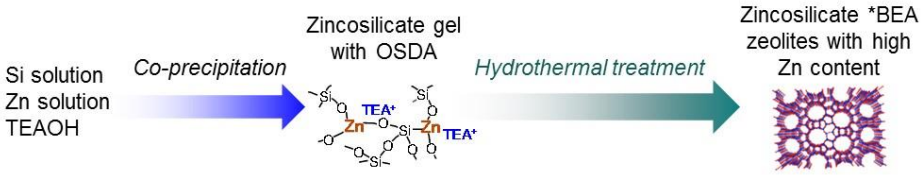

Figure 6-3 Schematic images for synthesis of zincosilicate zeolites from zincosilicate gels prepared by an organic structure-directing agent involved co-precipitation method

Chapter 5 presents a method to increase homogeneity of zinc and silicate species with a particular focus on mixing method of raw materials in liquid phase. Only the mixture with high homogeneity of zinc and silicate species, pure CHA zeolite was obtained, otherwise amorphous phase or layered silicate materials are formed. For the synthesis of zincosilicate CHA zeolite, Li cation is needed for the nucleation, but crystal growth can proceed with only TMAdaOH.

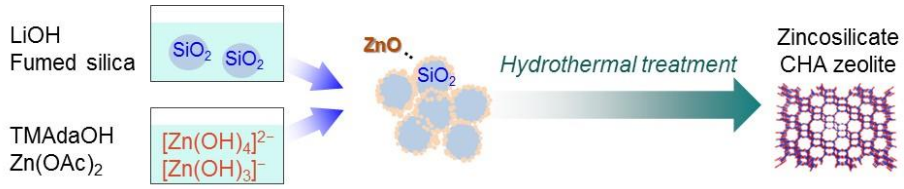

Figure 6-4 Schematic images for synthesis of new zincosilicate zeolites with CHA topology by focusing on mixing procedures of raw materials in liquid phase

In this dissertation, various methods to synthesize zinc-substituted zeolites were demonstrated, by focusing on the mixing procedures. Several general aspects to achieve the synthesis of zinc-substituted zeolites were suggested as follows.

- Homogeneous zinc and silicate mixture should be prepared before hydrothermal treatment to prevent formation of ZnO species in the synthesis both with and without OSDAs.
- Synthesis of zinc-containing zeolites in an OSDA-free manner can be achieved by using seed crystals and CBU hypothesis.
- Certain amount of Al is mostly needed for the successful formation of zeolite framework with zinc in the OSDA-free manner and zincoaluminosilicate gels are

effective to introduce both Zn and Al to zeolite framework.

- The use of OSDAs suitable for the targeted zeolite structure helps formation of zincosilicate framework and homogenization of zinc and silica source with OSDA is effective to increase the content of Zn introduced to the zeolite framework.

It is important to choose the method depending on the targeted zeolites and desired properties. When the co-existence of Al in the framework is acceptable, OSDA-free synthesis using zincoaluminosilicate gels described in Chapter 2 and 3 will be preferable. For the applications which require pure zincosilicate frameworks, synthesis using OSDAs will be adequate. For the simple and cheap OSDAs, OSDA-involved co-precipitation method shown in Chapter 4 is applicable. When the OSDAs are rather complex and costly, the mixing method focusing on Zn state in synthetic solutions will be suitable as shown in Chapter 5. It is important to have the choices for various demand in accordance with the conditions and necessities.

Also, throughout the studies, detailed characterizations revealed characteristic Lewis acidic features and remarkable ion-exchange ability for divalent cations of zinc-substituted zeolites. The high affinity to divalent cations with negative charges generated by framework zinc was clearly shown for the first time by constructing mono-divalent ion-exchange isotherms. It was also found that there are two different local environments of Zn in the zeolite frameworks with different Lewis acidity.

The developed methods for the synthesis of zinc-containing zeolites are anticipated to be effectively applicable for other heteroatoms such as B, Ga, and Fe, and various zeolite frameworks. The generation of new class of zeolites by using the facile methods will open the door for many new applications which have not been accessible by the existing zeolites or zeolites prepared by complex procedure. Additionally, the co-precipitation method will provide the method to prepare zeolites with more than two types of heteroatoms incorporated together to the framework, which has been considered to be difficult because of the difference in reactivity between the different metals.

Furthermore, by combining the properties of framework metals and extra-framework metal species in ion-exchange sites, advanced materials with new or

improved properties compared to the existing one are expected to be provided. For example, catalysts with bifunctionality (combined functionalities derived from the framework and extra-framework metals) are anticipated to catalyze tandem reactions with high selectivity. For example, a zeolite combining both Brønsted acid sites effective for alcohol dehydrogenation and ion-exchanged Ni^{2+} active sites for olefin dimerization is expected to realize one-pot ethylene oligomerization reactions from ethanol to produce a heavier, more valuable molecules (Figure 6-5 (i)).[248] Combination of the Brønsted acid sites effective for alcohol dehydrogenation and zinc Lewis acid sites will enable, for example, formation of dimethyl terephthalate from biomass derived ethanol and dimethyl ester of furan-2,5-dicarboxilic acid thorough Diels–Alder cycloaddition–dehydration reactions of ethylene formed by ethanol dehydration (Figure 6-5 (ii)).

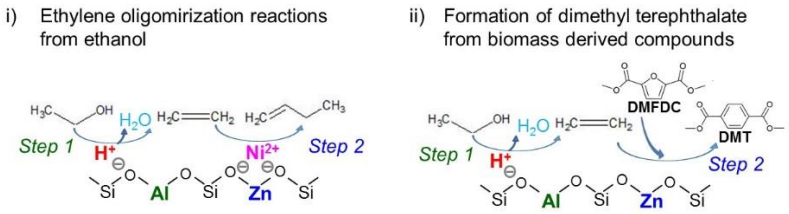

Figure 6-5 Schematic images for application of zincoaluminosilicate zeolites by combining the activities of framework and extra framework metals.

Furthermore, when the certain location of Zn (and other metals) in the zeolitic frameworks are able to be controlled, improvement in catalyst stability and selectivity will be achieved by careful tuning of the catalyst active sites. Taken together, the methods are expected to provide new approaches in, especially, catalytic applications.

The facile methods to incorporate zinc (and other metals) provided in this dissertation have versatile applicability, and the simplicity will make it possible to produce the advanced zeolites which can really be used in the industry.

References

(1) Davis, M. E. Ordered porous materials for emerging applications. *Nature* **2002**, *417*, 813–821.

(2) Thommes, M.; Kaneko, K.; Neimark, A. V.; Olivier, J. P.; Rodriguez-Reinoso, F.; Rouquerol, J.; Sing, K. S. W. Physisorption of gases, with special reference to the evaluation of surface area and pore size distribution (IUPAC Technical Report). *Pure Appl. Chem.* **2015**, *87*, 1051–1069.

(3) Cundy, C. S.; Cox, P. A. The hydrothermal synthesis of zeolites: Precursors, intermediates and reaction mechanism. *Microporous Mesoporous Mater.* **2005**, *82*, 1–78.

(4) Cox, P.; Casci, J. L.; Stevens, P. Molecular modelling of templated zeolite synthesis. *Faraday Discuss.* **1997**, *106*, 473–487.

(5) Yaghi, O. M.; O'Keeffe, M.; Ockwig, N. W.; Chae, H. K.; Eddaoudi, M.; Kim, J. Reticular synthesis and the design of new materials. *Nature* **2003**, *423*, 705–714.

(6) Si, Y.; Chen, M.; Wu, L. Syntheses and biomedical applications of hollow micro-/nano-spheres with large-through-holes. *Chem. Soc. Rev.* **2016**, *45*, 690–714.

(7) Djojoputro, H.; Zhou, X. F.; Qiao, S. Z.; Wang, L. Z.; Yu, C. Z.; Lu, G. Q. Periodic mesoporous organosilica hollow spheres with tunable wall thickness. *J. Am. Chem. Soc.* **2006**, *128*, 6320–6321.

(8) Liu, J.; Yang, Q.; Zhang, L.; Yang, H.; Gao, J.; Li, C. Organic-inorganic hybrid hollow nanospheres with microwindows on the shell. *Chem. Mater.* **2008**, *20*, 4268–4275.

(9) Manchanda, A. S.; Kruk, M. Synthesis of Xylylene-Bridged Periodic Mesoporous Organosilicas and Related Hollow Spherical Nanoparticles. *Langmuir* **2016**, *32*, 900–908.

(10) Wang, Y.; Su, X.; Ding, P.; Lu, S.; Yu, H. Shape-controlled synthesis of hollow silica colloids. *Langmuir* **2013**, *29*, 11575–11581.

(11) Guo, W.; Wang, J.; Lee, S. J.; Dong, F.; Park, S. S.; Ha, C. S. A general pH-responsive supramolecular nanovalve based on mesoporous organosilica hollow nanospheres. *Chem. - A Eur. J.* **2010**, *16*, 8641–8646.

(12) Koike, N.; Chaikittisilp, W.; Shimojima, A.; Okubo, T. Surfactant-free synthesis of hollow mesoporous organosilica nanoparticles with controllable particle sizes and diversified organic moieties. *RSC Adv.* **2016**, *6*, 90435–90445.

(13) Aguirre, C. I.; Reguera, E.; Stein, A. Tunable colors in opals and inverse opal photonic crystals. *Adv. Funct. Mater.* **2010**, *20*, 2565–2578.

(14) Yamamoto, E.; Kitahara, M.; Tsumura, T.; Kuroda, K. Preparation of size-controlled monodisperse colloidal mesoporous silica nanoparticles and fabrication of colloidal crystals. *Chem. Mater.* **2014**, *26*, 2927–2933.

(15) Ohji, T.; Fukushima, M. Macro-porous ceramics: processing and properties. *Int. Mater. Rev.* **2012**, *57*, 115–131.

(16) Hartmann, M.; Machoke, A. G.; Schwieger, W. Catalytic test reactions for the evaluation of hierarchical zeolites. *Chem. Soc. Rev.* **2016**, *45*, 3313–3330.

(17) Wang, D. W.; Li, F.; Liu, M.; Lu, G. Q.; Cheng, H. M. 3D aperiodic hierarchical porous graphitic carbon material for high-rate electrochemical capacitive energy storage. *Angew. Chemie - Int. Ed.* **2008**, *47*, 373–376.

(18) Cheetham, A. K.; Férey, G.; Loiseau, T. Open-Framework Inorganic Materials. *Angew. Chemie Int. Ed.* **1999**, *38*, 3268–3292.

(19) Yamauchi, Y.; Sugiyama, A.; Morimoto, R.; Takai, A.; Kuroda, K. Mesoporous platinum with giant mesocages templated from lyotropic liquid crystals consisting of diblock copolymers. *Angew. Chemie - Int. Ed.* **2008**, *47*, 5371–5373.

(20) Attard, G. S.; Corker, J. M.; Göltner, C. G.; Henke, S.; Templer, R. H. Liquid-Crystal Templates for Nanostructured Metals. *Angew. Chemie Int. Ed.* **1997**, *36*, 1315–1317.

(21) Faik Demirörs, A.; Eser, B. E.; Dag, Ö. Liquid crystalline mesophases of pluronics (L64, P65, and P123) and transition metal nitrate salts. *Langmuir* **2005**, *21*, 4156–4162.

(22) Celik, O.; Dag, O. A new lyotropic liquid-crystalline system: Oligo(etylene oxide) Surfactants with Transition Metal Complexes. *Angew. Chem. Int. Ed.* **2001**, *40*, 3799–3803.

(23) Yang, P.; Deng, T.; Zhao, D.; Feng, P.; Pine, D.; Chmelka, B. F.; Whitesides, G. M.; Stucky, G. D.

Hierarchically Ordered Oxides. *Science (80-.).* **1998**, *282*, 2244–2246.
(24) Slowing, I. I.; Trewyn, B. G.; Giri, S.; Lin, V. S. Y. Mesoporous silica nanoparticles for drug delivery and biosensing applications. *Adv. Funct. Mater.* **2007**, *17*, 1225–1236.
(25) Yanagisawa, T.; Shimizu, T.; Kuroda, K.; Kato, C. The preparation of alkyltrimethylammonium-kanemite complexes and their conversion to microporous materials. *Bull. Chem. Soc. Jpn.* **1990**, *63*, 988–992.
(26) Kresge, C. T.; Leonowicz, M. E.; Roth, W. J.; Vartuli, J. C.; Beck, J. S. Ordered mesoporous molecular sieves synthesized by a liquid-crystal template mechanism. *Nature* **1992**, *359*, 710–712.
(27) Yang, P.; Gai, S.; Lin, J. Functionalized mesoporous silica materials for controlled drug delivery. *Chem. Soc. Rev.* **2012**, *41*, 3679.
(28) Jiang, C.; Hara, K.; Fukuoka, A. Low-temperature oxidation of ethylene over platinum nanoparticles supported on mesoporous silica. *Angew. Chemie - Int. Ed.* **2013**, *52*, 6265–6268.
(29) Frackowiak, E.; Béguin, F. Carbon materials for the electrochemical storage of energy in capacitors. *Carbon N. Y.* **2001**, *39*, 937–950.
(30) Monser, L.; Adhoum, N. Modified activated carbon for the removal of copper, zinc, chromium and cyanide from wastewater. *Sep. Purif. Technol.* **2002**, *26*, 137–146.
(31) Zhuang, X.; Wan, Y.; Feng, C.; Shen, Y.; Zhao, D. Highly Efficient Adsorption of Bulky Dye Molecules in Wastewater on Ordered Mesoporous Carbons. *Chem. Mater.* **2009**, *21*, 706–716.
(32) Ockwig, N. W.; Co, A. P.; Keeffe, M. O.; Matzger, A. J.; Yaghi, O. M. Porous , Crystalline , Covalent Organic Frameworks. **2005**, *310*, 1166–1171.
(33) Lu, W.; Yuan, D.; Zhao, D.; Schilling, C. I.; Plietzsch, O.; Muller, T.; Bräse, S.; Guenther, J.; Blümel, J.; Krishna, R.; et al. Porous polymer networks: Synthesis, porosity, and applications in gas storage/separation. *Chem. Mater.* **2010**, *22*, 5964–5972.
(34) Furukawa, H.; Yaghi, O. M. Storage of Hydrogen, Methane, and Carbon Dioxide in Highly Porous Covalent Organic Frameworks for Clean Energy Applications. *J. Am. Chem. Soc.* **2009**, *131*, 8875–8883.
(35) Hoffmann, F.; Cornelius, M.; Morell, J.; Fröba, M. Silica-based mesoporous organic-inorganic hybrid materials. *Angew. Chemie - Int. Ed.* **2006**, *45*, 3216–3251.
(36) Shea, K. J.; Loy, D. A.; Webster, O. Arylsilsesquioxane Gels and Related Materials. New Hybrids of Organic and Inorganic Networks. *J. Am. Chem. Soc.* **1992**, *114*, 6700–6710.
(37) Schaefer, D. W.; Beaucage, G.; Loy, D. A.; Shea, K. J.; Lin, J. S. Structure of Arylene-Bridged Polysilsesquioxane Xerogels and Aerogels. *Chem. Mater.* **2004**, *16*, 1402–1410.
(38) Hagiwara, Y.; Shimojima, A.; Kuroda, K. Alkoxysilylated-derivatives of double-four-ring silicate as novel building blocks of silica-based materials. *Chem. Mater.* **2008**, *20*, 1147–1153.
(39) Chaikittisilp, W.; Sugawara, A.; Shimojima, A.; Okubo, T. Microporous hybrid polymer with a certain crystallinity built from functionalized cubic siloxane cages as a singular building unit. *Chem. Mater.* **2010**, *22*, 4841–4843.
(40) Chaikittisilp, W.; Sugawara, A.; Shimojima, A.; Okubo, T. Hybrid porous materials with high surface area derived from bromophenylethenyl-functionalized cubic siloxane-based building units. *Chem. - A Eur. J.* **2010**, *16*, 6006–6014.
(41) Kuge, H.; Hagiwara, Y.; Shimojima, A.; Kuroda, K. Oligomeric alkoxysilanes with cagelike hybrids as cores: Designed precursors of nanohybrid materials. *Chem. - An Asian J.* **2008**, *3*, 600–606.
(42) Mal, N. K.; Fujiwara, M.; Tanaka, Y. Photocontrolled reversible release of guest molecules from coumarin-modified mesoporous silica. *Nature* **2003**, *421*, 350–353.
(43) Shimojima, A.; Liu, Z.; Ohsuna, T.; Terasaki, O.; Kuroda, K. Self-assembly of designed oligomeric siloxanes with alkyl chains into silica-based hybrid mesostructures. *J. Am. Chem. Soc.* **2005**, *127*, 14108–14116.
(44) Sakamoto, S.; Shimojima, A.; Miyasaka, K.; Ruan, J.; Terasaki, O.; Kuroda, K. Formation of two- and three-dimensional hybrid mesostructures from branched siloxane molecules. *J. Am. Chem. Soc.* **2009**, *131*, 9634–9635.
(45) Inagaki, S.; Guan, S.; Fukushima, Y.; Ohsuna, T.; Terasaki, O. Novel mesoporous materials with a uniform distribution of organic groups and inorganic oxide in their frameworks. *J. Am. Chem. Soc.* **1999**, *121*, 9611–9614.
(46) Melde, B. J.; Holland, B. T.; Blanford, C. F.; Stein, A. Mesoporous Sieves with Unified Hybrid Inorganic/Organic Frameworks. *Chem. Mater.* **1999**, *11*, 3302–3308.
(47) Asefa, T.; MacLachan, M. J.; Coombs, N.; Ozin, G. A. Periodic mesoporous organosilicas with organic

groups inside the channel walls. *Nature* **1999**, *402*, 867–871.
(48) Kapoor, M. P.; Inagaki, S. Synthesis of cubic hybrid organic-inorganic mesostructures with dodecahedral morphology from a binary surfactant mixture. *Chem. Mater.* **2002**, *14*, 3509–3514.
(49) Inagaki, S.; Guan, S.; Ohsuna, T.; Terasaki, O. An ordered mesoporous organosilica hybrid material with a crystal-like wall structure. *Nature* **2002**, *416*, 304–307.
(50) Kitagawa, S.; Kitaura, R.; Noro, S. Functional Porous Coordination Polymers. *Angew. Chemie Int. Ed.* **2004**, *43*, 2334–2375.
(51) Li, J.-R.; Kuppler, R. J.; Zhou, H.-C. Selective gas adsorption and separation in metal–organic frameworks. *Chem. Soc. Rev.* **2009**, *38*, 1477.
(52) Lee, J.; Farha, O. K.; Roberts, J.; Scheidt, K. A.; Nguyen, S. T.; Hupp, J. T. Metal–organic framework materials as catalysts. *Chem. Soc. Rev.* **2009**, *38*, 1450.
(53) Davis, M. E.; Lobo, R. F. Zeolite and Molecular Sieve Synthesis. *Chem. Mater.* **1992**, *4*, 756–768.
(54) Database of Zeolite Structures, http://www.iza-structure.org/databases/ (accessed October 30, 2017).
(55) Barrer, R. M. Synthesis of a zeolitic mineral with chabazite-like sorptive properties. *J. Chem. Soc.* **1948**, 127.
(56) Milton, R. M. MOLECULAR SIEVE ADSORBENTS. *US Pat. 2882243* **1959**.
(57) Barrer, R. M.; Denny, P. J. Hydrothermal Chemistry of the Silicates. Part IX Nitrogenous Alurninosilicates. *J. Chem. Soc.* **1961**, 971–982.
(58) Wilson, S. T.; Lok, B. M.; Messina, C. A.; Cannan, T. R.; Flanigen, E. M. Aluminophosphate Molecular Sieves. *J. Am. Chem. Soc.* **1982**, *104*, 1146–1147.
(59) Ng, E.; Chateigner, D.; Bein, T.; Valtchev, V.; Mintova, S. Capturing Ultrasmall EMT Zeolite from Template-Free Systems. **2012**, *335*, 70–74.
(60) Ng, E. P.; Goupil, J. M.; Vicente, A.; Fernandez, C.; Retoux, R.; Valtchev, V.; Mintova, S. Nucleation and crystal growth features of EMT-type zeolite synthesized from an organic-template-free system. *Chem. Mater.* **2012**, *24*, 4758–4765.
(61) Maldonado, M.; Oleksiak, M. D.; Chinta, S.; Rimer, J. D. Controlling crystal polymorphism in organic-free synthesis of Na-zeolites. *J. Am. Chem. Soc.* **2013**, *135*, 2641–2652.
(62) Ueda, S.; Kageyama, N.; Koizumi, M.; Kobayashi, S.; Fujiwara, Y.; Kyogoku, Y. Role of soluble species in the crystallization of mordenites. *J. Phys. Chem.* **1984**, *88*, 2128–2131.
(63) Wenyang, X.; Jianquan, L.; Wenyuan, L.; Huiming, Z.; Bingchang, L. Nonaqueous synthesis of ZSM-35 and ZSM-5. *Zeolites* **1989**, *9*, 468–473.
(64) Iton, L. E.; Brun, T. O.; Epperson, J. E.; Trouw, F.; White, J. W.; Henderson, S. J. Small-Angle Neutron-Scattering Studies of the Template-Mediated Crystallization of ZSM-5-Type Zeolite. *Langmuir* **1992**, *8*, 1045–1048.
(65) Warzywoda, J.; Edelman, R. D.; Thompson, R. W. Thoughts on the induction time in zeolite crystallization. *Zeolites* **1989**, *9*, 187–192.
(66) E. M. Flanigen, J. M. Bennett, R. W. Grose, J. P. Cohen, R. L. Patton, R. M. Kirchner, J. V. S. Silicalite, a new hydrophobic crystalline silica molecular sieve. *Nature* **1978**, *271*, 512–516.
(67) Brar, T.; France, P.; Smirniotis, P. G. Heterogeneous versus homogeneous nucleation and growth of zeolite A. *J. Phys. Chem. B* **2001**, *105*, 5383–5390.
(68) Ren, N.; Subotić, B.; Bronić, J.; Tang, Y.; Dutour Sikirić, M.; Mišić, T.; Svetličić, V.; Bosnar, S.; Antonić Jelić, T. Unusual pathway of crystallization of zeolite ZSM-5 in a heterogeneous system: Phenomenology and starting considerations. *Chem. Mater.* **2012**, *24*, 1726–1737.
(69) de Moor, P. P. E. A.; Beelen, T. P. M.; van Santen, R. A. In situ observation of nucleation and crystal growth in zeolite synthesis. A small-angle X-ray scattering investigation on Si-TPA-MFI. *J. Phys. Chem. B* **1999**, *103*, 1639–1650.
(70) Moliner, M.; Rey, F.; Corma, A. Towards the rational design of efficient organic structure-directing agents for zeolite synthesis. *Angew. Chemie - Int. Ed.* **2013**, *52*, 13880–13889.
(71) Koller, H.; Wölker, A.; Villaescusa, L. A.; Díaz-Cabañas, M. J.; Valencia, S.; Camblor, M. A. Five-coordinate silicon in high-silica zeolites. *J. Am. Chem. Soc.* **1999**, *121*, 3368–3376.
(72) Burton, A. W.; Zones, S. I.; Elomari, S. The chemistry of phase selectivity in the synthesis of high-silica zeolites. *Curr. Opin. Colloid Interface Sci.* **2005**, *10*, 211–219.
(73) Freyhardt, C. C.; Tsapatsis, M.; Lobo, R. F.; Balkus, K. J.; Davis, M. E. A high-silica zeolite with a 13-tetrahedral-atom pore opening. *Nature* **1996**, *381*, 295–298.

(74) Wagner, P.; Yoshikawa, M.; Lovallo, M.; Tsuji, K.; Davis, M. E. CIT-5 : a high-silica zeolite with 14-ring pores. *Chem. Commun.* **1997**, *22*, 2179–2180.
(75) Liu, M.; Yokoi, T.; Kondo, J. N.; Tatsumi, T. Synthesis of SFH-type aluminosilicate zeolite with 14-membered ring and its applications as solid acidic catalyst. *Microporous Mesoporous Mater.* **2014**, *193*, 166–172.
(76) Burkett, S. L.; Davis, M. E. Mechanism of Structure Direction in the Synthesis of Pure-Silica Zeolites. 2. Hydrophobic Hydration and Structural Specificity. *Chem. Mater.* **1995**, *7*, 1453–1463.
(77) Burkett, S. L.; Davis, M. E. Mechanism of Structure Direction in the Synthesis of Si-ZSM-5: An Investigation by Intermolecular 1H-29Si CP MAS NMR. *J. Phys. Chem.* **1994**, *98*, 4647–4653.
(78) Burkett, S. L.; Davis, M. E. Mechanisms of Structure Direction in the Synthesis of Pure-Silica Zeolites. 1. Synthesis of TPA/Si-ZSM-5. *Chem. Mater.* **1995**, *7*, 920–928.
(79) De Moor, P.-P. E. a; Beelen, T. P. M.; Komanschek, B. U.; Beck, L. W.; Wagner, P.; Davis, M. E.; Van Santen, R. Imaging the assembly process of the organic-mediated synthesis of a zeolite. *Chem. – A Eur. J.* **1999**, *5*, 2083–2088.
(80) Hui, K. S.; Chao, C. Y. H. Pure, single phase, high crystalline, chamfered-edge zeolite 4A synthesized from coal fly ash for use as a builder in detergents. *J. Hazard. Mater.* **2006**, *137*, 401–409.
(81) Chapman, K. W.; Chupas, P. J.; Nenoff, T. M. Radioactive iodine capture in silver-containing mordenites through nanoscale silver iodide formation. *J. Am. Chem. Soc.* **2010**, *132*, 8897–8899.
(82) Traa, Y.; Burger, B.; Weitkamp, J. Zeolite-based materials for the selective catalytic reduction of NOx with hydrocarbons. *Microporous Mesoporous Mater.* **1999**, *30*, 3–41.
(83) Brandenberger, S.; Kröcher, O.; Tissler, A.; Althoff, R. The State of the Art in Selective Catalytic Reduction of NOx by Ammonia Using Metal-Exchanged Zeolite Catalysts. *Catal. Rev.* **2008**, *50*, 492–531.
(84) Williams, B. A.; Babitz, S. M.; Miller, J. T.; Snurr, R. Q.; Kung, H. H. The roles of acid strength and pore diffusion in the enhanced cracking activity of steamed Y zeolites. *Appl. Catal. A Gen.* **1999**, *177*, 161–175.
(85) Hagiwara, K.; Ebihara, T.; Urasato, N.; Ozawa, S.; Nakata, S. Effect of vanadium on USY zeolite destruction in the presence of sodium ions and steam - Studies by solid-state NMR. *Appl. Catal. A Gen.* **2003**, *249*, 213–228.
(86) Caratzoulas, S.; Davis, M. E.; Gorte, R. J.; Gounder, R.; Lobo, R. F.; Nikolakis, V.; Sandler, S. I.; Snyder, M. A.; Tsapatsis, M.; Vlachos, D. G. Challenges of and Insights into Acid-Catalyzed Transformations of Sugars. *J. Phys. Chem. C* **2014**, *118*, 22815–22833.
(87) Dapsens, P. Y.; Mondelli, C.; Pérez-Ramírez, J. Design of Lewis-acid centres in zeolitic matrices for the conversion of renewables. *Chem. Soc. Rev.* **2015**, *44*, 7025–7043.
(88) Boronat, M.; Concepcion, P.; Corma, A.; Renz, M.; Valencia, S. Determination of the catalytically active oxidation Lewis acid sites in Sn-beta zeolites, and their optimisation by the combination of theoretical and experimental studies. *J. Catal.* **2005**, *234*, 111–118.
(89) Corma, A.; Domine, M. E.; Valencia, S. Water-resistant solid Lewis acid catalysts: Meerwein-Ponndorf-Verley and Oppenauer reactions catalyzed by tin-beta zeolite. *J. Catal.* **2003**, *215*, 294–304.
(90) Corma, A.; Nemeth, L. T.; Renz, M.; Valencia, S. Sn-zeolite beta as a heterogeneous chemoselective catalyst for Baeyer–Villiger oxidations. *Nature* **2001**, *412*, 423–425.
(91) Orazov, M.; Davis, M. E. Catalysis by framework zinc in silica-based molecular sieves. *Chem. Sci.* **2016**, *7*, 2264–2274.
(92) Gounder, R. Hydrophobic microporous and mesoporous oxides as Brønsted and Lewis acid catalysts for biomass conversion in liquid water. *Catal. Sci. Technol.* **2014**, *4*, 2877–2886.
(93) Román-Leshkov, Y.; Davis, M. E. Activation of carbonyl-containing molecules with solid lewis acids in aqueous media. *ACS Catal.* **2011**, *1*, 1566–1580.
(94) Baba, T.; Morikawa, Y.; Komatsu, N.; Ono, Y. Nature of acidic protons in metallosilicate molecular sieves as studied by variable temperature 1H MAS NMA. *Res. Chem. Intermed.* **2000**, *26*, 13–20.
(95) Camblor, M. a.; Corma, A.; Valencia, S. Spontaneous nucleation and growth of pure silica zeolite-B free of connectivity defects. *Chem. Commun.* **1996**, *20*, 2365.
(96) Flanigen, E. M.; Patton, R. L. Silica polymorph and process for preparing same. *US Pat. 4,073,865* **1978**.
(97) Moliner, M.; Corma, A. Advances in the synthesis of titanosilicates: From the medium pore TS-1 zeolite to highly-accessible ordered materials. *Microporous Mesoporous Mater.* **2014**, *189*, 31–40.
(98) Fan, W.; Duan, R. G.; Yokoi, T.; Wu, P.; Kubota, Y.; Tatsumi, T. Synthesis, crystallization mechanism, and

catalytic properties of titanium-rich TS-1 free of extraframework titanium species. *J. Am. Chem. Soc.* **2008**, *130*, 10150–10164.

(99) Corma, A.; Camblor, M. A.; Esteve, P.; Martínez, A.; Pérez-Pariente, J. Activity of Ti-Beta Catalyst for the Selective Oxidation of Alkenes and Alkanes. *J. Catal.* **1994**, *145*, 151–158.

(100) Camblor, M. A.; Corma, A.; Martinez, A.; Perez-Pariente, J. Synthesis of a Titaniumsilicoaluminate lsomorphous to Zeolite Beta and its Application as a Catalyst for the Selective Oxidation of Large Organic Molecules. *Chem. Commun.* **1992**, *49*, 589–590.

(101) Camblor, M. A.; Costantini, M.; Corma, A.; Gilbert, L.; Esteve, P.; Martínez, A.; Valencia, S. Synthesis and catalytic activity of aluminium-free zeolite Ti-B oxidation catalysts. *Chem. Commun.* **1996**, *11*, 1339–1340.

(102) Blasco, T.; Camblor, M. A.; Corma, A.; Esteve, P.; Martínez, A.; Prieto, C.; Valencia, S. Unseeded synthesis of Al-free Ti-beta zeolite in fluoride medium: a hydrophobic selective oxidation catalyst. *Chem. Commun.* **1996**, *3*, 2367–2368.

(103) Camblor, M. A.; Corma, A.; Esteve, P.; Martínez, A.; Valencia, S. Epoxidation of unsaturated fatty esters over large-pore Ti-containing molecular sieves as catalysts: Important role of the hydrophobic-hydrophilic properties of the molecular sieve. *Chem. Commun.* **1997**, *8*, 795–796.

(104) Mal, N. K.; Ramaswamy, V.; Ganapathy, S.; Ramaswamy, A. V. Synthesis and Characterization of Crystalline, Tin-silicate Molecular Sieves with MFI Structure. *J. Chem. Soc., Chem. Comn.* **1994**, 1933–1934.

(105) Mal, N. K.; Ramaswamy, V.; Rajamohanan, P. R.; Ramaswamy, A. V. Sn-MFI molecular sieves: synthesis methods, 29Si liquid and solid MAS-NMR, 119Sn static and MAS NMR studies. *Microporous Mater.* **1997**, *12*, 331–340.

(106) Mal, N. K.; Ramaswamy, A. V. Synthesis and catalytic properties of large-pore Sn- b and Al-free Sn- b molecular sieves. *Chem. Commun.* **1997**, *8*, 425–426.

(107) van der Waal, J. C.; Rigutto, M. S.; Van Bekkum, H. Synthesis of all-silica zeolite beta. *J. Chem. Soc., Chem. Comn.*. **1994**, 1241–1242.

(108) Perez-Pariente, J.; Martens, J. A.; Jacobs, P. A. Factors affecting the synthesis efficiency of zeolite BETA from aluminosilicate gels containing alkali and tetraethylammonium ions. *Zeolites* **1988**, *8*, 46–53.

(109) Tolborg, S.; Katerinopoulou, A.; Falcone, D. D.; Sadaba, I.; Osmundsen, C. M.; Davis, R. J.; Taarning, E.; Fristrup, P.; Holm, M. S. Incorporation of tin affects crystallization, morphology, and crystal composition of Sn-Beta. *J. Mater. Chem. A* **2014**, *2*, 20252–20262.

(110) Wu, P.; Komatsu, T.; Yashima, T.; Nakata, S.; Shoji, H. Modification of mordenite acidity by isomorphous substitution of trivalent cations in the framework sites using the atom-planting method. *Microporous Mater* **1997**, *12*, 25.

(111) Hammond, C.; Conrad, S.; Hermans, I. Simple and scalable preparation of highly active lewis acidic Sn-beta. *Angew. Chemie - Int. Ed.* **2012**, *51*, 11736–11739.

(112) Dapsens, P. Y.; Mondelli, C.; Kusema, B. T.; Verel, R.; Pérez-Ramírez, J. A continuous process for glyoxal valorisation using tailored Lewis-acid zeolite catalysts. *Green Chem.* **2014**, *16*, 1176–1186.

(113) Morales, M.; Dapsens, P. Y.; Giovinazzo, I.; Witte, J.; Mondelli, C.; Papadokonstantakis, S.; Hungerbühler, K.; Pérez-Ramírez, J. Environmental and economic assessment of lactic acid production from glycerol using cascade bio- and chemocatalysis. *Energy Environ. Sci.* **2015**, *8*, 558–567.

(114) Gabelica, Z.; Valange, S. Synthesis of MFI metallosilicate zeolites using metallic amino complexes as mineralizing agents: an overview. *Microporous Mesoporous Mater.* **1999**, *30*, 57–66.

(115) De Vos, D. E.; Feijen, E. J. P.; Schoonheydt, R. A.; Jacobs, P. A. Influences of Ligand and of Zeolite Topology on the Structure of CoII Schiff Base Chelates in Faujasite Type Zeolites. *J. Am. Chem. Soc.* **1994**, *116*, 4746–4752.

(116) Meng, Y.; Genuino, H. C.; Kuo, C. H.; Huang, H.; Chen, S. Y.; Zhang, L.; Rossi, A.; Suib, S. L. One-step hydrothermal synthesis of manganese-containing MFI-type zeolite, Mn-ZSM-5, characterization, and catalytic oxidation of hydrocarbons. *J. Am. Chem. Soc.* **2013**, *135*, 8594–8605.

(117) Dong, M.; Wang, J.; Sun, Y. Synthesis of zincosilicate mordenite using citric acid as complexing agent. *Microporous Mesoporous Mater.* **2001**, *43*, 237–243.

(118) Zhou, Y.; Jin, Y.; Wang, M.; Zhang, W.; Xie, J.; Gu, J.; Wen, H.; Wang, J.; Peng, L. One-Pot Synthesis of Zeolitic Strong Solid Bases: A Family of Alkaline-Earth Metal-Containing Silicalite-1. *Chem. - A Eur. J.* **2015**, *21*, 15412–15420.

(119) Borjas Garcia, S. E.; Yamamoto, K.; Muramatsu, A. Synthesis of Ti-Beta via mechanochemical route. *J.*

Mater. Sci. **2008**, *43*, 2367–2371.
(120) Yamamoto, K.; Borjas García, S. E.; Muramatsu, A. Zeolite synthesis using mechanochemical reaction. *Microporous Mesoporous Mater.* **2007**, *101*, 90–96.
(121) Iida, T.; Sato, M.; Numako, C.; Nakahira, A.; Kohara, S.; Okubo, T.; Wakihara, T. Preparation and characterization of Silicalite-1 zeolites with high manganese contents from mechanochemically pretreated reactants. *J. Mater. Chem. A* **2015**, *3*, 6215–6222.
(122) Palomo, C.; Oiarbide, M.; Halder, R.; Laso, A.; López, R. Enantioselective aza-Henry reactions assisted by Zn and N-methylephedrine. *Angew. Chemie - Int. Ed.* **2005**, *45*, 117–120.
(123) Fernandez-Lopez, R.; Kofoed, J.; Machuqueiro, M.; Darbre, T. A selective direct aldol reaction in aqueous media catalyzed by zinc-proline. *European J. Org. Chem.* **2005**, *24*, 5268–5276.
(124) Connell, G.; Dumesic, J. A. The generation of Bronsted and Lewis acid sites on the surface of silica by addition of dopant cations. *J. Catal.* **1987**, *105*, 285–298.
(125) Mccall, K. A.; Huang, C.-C.; Fierke, C. A. Zinc and Health: Current Status and Future Directions Function and Mechanism of Zinc Metalloenzymes. *J. Nutr* **2000**, *130*, 1437–1446.
(126) Butler, A. Acquisition and utilization of transition metal ions by marine organisms. *Science* **1998**, *281*, 207–210.
(127) Conner, W. C.; Kokes, R. J. Hydrogen Activation on Zinc Oxide. *J. Catal.* **1975**, *210*, 199–210.
(128) Kokes, R. J. Characterization of Adsorbed Intermediates on Zinc Oxide by Infrared Spectroscopy. *Acc. Chem. Res.* **1973**, *6*, 226–233.
(129) Schweitzer, N. M.; Hu, B.; Das, U.; Kim, H.; Greeley, J.; Curtiss, L. A.; Stair, P. C.; Miller, J. T.; Hock, A. S. Propylene hydrogenation and propane dehydrogenation by a single-site Zn2+ on silica catalyst. *ACS Catal.* **2014**, *4*, 1091–1098.
(130) Kolyagin, Y. G.; Ivanova, I. I.; Ordomsky, V. V; Gedeon, A.; Pirogov, Y. A. Methane Activation over Zn-Modified MFI Zeolite : NMR Evidence for Zn - Methyl Surface Species Formation. *J. Phys. Chem. C* **2008**, *112*, 20065–20069.
(131) Kolyagin, Y. G.; Ordomsky, V. V.; Khimyak, Y. Z.; Rebrov, A. I.; Fajula, F.; Ivanova, I. I. Initial stages of propane activation over Zn/MFI catalyst studied by in situ NMR and IR spectroscopic techniques. *J. Catal.* **2006**, *238*, 122–133.
(132) Penzien, J.; Müller, T. E.; Lercher, J. A. Zinc-ion exchanged zeolites for the intramolecular hydroamination of 6-aminohex-1-yne. *Chem. Commun.* **2000**, *122*, 1753–1754.
(133) Bermejo-Deval, R.; Orazov, M.; Gounder, R.; Hwang, S. J.; Davis, M. E. Active sites in Sn-beta for glucose isomerization to fructose and epimerization to mannose. *ACS Catal.* **2014**, *4*, 2288–2297.
(134) Penzien, J.; Abraham, A.; van Bokhoven, J. A.; Jentys, A.; Müller, T. E.; Sievers, C.; Lercher, J. A. Generation and Characterization of Well-Defined Zn 2+ Lewis Acid Sites in Ion Exchanged Zeolite BEA. *J. Phys. Chem. B* **2004**, *108*, 4116–4126.
(135) Patet, R. E.; Fan, W.; Vlachos, D. G.; Caratzoulas, S. Tandem Diels–Alder Reaction of Dimethylfuran and Ethylene and Dehydration to para-Xylene Catalyzed by Zeotypic Lewis Acids. *ChemCatChem* **2017**, *9*, 2523–2535.
(136) Bnmner, G. O.; Meier, W. M. Framework density distribution of zeolite-type tetrahedral nets. *Nature* **1989**, *337*, 146.
(137) Annen, M. J.; Davis, M. E.; Higgins, J. B.; Schlenker, J. L. VPI-7: the first zincosilicate molecular sieve containing three-membered T-atom rings. *J. Chem. Soc. Chem. Commun.* **1991**, 1175.
(138) Yoshikawa, M.; Zones, S. I.; Davis, M. E. Synthesis of VPI-8 I. The effects of reaction components. **1997**, *11*, 127–136.
(139) Yoshikawa, M.; Zones, S.; Davis, M. Synthesis of VPI-8 II. Mechanism of crystallization. *Microporous Mater.* **1997**, *11*, 137–148.
(140) Freyhardt, C. C.; Lobo, R. F.; Khodabandeh, S.; Lewis, J. E.; Tsapatsis, M.; Yoshikawa, M.; Camblor, M. a.; Pan, M.; Helmkamp, M. M.; Zones, S. I.; et al. VPI-8: A high-silica molecular sieve with a novel "pinwheel" building unit and its implications for the synthesis of extra-large pore molecular sieves. *J. Am. Chem. Soc.* **1996**, *118*, 7299–7310.
(141) McCusker, L. B.; Grosse-Kunstleve, R. W.; Baerlocher, C.; Yoshikawa, M.; Davis, M. E. Synthesis optimization and structure analysis of the zincosilicate molecular sieve VPI-9. *Microporous Mater.* **1996**, *6*, 295–309.
(142) Annen, M. J.; Davis, M. E. Raman and Si-29 Mas Nmr-Spectroscopy of Framework Materials Containing

3-Membered Rings. *Microporous Mater.* **1993**, *1*, 57–65.
(143) Röhrig, C.; Gies, H. A New Zincosilicate Zeolite with Nine‐Ring Channels. *Angew. Chemie Int. Ed. English* **1995**, *34*, 63–65.
(144) Camblor, M. A.; Lobo, R. F.; Roller, H.; Davis, M. E. Synthesis and Characterization of Zincosilicates with the SOD Topology. *Chem. Mater.* **1994**, *6*, 2193–2199.
(145) Takewaki, T.; Beck, L. W.; Davis, M. E. Synthesis of CIT-6, a zincosilicate with the *BEA topology. *Top. Catal.* **1999**, *9*, 35–42.
(146) Takewaki, T.; Beck, L. W.; Davis, M. E. Zincosilicate CIT-6: A Precursor to a Family of *BEA-Type Molecular Sieves. *J. Phys. Chem. B* **1999**, *103*, 2674–2679.
(147) Serrano, D. P.; Van Grieken, R.; Davis, M. E.; Melero, J. A.; Garcia, A.; Morales, G. Mechanism of CIT-6 and VPI-8 crystallization from zincosilicate gels. *Chem. - A Eur. J.* **2002**, *8*, 5153–5160.
(148) Steohen, L. Law.; Rohrbaugh, W. J. The Framework Topology of ZSM-18, a Novel Zeolite Containing Rings of Three (Si,Al)-O Species. *Science (80-.).* **1990**, *247*, 1319–1322.
(149) Palčić, A.; Abellán, F. Z.; Vicente, A.; Fernandez, C.; Georgieva, V.; Bronić, J.; Valtchev, V.; McCusker, L. B.; Baerlocher, C.; Brunner, G. O.; et al. Formation mechanism of three-membered ring containing microporous zincosilicate RUB-17. *CrystEngComm* **2015**, *17*, 7063–7069.
(150) Camblor, M. a.; Davis, M. E. 29Si MAS NMR Spectroscopy of Tectozincosilicates. *J. Phys. Chem.* **1994**, *98*, 13151–13156.
(151) Suzuki, Y.; Wakihara, T.; Kohara, S.; Itabashi, K.; Ogura, M. Mechanistic Study on the Synthesis of a Porous Zincosilicate VPI-7 Containing. **2011**, *115*, 443–446.
(152) Deimund, M. A.; Labinger, J.; Davis, M. E. Nickel-exchanged zincosilicate catalysts for the oligomerization of propylene. *ACS Catal.* **2014**, *4*, 4189–4195.
(153) Paolucci, C.; Di Iorio, J. R.; Ribeiro, F. H.; Gounder, R.; Schneider, W. F. Catalysis Science of NOx Selective Catalytic Reduction With Ammonia Over Cu-SSZ-13 and Cu-SAPO-34. *Adv. Catal.* **2016**, *59*, 1–4.
(154) Snyder, B. E. R.; Vanelderen, P.; Bols, M. L.; Hallaert, S. D.; Böttger, L. H.; Ungur, L.; Pierloot, K.; Schoonheydt, R. A.; Sels, B. F.; Solomon, E. I. The active site of low-temperature methane hydroxylation in iron-containing zeolites. *Nature* **2016**, *536*, 317–321.
(155) Serrano, D. P.; Van Grieken, R.; Melero, J. A.; García, A. Liquid phase rearrangement of long straight-chain epoxides over amorphous, mesostructured and zeolitic catalysts. *Appl. Catal. A Gen.* **2004**, *269*, 137–146.
(156) Andy, P.; Davis, M. Dehydrogenation of propane over platinum containing CIT-6. *Ind. Eng. Chem. Res.* **2004**, *43*, 2922–2928.
(157) McKeen, J. C.; Davis, M. E. Conductivity of mono- and divalent cations in the microporous zincosilicate VPI-9. *J. Phys. Chem. C* **2009**, *113*, 9870–9877.
(158) Dědeček, J.; Kaucký, D.; Wichterlová, B.; Gonsiorová, O. Co 2+ ions as probes of Al distribution in the framework of zeolites. ZSM-5 study. *Phys. Chem. Chem. Phys.* **2002**, *4*, 5406–5413.
(159) Gonzales, N. O.; Chakraborty, A. K.; Bell, A. T. A density functional study of the effects of metal cations on the Bronsted acidity of H-ZSM-5. *Catal. Letters* **1998**, *50*, 135–139.
(160) Dědeček, J.; Kaucký, D.; Wichterlová, B. Co2+ ion siting in pentasil-containing zeolites, part 3. Co2+ ion sites and their occupation in ZSM-5: A VIS diffuse reflectance spectroscopy study. *Microporous Mesoporous Mater.* **2000**, *35–36*, 483–494.
(161) Dědeček, J.; Sobalík, Z.; Wichterlová, B. Siting and Distribution of Framework Aluminium Atoms in Silicon-Rich Zeolites and Impact on Catalysis. *Catal. Rev. - Sci. Eng.* **2012**, *54*, 135–223.
(162) Pashkova, V.; Klein, P.; Dedecek, J.; Tokarová, V.; Wichterlová, B. Incorporation of Al at ZSM-5 hydrothermal synthesis. Tuning of Al pairs in the framework. *Microporous Mesoporous Mater.* **2015**, *202*, 138–146.
(163) Gábová, V.; Dědeček, J.; Čejka, J. Control of Al distribution in ZSM-5 by conditions of zeolite synthesis. *Chem. Commun.* **2003**, *10*, 1196–1197.
(164) Dedecek, J.; Balgová, V.; Pashkova, V.; Klein, P.; Wichterlová, B. Synthesis of ZSM-5 zeolites with defined distribution of Al atoms in the framework and multinuclear MAS NMR analysis of the control of Al distribution. *Chem. Mater.* **2012**, *24*, 3231–3239.
(165) Di Iorio, J. R.; Gounder, R. Controlling the Isolation and Pairing of Aluminum in Chabazite Zeolites Using Mixtures of Organic and Inorganic Structure-Directing Agents. *Chem. Mater.* **2016**, *28*, 2236–2247.
(166) Dusselier, M.; Davis, M. E. US Patent 2016/0243531 A1. 2016.

(167) Wang, L.; Sang, S.; Meng, S.; Zhang, Y.; Qi, Y.; Liu, Z. Direct synthesis of Zn-ZSM-5 with novel morphology. *Mater. Lett.* **2007**, *61*, 1675–1678.
(168) Iyoki, K.; Itabashi, K.; Okubo, T. Progress in seed-assisted synthesis of zeolites without using organic structure-directing agents. *Microporous Mesoporous Mater.* **2014**, *189*, 22–30.
(169) Itabashi, K.; Kamimura, Y.; Iyoki, K.; Shimojima, A.; Okubo, T. A working hypothesis for broadening framework types of zeolites in seed-assisted synthesis without organic structure-directing agent. *J. Am. Chem. Soc.* **2012**, *134*, 11542–11549.
(170) Kamimura, Y.; Tanahashi, S.; Itabashi, K.; Sugawara, A.; Wakihara, T.; Shimojima, A.; Okubo, T. Crystallization behavior of zeolite beta in OSDA-free, seed-assisted synthesis. *J. Phys. Chem. C* **2011**, *115*, 744–750.
(171) Iyoki, K.; Kamimura, Y.; Itabashi, K.; Shimojima, A.; Okubo, T. Synthesis of MTW-type Zeolites in the Absence of Organic Structure-directing Agent. *Chem. Lett.* **2010**, *39*, 730–731.
(172) Kamimura, Y.; Itabashi, K.; Kon, Y.; Endo, A.; Okubo, T. Seed-assisted synthesis of MWW-type zeolite with organic structure-directing agent-free Na-aluminosilicate gel system. *Chem. - An Asian J.* **2017**, *12*, 530–542.
(173) Iyoki, K.; Itabashi, K.; Chaikittisilp, W.; Elangovan, S. P.; Wakihara, T.; Kohara, S.; Okubo, T. Broadening the applicable scope of seed-directed, organic structure-directing agent-free synthesis of zeolite to zincosilicate components: A case of VET-type zincosilicate zeolites. *Chem. Mater.* **2014**, *26*, 1957–1966.
(174) Yun, J. H.; Lobo, R. F. Catalytic dehydrogenation of propane over iron-silicate zeolites. *J. Catal.* **2014**, *312*, 263–270.
(175) Itabashi, K.; Matsumoto, A.; Ikeda, T.; Kato, M.; Tsutsumi, K. Synthesis and characteristic properties of Rb-mordenite. *Microporous Mesoporous Mater.* **2007**, *101*, 57–65.
(176) Ikuno, T.; Chaikittisilp, W.; Liu, Z.; Iida, T.; Yanaba, Y.; Yoshikawa, T.; Kohara, S.; Wakihara, T.; Okubo, T. Structure-Directing Behaviors of Tetraethylammonium Cations toward Zeolite Beta Revealed by the Evolution of Aluminosilicate Species Formed during the Crystallization Process. *J. Am. Chem. Soc.* **2015**, *137*, 14533–14544.
(177) Lercher, J. A.; Grijndling, C.; Eder-Mirth, G. Infrared studies of the surface acidity of oxides and zeolites using adsorbed probe molecules. *Catal. Today* **1996**, *27*, 353–376.
(178) Choi, S. W.; Kim, W. G.; So, J. S.; Moore, J. S.; Liu, Y.; Dixit, R. S.; Pendergast, J. G.; Sievers, C.; Sholl, D. S.; Nair, S.; et al. Propane dehydrogenation catalyzed by gallosilicate MFI zeolites with perturbed acidity. *J. Catal.* **2017**, *345*, 113–123.
(179) Osmundsen, C. M.; Holm, M. S.; Dahl, S.; Taarning, E. Tin-containing silicates: structure-activity relations. *Proc. R. Soc. A Math. Phys. Eng. Sci.* **2012**, *468*, 2000–2016.
(180) Gunther, W. R.; Michaelis, V. K.; Caporini, M. A.; Griffin, R. G.; Román-Leshkov, Y. Dynamic nuclear polarization NMR enables the analysis of sn-beta zeolite prepared with natural abundance 119Sn precursors. *J. Am. Chem. Soc.* **2014**, *136*, 6219–6222.
(181) Parker, W. O.; Millini, R. Ti coordination in titanium silicalite-1. *J. Am. Chem. Soc.* **2006**, *128*, 1450–1451.
(182) Finiels, A.; Fajula, F.; Hulea, V. Nickel-based solid catalysts for ethylene oligomerization – a review. *Catal. Sci. Technol.* **2014**, *4*, 2412–2426.
(183) Brogaard, R. Y.; Olsbye, U. Ethene Oligomerization in Ni-containing Zeolites: Theoretical Discrimination of Reaction Mechanisms. *ACS Catal.* **2016**, *6*, acscatal.5b01957.
(184) Iwama, M.; Suzuki, Y.; Plévert, J.; Itabashi, K.; Ogura, M.; Okubo, T. Location of alkali ions and their relevance to crystallization of low silica X zeolite. *Cryst. Growth Des.* **2010**, *10*, 3471–3479.
(185) S D. W. Breck, in Zeolite Molecular Sieves, Structure, Chemistry, and Use, John Wiley & Sons, New York, pp. 529
(186) Mlinar, A. N.; Baur, G. B.; Bong, G. G.; Getsoian, A.; Bell, A. T. Propene oligomerization over Ni-exchanged Na-X zeolites. *J. Catal.* **2012**, *296*, 156–164.
(187) Ng, F. T. T.; Creaser, D. C. Ethylene dimerization over modified nickel exchanged Y-zeolite. *Appl. Catal. A, Gen.* **1994**, *119*, 327–339.
(188) Mlinar, A. N.; Ho, O. C.; Bong, G. G.; Bell, A. T. The effect of noncatalytic cations on the activity and selectivity of nickel-exchanged xzeolites for propene oligomerization. *ChemCatChem* **2013**, *5*, 3139–3147.
(189) Heveling, J.; van der Beek, A.; de Pender, M. Oligomerization of ethene over nickel-exchanged zeolite y into a diesel-range product. *Appl. Catal.* **1988**, *42*, 325–336.
(190) Boronat, M.; Viruela, P.; Corma, A. Theoretical study on the mechanism of the hydride transfer reaction

between alkanes and alkylcarbenium ions. *J. Phys. Chem. B* **1997**, *101*, 10069–10074.
(191) Kato, M.; Ikeda, T.; Kodaira, T.; Takahashi, S. Synthesis of Co-substituted Zeolites in the presence of cobalt complex with EDMA. *Microporous Mesoporous Mater.* **2011**, *142*, 444–453.
(192) Xie, B.; Song, J.; Ren, L.; Ji, Y.; Li, J.; Xiao, F. S. Organotemplate-free and fast route for synthesizing beta zeolite. *Chem. Mater.* **2008**, *20*, 4533–4535.
(193) Xie, B.; Zhang, H.; Yang, C.; Liu, S.; Ren, L.; Zhang, L.; Meng, X.; Yilmaz, B.; Müller, U.; Xiao, F.-S. Seed-directed synthesis of zeolites with enhanced performance in the absence of organic templates. *Chem. Commun.* **2011**, *47*, 3945–3947.
(194) Majano, G.; Delmotte, L.; Valtchev, V.; Mintova, S. Al-rich zeolite beta by seeding in the absence of organic template. *Chem. Mater.* **2009**, *21*, 4184–4191.
(195) Kamimura, Y.; Iyoki, K.; Elangovan, S. P.; Itabashi, K.; Shimojima, A.; Okubo, T. OSDA-free synthesis of MTW-type zeolite from sodium aluminosilicate gels with zeolite beta seeds. *Microporous Mesoporous Mater.* **2012**, *163*, 282–290.
(196) Kubota, Y.; Itabashi, K.; Inagaki, S.; Nishita, Y.; Komatsu, R.; Tsuboi, Y.; Shinoda, S.; Okubo, T. Effective fabrication of catalysts from large-pore, multidimensional zeolites synthesized without using organic structure-directing agents. *Chem. Mater.* **2014**, *26*, 1250–1259.
(197) Ogawa, A.; Iyoki, K.; Kamimura, Y.; Elangovan, S. P.; Itabashi, K.; Okubo, T. Seed-directed, rapid synthesis of MAZ-type zeolites without using organic structure-directing agent. *Microporous Mesoporous Mater.* **2014**, *186*, 21–28.
(198) Iyoki, K.; Itabashi, K.; Okubo, T. Seed-assisted, one-pot synthesis of hollow zeolite beta without using organic structure-directing agents. *Chem. - An Asian J.* **2013**, *8*, 1419–1427.
(199) Sogukkanli, S.; Iyoki, K.; Elangovan, S. P.; Itabashi, K.; Takano, M.; Liu, Z.; Inagaki, S.; Wakihara, T.; Kubota, Y.; Okubo, T. Rational seed-directed synthesis of MSE-type zeolites using a simple organic structure-directing agent by extending the composite building unit hypothesis. *Microporous Mesoporous Mater.* **2017**, *245*, 1–7.
(200) Han, O. H.; Kim, C. S.; Hong, S. B. Direct evidence for the nonrandom nature of Al substitution in zeolite ZSM-5: An investigation by 27Al MAS and MQ MAS NMR. *Angew. Chemie - Int. Ed.* **2002**, *41*, 469–472.
(201) Zhu, J.; Liu, Z.; Endo, A.; Yanaba, Y.; Yoshikawa, T.; Wakihara, T.; Okubo, T. Ultrafast, OSDA-free synthesis of mordenite zeolite. *CrystEngComm* **2017**, *19*, 632–640.
(202) Round, C. I.; Williams, C. D.; Latham, K.; Duke, C. V. A. Ni-ZSM-5 and Cu-ZSM-5 synthesized directly from aqueous fluoride gels. *Chem. Mater.* **2001**, *13*, 468–472.
(203) Kirschhock, C. E. A.; Ravishankar, R.; Looveren, L. Van; Jacobs, P. A.; Martens, J. A. Mechanism of Transformation of Precursors into Nanoslabs in the Early Stages of MFI and MEL Zeolite Formation from TPAOH−TEOS−H2O and TBAOH−TEOS−H2O Mixtures. *J. Phys. Chem. B* **1999**, *103*, 4972–4978.
(204) Kirschhock, C. E. A.; Ravishankar, R.; Verspeurt, F.; Grobet, P. J.; Jacobs, P. A.; Martens, J. A. Identification of Precursor Species in the Formation of MFI Zeolite in the TPAOH−TEOS−H2O System. *J. Phys. Chem. B* **1999**, *103*, 4965–4971.
(205) Kirschhock, C. E. A.; Kremer, S. P. B.; Grobet, P. J.; Jacobs, P. A.; Martens, J. A. New evidence for precursor species in the formation of MFI zeolite in the tetrapropylammonium hydroxide-tetraethyl orthosilicate-water system. *J. Phys. Chem. B* **2002**, *106*, 4897–4900.
(206) Kirschhock, C. E. A.; Buschmann, V.; Kremer, S.; Ravishankar, R.; Houssin, C. J. Y.; Mojet, B. L.; Santen, R. a Van; Grobet, P. J.; Jacobs, P. A.; Martens, J. A. Zeosil Nanoslabs : Building Blocks in nPr4N+-Mediated Synthesis of MFI Zeolite. *Angew. Chem. Int. Ed.* **2001**, *3010*, 2637–2640.
(207) Matsukata, M.; Ogura, M.; Osaki, T.; Kikuchi, E.; Mitra, A. Quantitative analyses for TEA+ and Na+ contents in zeolite beta with a wide range of Si/2Al ratio. *Microporous Mesoporous Mater.* **2001**, *48*, 23–29.
(208) Ma, Z.; Xie, J.; Zhang, J.; Zhang, W.; Zhou, Y.; Wang, J. Mordenite zeolite with ultrahigh SiO2/Al2O3 ratio directly synthesized from ionic liquid-assisted dry-gel-conversion. *Microporous Mesoporous Mater.* **2016**, *224*, 17–25.
(209) Zhou, D.; Lu, X.; Xu, J.; Yu, A.; Li, J.; Deng, F.; Xia, Q. Dry gel conversion method for the synthesis of organic-inorganic hybrid MOR zeolites with modifiable catalytic activities. *Chem. Mater.* **2012**, *24*, 4160–4165.
(210) Matsukata, M.; Nishiyama, N.; Ueyama, K. Synthesis of zeolites under vapor atmosphere. Effect of synthetic conditions on zeolite structure. *Microporous Mater.* **1993**, *1*, 219–222.
(211) Matsukata, M.; Ogura, M.; Osaki, T.; Raja, P.; Rao, H. P.; Nomura, M.; Kikuchi, E. Conversion of dry gel to

microporous crystals in gas phase. *Top. Catal.* **1999**, *9*, 77–92.
(212) Inagaki, S.; Nakatsuyama, K.; Saka, Y.; Kikuchi, E.; Kohara, S.; Matsukata, M. Elucidation of medium-range structure in a dry gel-forming *BEA-type zeolite. *J. Phys. Chem. C* **2007**, *111*, 10285–10293.
(213) Matsukata, M.; Osaki, T.; Ogura, M.; Kikuchi, E. Crystallization behavior of zeolite beta during steam-assisted crystallization of dry gel. *Microporous Mesoporous Mater.* **2002**, *56*, 1–10.
(214) Jappar, N.; Xia, Q.; Tatsumi, T. Oxidation activity of Ti-beta synthesized by a dry-gel conversion method. *J. Catal.* **1998**, *180*, 132–141.
(215) Bandyopadhyay, R.; Kubota, Y.; Sugimoto, N.; Fukushima, Y.; Sugi, Y. Synthesis of borosilicate zeolites by the dry gel conversion method and their characterization. *Microporous Mesoporous Mater.* **1999**, *32*, 81–91.
(216) Wakihara, T.; Kohara, S.; Sankar, G.; Saito, S.; Sanchez-Sanchez, M.; Overweg, A. R.; Fan, W.; Ogura, M.; Okubo, T. A new approach to the determination of atomic-architecture of amorphous zeolite precursors by high-energy X-ray diffraction technique. *Phys. Chem. Chem. Phys.* **2006**, *8*, 224–227.
(217) Kohara, S.; Itou, M.; Suzuya, K.; Inamura, Y.; Sakurai, Y.; Ohishi, Y.; Takata, M. Structural studies of disordered materials using high-energy x-ray diffraction from ambient to extreme conditions. *J. Phys. Condens. Matter* **2007**, *19*, 1–15.
(218) Bania, K. K.; Deka, R. C. Experimental and theoretical evidence for encapsulation and tethering of 1,10-phenanthroline complexes of Fe, Cu, and Zn in zeolite-Y. *J. Phys. Chem. C* **2012**, *116*, 14295–14310.
(219) NIST chemistry web-book, http://webbook.nist.gov/cgi/cbook.cgi?ID=C121448&Units=SI&Mask=400 (accessed November 30, 2017).
(220) Song, C.; Li, X.; Zhu, X.; Liu, S.; Chen, F.; Liu, F.; Xu, L. Influence of the state of Zn species over Zn-ZSM-5/ZSM-11 on the coupling effects of cofeeding n-butane with methanol. *Appl. Catal. A Gen.* **2016**, *519*, 48–55.
(221) Ivanova, I. I.; Kolyagin, Y. G.; Ordomsky, V. V.; Asachenko, E. V.; Pasynkova, E. M.; Pirogov, Y. A. Surface species formed during propane aromatization over Zn/MFI catalyst as determined by in situ spectroscopic techniques. *J. Mol. Catal. A Chem.* **2009**, *305*, 47–53.
(222) Naudin, C.; Bonhomme, F.; Bruneel, J. L.; Ducasse, L.; Grondin, J.; Lassègues, J. C.; Servant, L. Rotational isomerism of the tetraethylammonium cation in solution and in the solid state. *J. Raman Spectrosc.* **2000**, *31*, 979–985.
(223) Goto, T.; Takekiyo, T.; Yoshimura, Y. Raman spectroscopic study on the hydration structure of tetraethylammonium chloride in water. *J. Phys. Conf. Ser.* **2008**, *121* (4), 42005.
(224) Takekiyo, T.; Yoshimura, Y. Raman spectroscopic study on the hydration structures of tetraethylammonium cation in water. *J. Phys. Chem. A* **2006**, *110*, 10829–10833.
(225) O'Brien, M. G.; Beale, A. M.; Catlow, C. R. A.; Weckhuysen, B. M. Unique organic-inorganic interactions leading to a structure-directed microporous aluminophosphate crystallization as observed with in situ Raman spectroscopy. *J. Am. Chem. Soc.* **2006**, *128*, 11744–11745.
(226) Moliner, M.; Martínez, C.; Corma, A. Synthesis strategies for preparing useful small pore zeolites and zeotypes for gas separations and catalysis. *Chem. Mater.* **2014**, *26*, 246–258.
(227) Olsbye, U.; Svelle, S.; Lillerud, K. P.; Wei, Z. H.; Chen, Y. Y.; Li, J. F.; Wang, J. G.; Fan, W. B. The formation and degradation of active species during methanol conversion over protonated zeotype catalysts. *Chem. Soc. Rev.* **2015**, *44*, 7155–7176.
(228) Dai, W.; Sun, X.; Tang, B.; Wu, G.; Li, L.; Guan, N.; Hunger, M. Verifying the mechanism of the ethene-to-propene conversion on zeolite H-SSZ-13. *J. Catal.* **2014**, *314*, 10–20.
(229) Beale, A. M.; Gao, F.; Lezcano-Gonzalez, I.; Peden, C. H. F.; Szanyi, J. Recent advances in automotive catalysis for NO x emission control by small-pore microporous materials. *Chem. Soc. Rev.* **2015**, *44*, 7371–7405.
(230) Deimund, M. A.; Harrison, L.; Lunn, J. D.; Liu, Y.; Malek, A.; Shayib, R.; Davis, M. E. Effect of Heteroatom Concentration in SSZ-13 on the Methanol-to-Olefins Reaction. *ACS Catal.* **2016**, *6*, 542–550.
(231) Wulfers, M. J.; Teketel, S.; Ipek, B.; Lobo, R. F. Conversion of methane to methanol on copper-containing small-pore zeolites and zeotypes. *Chem. Commun.* **2015**, *51*, 4447–4450.
(232) Chen, J. Q.; Bozzano, A.; Glover, B.; Fuglerud, T.; Kvisle, S. Recent advancements in ethylene and propylene production using the UOP/Hydro MTO process. *Catal. Today* **2005**, *106*, 103–107.
(233) Van Speybroeck, V.; Hemelsoet, K.; Joos, L.; Waroquier, M.; Bell, R. G.; Catlow, C. R. A. Advances in theory and their application within the field of zeolite chemistry. *Chem. Soc. Rev.* **2015**, *44*, 7044–7111.
(234) Grundner, S.; Markovits, M. A. C.; Li, G.; Tromp, M.; Pidko, E. A.; Hensen, E. J. M.; Jentys, A.;

Sanchez-Sanchez, M.; Lercher, J. A. Single-site trinuclear copper oxygen clusters in mordenite for selective conversion of methane to methanol. *Nat. Commun.* **2015**, *6*, 7546.

(235) Paolucci, C.; Parekh, A. A.; Khurana, I.; Di Iorio, J. R.; Li, H.; Albarracin Caballero, J. D.; Shih, A. J.; Anggara, T.; Delgass, W. N.; Miller, J. T.; et al. Catalysis in a cage: Condition-dependent speciation and dynamics of exchanged Cu cations in SSZ-13 zeolites. *J. Am. Chem. Soc.* **2016**, *138*, 6028–6048.

(236) Tomkins, P.; Ranocchiari, M.; Van Bokhoven, J. A. Direct Conversion of Methane to Methanol under Mild Conditions over Cu-Zeolites and beyond. *Acc. Chem. Res.* **2017**, *50*, 418–425.

(237) Bulánek, R.; Wichterlová, B.; Sobalík, Z.; Tichý, J. Reducibility and oxidation activity of Cu ions in zeolites effect of Cu ion coordination and zeolite framework composition. *Appl. Catal. B Environ.* **2001**, *31*, 13–25.

(238) Dědeček, J.; Čapek, L.; Sazama, P.; Sobalík, Z.; Wichterlová, B. Control of metal ion species in zeolites by distribution of aluminium in the framework: From structural analysis to performance under real conditions of SCR-NOx and NO, N2O decomposition. *Appl. Catal. A Gen.* **2011**, *391*, 244–253.

(239) Kuroda, Y.; Iwamoto, M. Characterization of cuprous ion in high silica zeolites and reaction mechanisms of catalytic NO decomposition and specific N2 adsorption. *Top. Catal.* **2004**, *28*, 111–118.

(240) Han, S.; Cheng, J.; Zheng, C.; Ye, Q.; Cheng, S.; Kang, T.; Dai, H. Effect of Si/Al ratio on catalytic performance of hydrothermally aged Cu-SSZ-13 for the NH3-SCR of NO in simulated diesel exhaust. *Appl. Surf. Sci.* **2017**, *419*, 382–392.

(241) Dutra, A. J. B.; Paiva, P. R. P.; Tavares, L. M. Alkaline leaching of zinc from electric arc furnace steel dust. *Miner. Eng.* **2006**, *19*, 478–485.

(242) McBride, R. A.; Kelly, J. M.; McCormack, D. E. Growth of well-defined ZnO microparticles by hydroxide ion hydrolysis of zinc salts. *J. Mater. Chem.* **2003**, *13*, 1196–1201.

(243) Mosquedajimenez, B. Reduction of nitric oxide by propene and propane on Ni-exchanged mordenite. *Appl. Catal. B Environ.* **2003**, *43*, 105–115.

(244) Mosqueda-Jimenez, B.; Jentts, A.; Seshan, K.; Lercher, J. A. Structure-activity relations for Ni-containing zeolites during NO reductionII. Role of the chemical state of Ni. *J. Catal.* **2003**, *218*, 375–385.

(245) Kinger, G.; Lugstein, A.; Swagera, R.; Ebel, M.; Jentys, A.; Vinek, H. Comparison of impregnation, liquid- and solid-state ion exchange procedures for the incorporation of nickel in HMFI, HMOR and HBEA. *Microporous Mesoporous Mater.* **2000**, *39*, 307–317.

(246) Lepetit, C.; Che, M. Discussion on the Coordination of Ni2+ Ions to Lattice Oxygens in Calcined Faujasite-Type Zeolites Followed by Diffuse Reflectance Spectroscopy. *J. Phys. Chem.* **1996**, *100*, 3137–3143.

(247) Ortega-Domínguez, R. A.; Vargas-Villagrán, H.; Peñaloza-Orta, C.; Saavedra-Rubio, K.; Bokhimi, X.; Klimova, T. E. A facile method to increase metal dispersion and hydrogenation activity of Ni/SBA-15 catalysts. *Fuel* **2017**, *198*, 110–122.

(248) Labinger, J. A.; Leitch, D. C.; Bercaw, J. E.; Deimund, M. A.; Davis, M. E. Upgrading Light Hydrocarbons: A Tandem Catalytic System for Alkane/Alkene Coupling. *Top. Catal.* **2015**, *58*, 494–501.

List of Publications

Publications related to this dissertation

1. **Natsume Koike**, Watcharop Chaikittisilp, Kenta Iyoki, Yutaka Yanaba, Takeshi Yoshikawa, Shanmugam Palani Elangovan, Keiji Itabashi and Tatsuya Okubo, "Organic-free synthesis of zincoaluminosilicate zeolites from homogeneous gels prepared by a co-precipitation method", *Dalton Transactions*, 46, 10837–10846, 2017.

2. **Natsume Koike**, Kenta Iyoki, Sye Hoe Keoh, Watcharop Chaikittisilp and Tatsuya Okubo, "Synthesis of a new microporous zincosilicate with CHA zeolite topology as efficient platforms for ion-exchange of divalent cations", *Chemistry-A European Journal*, 24, 808–812, 2018.

3. **Natsume Koike**, Watcharop Chaikittisilp, Kenta Iyoki, Yutaka Yanaba, Shanmugam Palani Elangovan, Keiji Itabashi and Tatsuya Okubo, "Organic-free synthesis of zincoaluminosilicate zeolites with MFI topology having high ion-exchange ability of divalent cations", *In preparation.*

4. **Natsume Koike**, Watcharop Chaikittisilp, Kenta Iyoki, Yutaka Yanaba, Shanmugam Palani Elangovan, Keiji Itabashi and Tatsuya Okubo, "Synthesis of zincosilicate zeolites from zincosilicate gels prepared by an organic structure-directing agentinvolved co-precipitation method", *In preparation.*

Other publications

1. **Natsume Koike,** Takaaki Ikuno, Tatsuya Okuboand Atsushi Shimojima, "Synthesis of monodisperse organosilica nanoparticleswith hollow interiors and porous shells using silicananospheres as templates", *Chemical Communications*, 49, 4998–5000, 2013.

2. **Natsume Koike**, Sou Hosokai, Atsushi Takagaki, Shun Nishimura, Ryuji Kikuchi, Kohki Ebitani, Yoshizo Suzukiand S. Ted Oyama, "Upgrading of pyrolysis bio-oil using nickel

phosphide catalysts", *Journal of Catalysis*, 333, 115–126, 2016.

3. **Natsume Koike**, Watcharop Chaikittisilp, Atsushi Shimojima and Tatsuya Okubo, "Surfactant-free synthesis of hollow mesoporous organosilica nanoparticles with controllable particle sizes and diversified organic moieties", *RSC Advances*, 6, 90435–90445, 2016.

4. Sibel Sogukkanli, Kenta Iyoki, Shanmugam P. Elangovan, Keiji Itabashi, **Natsume Koike**, Miku Takano, Yoshihiro Kubota and Tatsuya Okubo, "Seed-directed synthesis of zincoaluminosilicate MSE-type zeolites using co-precipitated gels with tetraethylammonium hydroxide as a simple organic structure directing agent", *Microporous and Mesoporous Materials*, 257, 272–280, 2018.

5. Watcharop Chaikittisilp, **小池夏萌**,「第 4 章第 1 節多孔性有機シリカハイブリッド材料」, 『ナノ空間材料ハンドブック』, エヌ・ティー・エス出版, 313–324,2016.

Acknowledgement

My deepest appreciation goes to my supervisor, Professor Tatsuya Okubo, who is leading me and always encourages me to challenge. Thanks for his guidance and support, I have gained a lot of knowledge and experiences. I would like to thank Associate Professor Toru Wakihara for his continuous encouragement and valuable comments during the study. The constructive and positive advices make me moving forward. I would like to express my sincere appreciation to Dr. Keiji Itabashi and Dr. Shanmugam P. Elangovan. The deep understanding and experiences in zeolite synthesis impressed me and always gives me new findings. I am deeply grateful to Assistant Professor Watcharop Chailittisilip, who teaches me many things important for a researcher. He is very brilliant and always gives me insightful advices. I greatly appreciate Assistant Professor Kenta Iyoki for the help and constructive advices. He is always kind and motivates me to enjoy research.

I would like to express my appreciation to Professor Masaru Ogura especially for access to an FT-IR instrument and valuable discussions which helps me a lot. I have greatly benefited from Professor Yoshiharu Kubota and Associate Professor Satoshi Inagaki for advices especially about catalysis.

The other committee members, Associate Professor Ryuji Kikuchi, Associate Professor Masashi Okubo, Professor Kazuya Yamaguchi, and Professor Shigeo Maruyama are truly acknowledged for their fruitful comments and discussion, which gives me new view points and helps to improve the dissertation.

Mr Hirokazu Abo and Mr Atsushi Masumoto (Shimadzu Corporation) are acknowledged for the measurements of deep UV spectra. For SEM observation, I am obliged to Mr. Isao Otsuka in the Center for Nano Lithography & Analysis. I would like to thank Associate Professor Takeshi Yoshikawa and Mr. Yutaka Yanaba for the solid-state NMR analysis. I owe an important debt to Dr. Keoh Sye Hoe for preparations of OSDAs in Chapter 5. Mr. Hiroki Yamada and Mr. Hirofumi Horikawa are acknowledged for the HEXTS analysis. I am particularly grateful for the help given by Mr. Wang Bangda for many ion-exchange experiments. I received generous support from Ogura laboratory for FT-IR analysis. I am particularly grateful for the assistance given by Mr. Shohei Harada, Mr. Kiyoyuki Yamazaki,

and Mr. Yusuke Ohata. For Raman spectroscopy, members in Yamada laboratory helped me a lot for the measurements.

I would like to thank secretaries, Ms. Kazuko Yokoyama, Ms. Yoshie Hayashi, Ms. Ayako Saito, Ms. Tomoko Yoshihara, Ms. Keiko Kotani and Ms. Ikuko Kinumatsu for the documental supports and warm encouragements.

I would like to thank all the members in Okubo-Shimojima Laboratory and Okubo-Wakihara Laboratory for their continuous experimental or daily life supports. I am happy to work here with them while encouraging each other.

For financial support, I appreciate JSPS and the Program for Leading Graduate Schools, “Global Leader Program for Social Design and Management (GSDM)”, by MEXT.

Last but not least, I would like to thank my family. With their continuous warm support, I am able to focus on my research.

December 19th, 2017

Natsume Koike